TURUN YLIOPISTON JULKAISUJA
ANNALES UNIVERSITATIS TURKUENSIS

SARJA - SER. D OSA - TOM. 885

MEDICA - ODONTOLOGICA

IMAGING OF THE VULNERABLE ATHEROSCLEROTIC PLAQUE

Pre-Clinical Evaluation of PET Tracers for Vascular Inflammation

by

Iina Laitinen

TURUN YLIOPISTO
UNIVERSITY OF TURKU
Turku 2009

From Turku PET Centre and Department of Clinical Physiology and Nuclear Medicine, University of Turku, Turku, Finland

Supervised by

Professor Juhani Knuuti, MD, PhD
Turku PET Centre
University of Turku
Turku, Finland

and

Adjunct Professor Anne Roivainen, PhD
Turku PET Centre and Turku Centre for Disease Modelling
University of Turku
Turku, Finland

Reviewed by

Professor Juha Hartikainen, MD, PhD
Department of Cardiology
Kuopio University Hospital
Kuopio, Finland

and

Senior Lecturer Lars Johansson, PhD
Institute of Oncology, Radiology and Clinical Immunology
Unit of Radiology
Uppsala University
Uppsala, Sweden

Dissertation opponent

Professor Petri Kovanen, MD, PhD
Wihuri Research Institute
Helsinki, Finland

ISBN 978-951-29-4148-3 (PRINT)
ISBN 978-951-29-4149-0 (PDF)
ISSN 0355-9483
Painosalama Oy – Turku, Finland 2009

to my family

ABSTRACT

Iina Laitinen

IMAGING OF THE VULNERABLE ATHEROSCLEROTIC PLAQUE
Pre-Clinical Evaluation of PET Tracers for Vascular Inflammation
From Turku PET Centre and Department of Clinical Physiology and Nuclear Medicine, University of Turku, Turku, Finland
Annales Universitatis Turkuensis
Painosalama Oy, Turku, Finland 2009

Atherosclerosis is a vascular inflammatory disease causing coronary artery disease, myocardial infarct and stroke, the leading causes of death in Finland and in many other countries. The development of atherosclerotic plaques starts already in childhood and is an ongoing process throughout life. Rupture of a plaque and the following occlusion of the vessel is the main reason for myocardial infarct and stroke, but despite extensive research, the prediction of rupture remains a major clinical problem. Inflammation is considered a key factor in the vulnerability of plaques to rupture. Measuring the inflammation in plaques non-invasively is one potential approach for identification of vulnerable plaques.

The aim of this study was to evaluate tracers for positron emission tomography (PET) imaging of vascular inflammation. The studies were performed with a mouse model of atherosclerosis by using *ex vivo* biodistribution, autoradiography and *in vivo* PET and computed tomography (CT). Several tracers for inflammation activity were tested and compared with the morphology of the plaques. Inflammation in the atherosclerotic plaques was evaluated as expression of active macrophages.

Systematic analysis revealed that the uptake of ^{18}F-FDG and ^{11}C-choline, tracers for metabolic activity in inflammatory cells, was more prominent in the atherosclerotic plaques than in the surrounding healthy vessel wall. The tracer for $\alpha_v\beta_3$ integrin, ^{18}F-galacto-RGD, was also found to have high potential for imaging inflammation in the plaques. While ^{11}C-PK11195, a tracer targeted to receptors in active macrophages, was shown to accumulate in active plaques, the target-to-background ratio was not found to be ideal for *in vivo* imaging purposes.

In conclusion, tracers for the imaging of inflammation in atherosclerotic plaques can be tested in experimental pre-clinical settings to select potential imaging agents for further clinical testing. ^{18}F-FDG, ^{18}F-galacto-RGD and ^{11}C-choline choline have good properties, and further studies to clarify their applicability for atherosclerosis imaging in humans are warranted.

Keywords: Animal models, atherosclerosis, biodistribution, inflammation, PET.

TIIVISTELMÄ

Iina Laitinen

REPEYTYMISALTTIIN ATEROSKLEROOTTISEN PLAKIN KUVANTAMINEN
Tulehdukseen hakeutuvien PET-merkkiaineiden prekliininen testaus

Valtakunnallinen PET-keskus, Kliinisen fysiologian ja isotooppilääketieteen oppiaine,
Kliininen laitos, Turun yliopisto
Annales Universitatis Turkuensis
Painosalama Oy, Turku, Finland 2009

Ateroskleroosi on verisuonten tulehdustauti, joka on yleisimpien kuolinsyidemme sepelvaltimotaudin, sydäninfarktin sekä aivoinfarktin taustalla. Ateroskleroottisten valtimomuutosten eli plakkien kehittyminen alkaa jo lapsuudessa ja kestää läpi elämän. Plakin repeytyminen ja sitä seuraava verisuonta tukkivan hyytymän muodostuminen on yleisin sydän- ja aivoinfarktin syy. Laajoista tutkimuksista huolimatta repeytymisen ennakointi on edelleen kliinisesti erittäin haastavaa. Nykyisin tiedetään, että tulehdusreaktio on tärkeä tekijä repeytymisalttiin plakin muodostumisessa. Positroniemissiotomografialla (PET) voitaisiin mahdollisesti löytää nämä tulehtuneet, repeytymisalttiit ateroskleroottiset plakit ennen kliinisiä oireita.

Tämän väitöskirjatyön tavoitteena oli prekliinisesti arvioida tiettyjen PET-merkkiaineiden soveltuvuutta verisuonitulehduksen kuvantamiseen. Tulehdusaktiivisuutta mittaavien radiolääkeaineiden kerääntymistä verrattiin plakkien rakenteeseen. Plakkien tulehduksen mittarina käytettiin aktiivisten makrofagisolujen esiintymistä plakeissa. Työssä käytettiin ateroskleroosin hiirimallia ja biodistribuutio-, autoradiografia-, tietokone-tomografiamittauksia (ex vivo), sekä PET-kuvantamista (in vivo).

Systemaattinen analyysi osoitti, että solujen aineenvaihdunnan aktiivisuutta kuvastavat radiolääkeaineet, ^{18}F-FDG ja ^{11}C-koliini, kerääntyivät tulehduksellisiin kohtiin ateroskleroottisissa plakeissa. Verisuonten uudistuotantoon liittyvä $\alpha_v\beta_3$-integriiniin sitoutuva ^{18}F-galacto-RGD todettiin myös lupaavaksi merkkiaineeksi ateroskleroosiin liittyvän tulehduksen kuvantamisessa. Sitä vastoin makrofageihin kerääntyvän ^{11}C-PK11195:n taustakertymä havaittiin liian korkeaksi PET-kuvantamista ajatellen.

Yhteenvetona voidaan todeta, että ateroskleroottisten plakkien tulehdusta havaitsevia merkkiaineita voidaan testata kokeellisesti eläinmallissa ja siten valita lupaavimmat kliinisiin jatkotutkimuksiin. Testatuista merkkiaineista ^{18}F-FDG:llä, ^{18}F-galacto-RGD:llä ja ^{11}C-koliinilla oli PET-kuvantamisen kannalta hyviä ominaisuuksia ja niiden käyttöä ateroskleroosin kuvantamisessa potilailla tulisi harkita.

Avainsanat: Ateroskleroosi, eläinmallit, biodistribuutio, PET-kuvantaminen, tulehdus.

TABLE OF CONTENTS

1 INTRODUCTION....11

2 REVIEW OF THE LITERATURE....12

2.1 Atherosclerosis....12
2.1.1 Progression of atherosclerotic plaque....13
2.1.2 Characterisation of vulnerable plaque....16

2.2 Animal and human models of atherosclerosis....19
2.2.1 Mouse models....20
2.2.2 Rabbit models....22
2.2.3 Pig models....23
2.2.4 Clinical models....23

2.3 Imaging of atherosclerosis and plaque vulnerability....24
2.3.1 Angiography....24
2.3.2 Intravascular ultrasound....24
2.3.3 Ultrasound....26
2.3.4 Computed tomography....26
2.3.5 MRI....27
2.3.6 Optical imaging....28
2.3.7 Nuclear imaging....28

2.4 Targets for nuclear imaging of atherosclerosis....30
2.4.1 Imaging of inflammation....33
2.4.2 Imaging of matrix degradation....35
2.4.3 Imaging of apoptosis....35
2.4.4 Imaging of angiogenesis....36
2.4.5 Imaging of thrombogenic factors....36

2.5 Future aspects....36

3 OBJECTIVES OF THE STUDY....38

4 METHODS AND EXPERIMENTAL ANIMALS....39

4.1 Radiotracers and metabolite analysis....39
4.1.1 Production of radiotracers....39
4.1.2. Other used radiotracers....41
4.1.3. Radiometabolite analysis....41

4.2 Experimental animals....41

4.3 Biodistribution studies....42

4.4 Autoradiography of aortic sections....44

4.5 PET imaging....45

4.6 *In vitro* studies....46

4.6.1 *In vitro* distribution of ^{18}F-FDG in human artery samples 46
4.6.2 Specific binding 47
4.6.3 Biochemical measurements 47
4.7 Histology and immunohistochemistry 47
4.8 Statistical analyses 48

5 RESULTS 50

5.1 Characterisation of the animal model 50
5.2 Biodistribution of tracers 50
5.3 Biodistribution of tracers in the plaques 51
5.3.1 Correlation to inflammation and morphology 53
5.3.2 Correlation to other immunohistochemical stainings 53
5.4 Mechanism of ^{18}F-FDG binding 54
5.4.1 ^{18}F-Fluoride 54
5.4.2 Patient samples 54
5.5 In vitro binding of ^{3}H-PK11195 54
5.6 Evaluation of ^{18}F-galacto-RGD 56
5.6.1 Dual tracer comparison 56
5.6.2 Small animal PET-CT 56
5.6.3 *In vitro* binding of ^{18}F-galacto-RGD in mouse aorta sections 56
5.7 Radiometabolite analysis of ^{11}C-choline 56

6 DISCUSSION 58

6.1 Animal model 58
6.2 Evaluation of tracers for atherosclerosis imaging 60
6.2.1. ^{18}F-FDG 60
6.2.2. ^{11}C-PK11195 61
6.2.3 ^{18}F-galacto-RGD 62
6.2.4 ^{11}C-Choline 64
6.3 Correlation of biodistribution to inflammation 66
6.4 Methods 67
6.5 Future directions 68

7 SUMMARY AND CONCLUSIONS 70

8 ACKNOWLEDGEMENTS 71

9. REFERENCES 74

ORIGINAL PUBLICATIONS 83

ABBREVIATIONS

%ID/g	Percentage of injected dose per gram of tissue
[^{11}C]PK11195	N-Methyl-^{11}C-(R)-1-(2-chlorophenyl)-N-(1-methylpropyl)-3-isoquinoline carboxamide
[^{18}F]FDG	2-^{18}F-Fluoro-2-deoxy-D-glucose
[^{18}F]-gal-RGD [^{18}F]-galacto-RGD	^{18}F-galacto-(cyclo(Arg-Gly-Asp-DPhe-Val-)
[^{18}F]FCH	^{18}F-Fluoromethylcholine
ADP	Adenosine diphosphate
AHA	American Heart Association
APOBEC-1	Apolipoprotein B mRNA editing enzyme, catalytic polypeptide-1
ApoB	Apolipoprotein B
ApoE	Apolipoprotein E
CT	Computed tomography
ECG	Electrocardiogram
Gd-DTPA	Gadolinium-diethylene triamine pentaacetic acid
GPVI	Glycoprotein VI antibody
HDL	High density lipoprotein
HPLC	High-performance liquid chromatography
ICAM-1	Inter-cellular adhesion molecule-1
IL	Interleukin
ILS	Interstitial lung disease
i.v.	Intravenous(ly)
IP	Imaging plate
ID	Injected dose
IVUS	Intravascular ultrasound
LDL	Low density lipoprotein
LDLR	Low density lipoprotein receptor
LDLR$^{-/-}$ ApoB$^{100/100}$	Genetically engineered mouse deficient for LDLR and expressing only ApoB100-form (deficient for ApoB48)
LDLR/ApoB48	same as LDLR$^{-/-}$ ApoB$^{100/100}$
LOX-1	Lectin-like oxidised LDL receptor-1
MCP-1	Monocyte chemotactic protein-1
MRI	Magnetic resonance imaging
NO	Nitric oxide
PBR	Peripheral benzodiazepine receptor
PET	Positron emission tomography
RGD	Arginine (R), glycine (G), aspartate (D) motif
ROI	Region of interest
RT	Room temperature
SD	Standard deviation

SHAPE	Society for Heart Attack Prevention and Eradication
SMC	Smooth muscle cell
SPECT	Single photon emission computed tomography
SR	Scavenger receptor
TF	Tissue factor
TNF-α	Tumour necrosis factor-alpha
VCAM-1	Vascular cell adhesion molecule-1
VEGF	Vascular endothelial growth factor
VLDL	Very-low-density lipoprotein

LIST OF ORIGINAL PUBLICATIONS

This dissertation is based on the following original publications, which are referred to in the text by the corresponding Roman numerals, I – IV.

I. Laitinen, I., Marjamäki, P., Haaparanta, M., Savisto, N., Laine, V.J.O., Soini, S.L., Wilson, I., Leppänen, P., Ylä-Herttuala, S., Roivainen, A., Knuuti, J. Non-specific binding of [^{18}F]FDG to calcifications in atherosclerotic plaques. Experimental study of mouse and human arteries. *European Journal of Nuclear Medicine and Molecular Imaging,* 2006 Dec; 33(12):1461-1467.

II. Laitinen, I., Marjamäki, P., Haaparanta, M., Någren, K., Laine, V.J.O., Leppänen, P., Ylä-Herttuala, S., Roivainen, A., Knuuti, J. Uptake of inflammatory cell marker [^{11}C]PK11195 into mouse atherosclerotic plaques. *European Journal of Nuclear Medicine and Molecular Imaging*, 2009 Jan;36(1):73-80.

III. Laitinen, I.,* Saraste, A.,* Weidl, E., Poethko, T., Weber, A.W., Nekolla, S.G., Leppänen, P., Ylä-Herttuala, S., Hölzlwimmer, G., Walch, A., Esposito, I., Wester, H.-J., Knuuti, J., Schwaiger, M. Evaluation of $\alpha_v\beta_3$ integrin -targeted PET tracer ^{18}F-Galacto-RGD for imaging of vascular inflammation in atherosclerotic mice. *Circulation Cardiovascular Imaging* 2009 Jul;2(4):331-338.

IV. Laitinen, I., Luoto, P., Någren, K., Marjamäki, P., Silvola, J., Hellberg, S., Laine. V.J.O., Ylä-Herttuala, S., Knuuti, J., Roivainen, A. Uptake of [^{11}C]choline into mouse atherosclerotic plaques. *Manuscript submitted for publication.*

* Equal contribution

1 INTRODUCTION

Atherosclerosis is a life-long vascular inflammatory disease. It is characterised by accumulation of lipids into the arterial wall and progression of atherosclerotic lesions, also called atherosclerotic plaques. Rupture of an atherosclerotic plaque is the main cause of acute cardiac events and stroke. The term "vulnerable plaque" refers to often modestly stenotic plaques, prone to rupture and cause clinical complications. Autopsy series have characterised these vulnerable rupture-prone plaques as comprising a thin fibrous cap, a large lipid-rich pool, increased macrophage activity with reduced collagen synthesis, and increased expression of collagenases and smooth-muscle apoptosis. Inflammation is currently considered critical for the pathogenesis of atherosclerosis and an important determinant of the outcome of macrovascular disease. Plaques containing a large number of inflammatory cells, mainly macrophages, are more vulnerable than plaques with only few inflammatory cells.

The association between the degree of arterial stenosis and plaque vulnerability is weak (Falk 1995). Conventional anatomical imaging may not provide sufficient information for risk assessment, and therefore, detection and identification of rupture-prone atherosclerotic plaques remains a great clinical challenge. Non-invasive imaging of inflammation within atherosclerotic lesions may be useful to predict future risk of plaque rupture, and to allow monitoring of anti-atherosclerotic therapies that are essential for efficient prevention of the acute events. Recent experimental and human studies have provided evidence that positron emission tomography (PET) imaging using fluorine-18 labelled 2-fluoro-2-deoxy-D-glucose (^{18}F-FDG), a glucose analogue that is taken up by the metabolically active macrophages, could provide an index of inflammation in atherosclerotic lesions (Rudd *et al*. 2002, Tawakol *et al*. 2006). However, due to the intense uptake of ^{18}F-FDG in the myocardium, which complicates imaging of coronary arteries, and the dependence of its uptake on metabolic conditions, better imaging agents for plaque inflammation and vulnerability are needed. Translational *ex vivo* animal studies are needed to evaluate the feasibility of potential radiotracers to be used for *in vivo* imaging.

This study evaluates the inflammation targeting tracers ^{18}F-FDG, ^{11}C-PK11195, ^{18}F-galacto-RGD and ^{11}C-choline for the imaging of vascular inflammation associated with atherosclerosis by using a mouse model of atherosclerosis.

2 REVIEW OF THE LITERATURE

2.1 Atherosclerosis

Atherosclerosis is a complex disease characterised by the thickening of the vascular wall via accumulation of lipids to the artery wall. It is the primary cause of coronary artery disease and cerebrovascular disease, which are the two most common causes of illness and death worldwide (Rader and Daugherty 2008). Atherosclerosis starts early in childhood and develops gradually, forming atheromas, atherosclerotic lesions, and later, complex plaques in major arteries (Figure 1). Clinical manifestations of atherosclerosis are often unsuspected and can lead to sudden death. Acute myocardial infarction, stroke, unstable angina and sudden cardiac death all result from the development of an occlusive thrombus over a disrupted atherosclerotic plaque. The risk of a thrombotic event is related more to the instability of the plaque than to the extent of the disease (Fuster *et al.* 1992). Therefore, characterisation of a vulnerable plaque and understanding the events leading to its development are under intensive investigation.

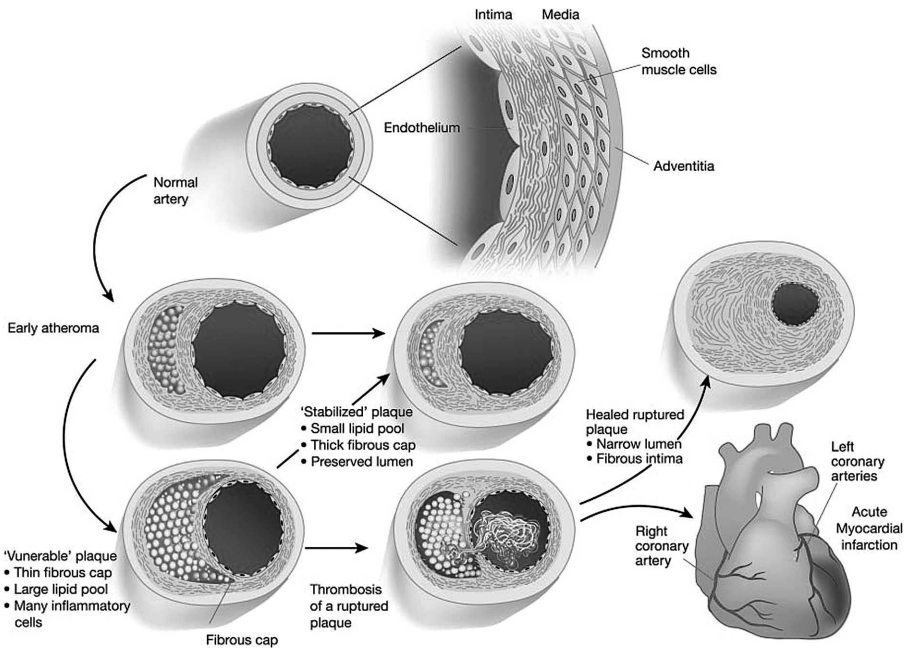

Figure 1: Development of vulnerable plaque. Reprinted with permission from the Nature Publishing Group (Libby 2002)

More than 200 risk factors for atherosclerosis have been identified (Naghavi *et al* 2006). The most commonly known are the typical cholesterol profile of high LDL (low-density lipoprotein) and low HDL (high density lipoprotein) plasma concentration, high blood pressure, diabetes, smoking, male gender, obesity, family history and stress. The risk of developing clinical events increases with every added risk factor, and prevention of atherosclerosis is focused on reducing the risk factors. Some patients are asymptomatic all their lives, while others start to show ischemic symptoms, typically after 50 years of age. Diagnosis of atherosclerosis is based on clinical symptoms, physiological tests and imaging techniques. Atherosclerosis can be treated, although not completely cured, with life-style changes and drug treatment. The acute clinical symptoms are treated by intense medication, balloon angioplasty and stenting, bypass surgery or endarcrectomy. Ischemic events may, however, be lethal or damage the tissue leading to severe complications.

2.1.1 Progression of atherosclerotic plaque

Fatty streak

Progression of atherosclerosis starts already in childhood or at adolescence with the formation of the first recognised arterial defects, fatty streaks. The order of events is not fully understood, but it involves the accumulation of lipids in the vascular wall due to the plasma hypercholesterolemia and defect of efflux of lipids, endothelial dysfunction and inflammation. Atherosclerotic plaque formation has been shown to develop first at the curvatures and bifurcations of the arteries where the endothelium is exposed to local blood flow disturbances (Ravensbergen *et al.* 1998). The endothelium is important for maintaining normal vascular function, and it has been claimed that sheer stress causes endothelial dysfunction, which is recognised as the first event in atherosclerosis. The shear stress is further enhanced by hypertension, a recognised risk factor (Gimbrone *et al.* 1997). Humoral factors, such as advanced hypercholesterolemia, advanced glycation end-products in diabetes, chemical irritants in tobacco smoke and immunocomplexes also contribute to endothelial dysfunction. Endothelial dysfunction is characterised by decreased nitric oxide (NO) synthesis. The decreasing of NO bioavailability is probably a multifactorial process. The increased vascular superoxide production and other reactive oxygen species react rapidly with NO and cofactors, resulting in loss of bioactivity and production of NO. This leads to the loss of normal NO functions in vessels, such as loss of normal endothelium-dependent vasodilation, inhibition of leukocyte adhesion, maintenance of smooth muscle cells in a non-proliferative state, and inhibition of platelet aggregation (Mahmoudi *et al.* 2007). The endothelium starts to express surface receptors (vascular cell adhesion molecule-1 (VCAM-1), inter-cellular adhesion molecule-1 (ICAM-1) and P-selectin) and chemoattractants (monocyte chemotactic protein-1 (MCP-1)) to draw monocytes, lymphocytes, mast cells and neutrophils into the arterial wall starting the initial inflammatory reaction at the vessel wall (Li *et al.* 1993). After internalisation, monocytes mature into macrophages. This is further enhanced with oxidised LDL in

the blood steam and the vessels (Rajavashisth *et al.* 1990). Macrophages express scavenger receptors (SR-A, CD36) and lectin-like oxidised LDL receptor-1 (LOX-1) for lipoprotein phagocytosis, and turn into lipid-laden macrophages, also called foam cells. Confluent lipid accumulation in the intima together with foam cells is called a fatty streak or a type I lesion as classified by the American Heart Association (Stary *et al.* 1995).

Fibroatheroma

Macrophages and T lymphocytes secrete a range of cytokines such as interleukin-1 (IL-1), tumour necrosis factor-alpha (TNF-α), proteolytic enzymes and growth factors, thus maintaining and escalating the local inflammation. This also serves as a stimulus to medial smooth muscle cells to produce proteinases which facilitate their migration to intima and growth factors for proliferation (Libby and Theroux 2005). Smooth muscle cells start to produce collagen, elastin and other matrix proteins, which eventually form a fibrous cap to the developing lesion. Proteoglycans bind lipoproteins, which prolong their residence in the arterial intima, and make them more susceptible to oxidation and glycation (Williams and Tabas 1998). Increasing accumulation of extracellular lipid and cell proliferation cause cell death either by apoptosis or necrosis. The formed lipid-rich necrotic core enlarges and provokes further inflammation. The core can ultimately occupy 30-50% of arterial volume. This type of lesion is called fibroatheroma (type II and III) and can be found in humans at age 15-30 years, continuing throughout life. Calcifications also occur, initially as small aggregates and later as large nodules. The mechanism of calcification is very much like that in bone formation and is mediated by osteopontin and other non-collagenous bone-associated proteins (Fuster *et al.* 2005). The coronary calcification is composed mainly of hydroxyapatite and organic matrix (collagen).

Advanced lesion, thin cap fibroatheroma

Advanced atherosclerotic lesions occur typically in persons aged >55 years and is characterised by the developing of a thin-cap fibroatheroma, also called vulnerable plaque when possessing certain characteristics. Advancing lesions first grow outwards, in a process called vascular remodelling (Glagov *et al.* 1987). The lumen may retain the same size, and since no flow-limiting growth can be seen in traditional angiography, these plaques are left undetected. When the enlargement of the plaque exceeds the limits of effective diffusion of oxygen and nutrients, the surrounding vasa vasorum, the small vessels feeding the artery, start to proliferate and invade the plaque media (Fleiner *et al*. 2004). This neovascularisation, also called angiogenesis, can be triggered by hypoxia or probably also via a hypoxia-independent way by inflammation (Fuster *et al.* 2005). Macrophages and other cells secrete pro-angiogenic factors such as $\alpha_v\beta_3$-integrin. The formed neovessels are fragile and leaky, and predispose the plaque to rupture by leaking erythrocytes into the lesion and forming a small thrombus. The cholesterol-rich red blood cells also increase the size of the necrotic core and induce phagocytosis. The number of neovessels is increased in ruptured plaques compared to stable ones (Moreno *et al.* 2004). Neovessels are associated with

macrophages and T cells and have been suggested as a way for further macrophage infiltration (Fuster *et al.* 2005). The main cause of the turning of mostly harmless fibroatheromas into dangerous rupture prone plaques lies in the thinning of the protective fibrous tissue. Inflammatory cells have an important role in secreting enzymes which degrade the fibrous cap. Macrophages and mast cells have been detected at the site of the rupture of the plaque. These cells secrete proteolytic enzymes, plasminogen activators and matrix metalloproteinases (MMPs), which degrade the extracellular matrix and weaken the fibrous cap (Moreno *et al.* 1994, Kaartinen *et al.* 1994).

Complex lesions and thrombosed lesions

Two mechanisms contribute to plaque rupture: physical forces and an active degrading process within the cap of the plaque. These can work independently or in conjunction., The most commonly found rupture site is a fibroatheroma with disruption of the thin fibrous cap where the overlying thrombus is continuous with the lipid core (Virmani *et al.* 2000). The thin cap is weakest when occupied by macrophages and foam cells. Ruptures most often occur in the shoulder region of the plaque. Macrophages and mast cells on the thin cap also secrete proteolytic enzymes and degrade extracellular matrix by phagocytosis, thus weakening the cap and predisposing it to rupture (Shah *et al.* 2001).

A thrombus is formed when thrombogenic substrates of the plaque content are exposed to the circulation. Lipid-rich plaques have been shown to be the most thrombogenic of all arterial sites (Fernandez-Ortiz *et al.* 1994). Tissue factor (TF), a small glycoprotein especially rich in apoptotic macrophages, initiates the clotting cascade and is believed to be a major regulator in coagulation (Nemerson 1998). TF forms a complex with coagulation factors, leading to thrombin generation. A thrombus in the coronary artery can cause acute occlusion or subocclusion and can lead to unstable angina or other acute coronary symptoms. Thrombus formation can also be caused by plaque erosion (Farb *et al.* 1996) where the lipid core has not been exposed; only the endothelium is absent. Protrusion of a calcific nodule through the endothelium has also been documented as a cause of thrombosis (Virmani *et al.* 2000). In these cases, the formation of thrombi may be caused by a hyper-thrombotic state triggered by systemic factors (Fuster *et al.* 1992). Many of the traditional risk factors also affect the thrombogenicity of the blood, for example, smoking increases catecolamine release and activates platelets (Badimon *et al.*1999). Circulating tissue factor also triggers systemic procoagulant activity (Sambola *et al.* 2003).

There is some evidence that unstable plaques can manifest as successive, clinically silent thrombi for days or weeks before occlusive thrombus formation (Rittersma *et al.* 2005). The rupture site is then healed, and the plaque volume increases, making the site vulnerable for another rupture. This may mean that disruption of the plaque may not be the decisive and only event causing the clinical event. This finding also provides the rationale for the quest to find biomarkers to elucidate these silent events before the severe events.

Atherosclerosis affects multiple vascular locations and involves most arterial vessels. Typically, the plaques that rupture are located in proximal segments or at least in the middle part of coronary vessels. However, most plaques in general remain stable. It is also possible the there are several plaques that are prone to rupture (Goldstein *et al.* 2000) although it is currently thought that only one to three vulnerable lesions typically exist simultaneously (Narula *et al.* 2008). The most prominently involved site in plaque formation is the abdominal aorta, but it is very rarely the site of any luminal thrombosis (van der Wal and Becker 1999). Instead, in the small diameter vessels the outcome of thrombus formation frequently leads to severe clinical symptoms, myocardial infarction in coronary arteries, and stroke in carotid artery.

2.1.2 Characterisation of vulnerable plaque

The term vulnerable plaque is used to describe an atherosclerotic lesion prone to develop an occlusion and lead to an acute clinical event. The terms high-risk lesion, unstable plaque, thrombus-prone plaque are also used, as well as the retrospectively used term culprit lesion of the plaques underlying a thrombosis. Chronic atherosclerotic disease becomes acute with the progression of vulnerable plaque or thrombosis, and therefore factors leading to it have been under comprehensive research. The characterisation of vulnerable plaque is based mainly on retrospective histological studies of autopsy samples, and may not fully describe the situation prior to the thrombus formation.

Plaque vulnerability is associated with several mechanisms in a complex interplay of mechanical forces and inflammation, which induces matrix remodelling, angiogenesis and apoptosis (Table 1). In large post-mortem studies, the ruptured lesion has been shown to have a large lipid core with a thin fibrous cap (Falk 2006), although also other types of culprit lesions have been reported (Virmani *et al.* 2000, Davies 1992). The inflammatory processes in the plaque are shown to be closely linked with

Table 1: Factors affecting to plaque vulnerability.

Inflammation	**Fibrous cap thinning**	**Intraplaque haemorrhage**	**Morphology**
Macrophage infiltrations	Matrix degradation (MMP's, cathepsins) and factors regulating their functions	Angiogenesis = neo-vascularisation	Size of the plaque
T-cell accumulation	SMC apoptosis		Size of the necrotic core
Cytokines and their regulation	Reduced SMC proliferation		Location of the plaque
Macrophage apoptosis	Reduced collagen synthesis		Hemodynamics
			Sheer stress

the rupture of the fibrous cap. However, the factors leading to rupture are still poorly understood due to the lack of adequate methods to follow the progress in detail and to distinguish clinically relevant plaques before the acute event.

Inflammation

Atherosclerosis is considered an inflammatory disease, because of the key role of inflammation in all stages of the disease (Ross 1999). As described above, the initiation of plaque occurs as a compensatory inflammatory response to endothelial dysfunction and lipid accumulation and continues throughout the progression of the plaque. Many inflammatory cells are involved in the progression and stability of atherosclerotic plaque, but the main contributor, not only by number but also by function, is the monocyte/macrophage. Monocytes and also T-cells infiltrate lesions at all stages and induce chronic inflammation in the plaques. The largest concentrations of macrophages can be found at the thin fibrous cap and shoulder regions in lipid-rich lesions and at the site of the rupture (Lendon *et al.* 1991, van der Wal *et al.* 1994, Moreno *et al.* 1994). Inflammation is close associated with the initiation of the plaque rupture by mechanisms leading to instability of the fibrous cap. Activated T-cells, interferon-gamma (IFN-γ) and uptake of lipids can induce macrophages to produce TF, a very potent trigger of thrombosis (Jander *et al.* 1998). Macrophage and T-cell infiltration has been reported to be enhanced in those carotid arteries which raise symptoms, versus asymptomatic ones (Spagnoli *et al.* 2004, Jander *et al.* 1998) or to correlate with symptom severity in coronary artery disease (MacNeill *et al.* 2004). In post-mortem analysis, ruptures of plaques have been demonstrated to occur at the thin inflamed cap of fibrous tissue (Falk 1995).

The uncontrolled vicious cycle of inflammation and cell death lies in the lipid pools of lesions. Extracellularly and intracellularly accumulating modified LDL promote inflammation and induce cell death (Öörni and Kovanen 2009). Cell death, especially through necrosis induces more damage and inflammation in the tissue. Macrophages and other phagocytes in an attempt to protect the tissue phagocytose the debris and later undergo apoptosis. Macrophage apoptosis has been shown to be increased in early lesions, but defective phagocytosis of apoptotic macrophages in the later stages promotes necrosis and enhances inflammatory response (Tabas 2005).

Throughout these phases, macrophages and other leukocytes present in the plaque secrete various cytokines and chemokines, which can have pro- or anti-inflammatory properties, e.g. interleukin-10 (IL-10), transforming growth factor-beta1 (TGF-β1), adding to the complexity of the plaque. IFN-γ, interleukin-18 (IL-18), TNF-α and MCP-1 have been associated with the progression of lesions (Whitmann *et al.* 2000, Whitmann *et al.* 2002, Stoll and Bendszus 2006). The increased expression of cell adhesion molecules on the endothelium, activated by cytokines, is probably the cause of acute macrophage infiltration into the vulnerable plaques (DeGraba *et al.* 1998).

Systemic inflammation is also linked to unstable plaque formation. Acute-phase reactants C-reactive protein (CRP) and serum amyloid A (SAA), are elevated in

unstable coronary disease patients and patients at high risk of stroke (stenotic carotid arteries) (Ridger *et al.* 2004).

Controlling inflammation by medication has been shown to decrease the risk of acute events. Acetylsalicylic acid (aspirin) has anti-thrombotic effects and also anti-inflammatory effects by inhibiting cyclooxygenase-2 (COX-2) expression in inflammation in the plaques, and by decreasing the adherence of monocytes (Cipollone *et al.* 2005, Khan and Mehta 2005). Also statins, in addition to their acknowledged lipid lowering effect, can prevent and possibly also reverse ongoing inflammation and tissue damage (Ridker *et al.* 1999, Pucci *et al.*2007*,* Ridker *et al.* 2009). Less studied is the effect of cortisone on the inflammation of the plaques. Pharmacological inhibition of 11ß-HSD1, the enzyme which converts inactive cortisone into active cortisol in cells, has been shown to slow plaque progression in mice (Hermanowski-Vosatka *et al.* 2005).

Fibrous cap thinning

As a part of the remodelling of the plaque, macrophages and mast cells secrete, upon activation, plasminogen activators and matrix metalloproteinases (MMPs), which degrade the components of the extracellular matrix (ECM) (Galis *et al.* 1995). This enables the outward growth of the plaque and neovessel formation, but consequently, when occurring in the fibrous cap area, also the thinning of the cap. The various types of MMPs in the plaque include collagenases, elastases, gelatinases and stromelysins. The functions of MMPs are regulated by specific inhibitors, but this balance is disrupted in advanced plaque. Quantification of MMPs and their inhibitors in blood correlates to atherogenesis in humans (Zureic *et al.* 2002). Particulary MMP-9 is found to be associated with plaque rupture in the carotid and coronary arteries. MMP-9 protein levels and activity have been elevated in patients with recent occurrence of cerebrovascular events (Loftus *et al.* 2000, Papalambros *et al.* 2004). In an experimental setting, activation of MMP-9 production in macrophages induced plaque disruption, showing direct evidence of the role of MMP-9, and highlighting it as a potential therapeutic target (Gough *et al.* 2006).

Smooth muscle cell (SMC) apoptosis contributes to destabilisation of the plaque. Fibrous cap regions are characterised by reduced SMC and ECM content (Virmani *et al.* 2000). SMCs produce collagen which stabilises the forming plaque. Direct interaction of macrophages and SMCs induce SMC death (Boyle *et al.* 2001). Also proliferation of SMC has been found to be reduced in vulnerable plaques (Bennett *et al.* 1998) In addition, activated mast cells also contribute to the stability by producing inhibitors of collagen synthesis (Leskinen *et al.* 2003).

Intraplaque haemorrhage

Vulnerable plaques may contain large areas of haemorrhage originating from neovessels (Virmani *et al.* 2005). This intraplaque haemorrhage has been claimed to be one of the mediating factors in making the stable plaques vulnerable to rupture and, therefore, has placed plaque angiogenesis under investigation. A study of advanced

human atherosclerotic plaques concluded that microvessel formation is strongly correlated with both plaque rupture and the signature features of vulnerable plaques (Moreno *et al.* 2004). In intraplaque haemorrhage, the rapid accumulation of erythrocytes is followed by macrophage infiltration. Erythrocyte membranes contain a large amount of cholesterol, which then ends up enlarging the plaque size and further activationing macrophages (Kolodgie 2003). Intraplaque haemorrhage in carotid artery lesions has been investigated with magnetic resonance imaging (MRI), finding an association with the plaque formation (Takaya *et al.* 2005).

Studies on angiogenesis in animal models are limited, since neovessel formation in the plaques is rare in experimental animals. In mice, even the extensive advanced lesions have little or no angiogenesis. In $LDLR^{-/-}$ $ApoB^{100/100}$ mice plaques, a very faint vascular endothelial growth factor (VEGF) signal has been detected (Heinonen *et al.* 2007).

Plaque morphology

Some plaque morphological characteristics have been linked with the rupture. The size of the plaque volume, but not necessarily stenosis, has been found to be linked with the risk of rupture as a determing factor (Narula *et al.* 2008). However, the plaques with significant luminal narrowing may cause angina and exercise-induced ischemia independently of the contents or the vulnerability of the plaque (Libby and Theroux 2005).

In addition, the positive remodelling of the vessel at the site of plaque, as well as spotty calcification also seem to have some value in characterising plaque vulnerability (Pletcher *et al.* 2004). One hypothesis is that the rupture of atherosclerotic plaque may be provoked by micro-calcifications in intima. If located near the thin cap these cell-size particles can cause high interfacial stress to the site and make the cap even more fragile (Vengrenyuk *et al.* 2006)

2.2 Animal and human models of atherosclerosis

Many biological processes can be studied in cell and tissue cultures, but to understand the functions of whole organisms and complex diseases, animal models are needed. Human atherosclerotic plaques are not easily accessible, and monitoring the progressing disease is challenging with the current technologies. Furthermore, studying a slowly progressing, life-long syndrome is time-consuming.

The development of gene manipulation methods in experimental animals has made it possible to understand better the biology and pathology of many diseases. For a complex disease such as atherosclerosis, there are several potential animal models to be used for research. Moreover, there is no animal model currently recognised as a standard model for either atherosclerosis or the vulnerable plaque (Schapira *et al.* 2007). The development of atherosclerosis and factors affecting it, the effect of diet or drugs, lipid metabolism, plaque rupture and stages leading to it may all require different characteristics for the model. In drug development experiments, the animal

model should also respond to statin treatment, which is the standard medication in atherosclerosis. The most often used endpoints are the changes in plaque burden or composition, combined with histological evidence and data of plasma biomarkers. When studying vulnerable plaques, an animal model would ideally need to possess plaques that are histologically similar to human end-stage lesions, and also have resemblance in lipid metabolism and coagulation. The latter is often neglected, and luminal thrombi occur very rarely in most used animal models, since regulation of blood coagulation differs in mice and humans (Carmeliet *et al.* 1998). In addition, the plaques would need to possess the same susceptibility to disrupt as in humans. There has been a lot of debate on whether plaque ruptures can be seen in experimental animals, especially in mice, and wheter they can be used as an endpoint (Jackson *et al.* 2007, Jackson 2007b, Falk *et al.* 2007, and Schwartz *et al*. 2007). The hard endpoints typical in epidemiological research such as myocardial infarction, cardiac dysfunction and premature death are very limited in mouse studies (Schapira *et al.* 2007). Some of the existing models could actually be considered as models of hypercholesterolemia, not exactly atherosclerosis, if these hard endpoints are missing.

In small animals such as the mouse, interpretation of the results may be difficult simply because of the size of the animal and the vessels, and differences in hemodynamics. Differences in lipid metabolism, blood coagulation and immunity also need to be taken into account. Primates and pigs most resemble human biology and therefore would be ideal models for many diseases, but costly maintenance, slow progression of the pathological condition, slow reproduction, and ethical issues hinder the use of these large animals.

2.2.1 Mouse models

Mice are highly resistant to atherosclerosis as compared to humans and therefore genetic variants have been created either by spontaneous mutations or by gene manipulation methods. There are two main reasons for resistance in wild type mice. First, mouse liver converts fewer very-low-density lipoprotein (VLDL) particles to LDL compared to human liver, because it can secrete both apolipoprotein B48 (ApoB48) containing lipoproteins and apolipoprotein B100 (ApoB100), the apoB48 being several fold more effective in clearing the lipoproteins. Second, mice do not express cholesteryl ester transfer protein, thus lacking the feedback mechanism of transferring cholesterol esters from HDL to VLDL (Agellon *et al*. 1991).

The first mouse models of atherosclerosis were created in the beginning of the 1990's after the invention of gene transfer and knock-out methods. Atherosclerosis is most often further induced by fat feeding, the Western-type diet being the most common. Most mouse models are bred on C57Bl/6 background and, therefore, this is most often used as a control strain in studies. The C57Bl/6 strain is susceptible to atherosclerosis, but only very small fatty streaks can be seen after prolonged fat-feeding (Paigen *et al.* 1990).

ApoE$^{-/-}$

ApoE glycoprotein is a structural component of lipoproteins and is responsible for the clearance of lipoproteins through the LDL receptor (LDLR) (Mahley 1988). ApoE-deficient mice spontaneously develop severe hypercholesterolemia with four-to-five-fold higher cholesterol concentration compared to C57Bl/6 mice and atherosclerosis, which can be further increased by a Western-type diet. These mice develop complex lesions with a fibrous cap, later also calcification (Rosenfeld *et al.* 2000). Induced and spontaneous ruptures have been reported (Reddick *et al.* 1998, der Thusen *et al.* 2002, Johnson *et al.* 2005), especially in crossbred LDLR$^{-/-}$ApoE$^{-/-}$ mice (Jackson *et al* 2007). Ruptures are seen in the brachiocephalic artery and are characterised as disruptions in the fibrous cap accompanied by lesion-intruding haemorrhage (Johnson *et al.* 2005). There has been some debate on whether spontaneous ruptures can be seen in mice and whether ruptures are in fact artefacts (Falk *et al* 2007). Luminal thrombosis or myocardial infarctions have not been reported.

ApoE is synthesised in the liver, brain and other tissues, including macrophages in the vessel wall. The lack of ApoE in macrophages influences inflammatory responses and, therefore, the use of ApoE mouse has been questioned (Curtiss and Boisvert 2000). The main reason for criticism against the use of this this mouse model is the lipoprotein profile, which very poorly resembles the human situation, and the extensive aggressive atherosclerosis affecting the composition of the lesions. Nevertheless, the ApoE deficient mice are still the most widely used model.

LDLR knockout mouse

Thw LDLR knockout mouse was one of the first models for atherosclerosis. In humans, the deficiency of the LDL receptor is known as familial hypercholesterolemia and is lethal at a young age if left untreated. The LDLR$^{-/-}$ mice have delayed clearance of LDL and other lipoproteins and, therefore, have increased plasma LDL concentrations. However, the progression of atherosclerosis is moderate. On a high fat diet, the lesions progress to complex plaques (Ishibashi *et al.* 1993). These mice exhibit xanthomas, a type of itchy skin lesions, and the possible loss of animals due to infected skin needs to be considered.

Mice with defective ApoB48

The ApoB protein exhibits in long ApoB100 form and in ApoB48 form, which is post-transcriptionally modified from the same gene by the apolipoprotein B mRNA editing enzyme, catalytic polypeptide-1 (*APOBEC-1*). The role of ApoB is different in human and mice. In mice, the liver expresses the ApoB48, and the ApoB48-containing lipoproteins are very effectively cleared from plasma, whereas ApoB100-particles remain for days in the circulation (Veniant *et al.* 2000). The knockout model of ApoB48 was made by targeted mutagenesis towards the ApoB gene, resulting in mice which produce only ApoB100 (ApoB$^{100/100}$) (Farese *et al.* 1996). Crossbred LDLR$^{-/-}$ ApoB$^{100/100}$ mice, also known as LDLR/ApoB48-double knockout, have severe hypercholesterolemia and the lipid profile resembles most that of humans. Cholesterol

accumulates in plasma to apoB100 containing LDL particles. These mice develop extensive atherosclerosis on normal chow which can be elevated further with the Western-type diet. (Veniant *et al.* 1998, Veniant *et al.* 2000) The plasma cholesterol levels and plaque burden depend on the age of the animal and the duration of fat feeding. After two months of feeding, the cross-sectional area of stenosis has been reported to be 58% in the aortic valve area (Leppänen *et al.* 2005). The lesions cover about 15% of the aorta, and feeding with the Western-type diet thickens the plaques. The lesions are advanced with macrophage infiltrates and large necrotic areas covered by a fibrous cap. Glucose levels remain unaffected, and the mice are not insulin-resistant (Heinonen *et al.* 2007).

Mechanical intervention

In addition to various genetic models, the plaque development can be further induced by ligation, denutation or by placing an extravascular collar on the vessel. Normally, in these models, genetically altered mice on a high fat diet are used and the device or operation is performed on the carotid artery. After operation, the animal is fed with a high-fat diet to further induce the plaque formation. Ligation and collar placing restrict the blood circulation and creates turbulence and changes in hemodynamics, which is believed to be very important of the creating of vulnerable plaques with a high risk of rupturing. Cheng *et al.* (2006) report vulnerable lesions with a thin fibrous cap and a large lipid core upstream of the collar and more stable lesions downstream.

Denutation is used more in larger animal models, but can also be used in mice. The endothelium of the vessel wall or an existing plaque is scraped off with a balloon catheter or other intravascular instrument. This creates an endothelial dysfunction in animals without prior plaques, to induce the plaque formation. Removal of the endothelium at the site of an existing plaque mimics plaque rupture or erosion and can create thrombus formation.

These surgical models have a considerable rate of animal loss and need skilled personnel to perform the operations. Proper control operations are essential. A sham-operation in the other carotid artery needs to be done to rule out the effect of wound healing in further experiments.

2.2.2 Rabbit models

Rabbits develop atherosclerotic lesions on a high cholesterol diet, and have been used extensively in atherosclerosis research (Yanni 2004). The most widely used New Zealand white (NZW) rabbit develops only fatty streaks and intimal thickening on a high fat diet, but advanced lesions can be induced by performing a balloon injury at the aorta or carotid artery and with a further fat-diet. The Watanabe heritable hyper-cholesterolemic rabbit is also used; these animals spontaneously develop lesions.

Rabbits are favoured when imaging arteries; the diameter of the rabbit aorta is 2-4mm, comparable to the size of human coronary arteries. The maintenance of rabbits is

expensive and another disadvantage is the relatively slow progression of the pathological condition and the required length of the studies.

2.2.3 Pig models

Domestic pigs and minipigs have been extensively used in medical research especially due to the similarities to human anatomy and physiology. For instance, the coronary arteries in pigs and humans are muscular, whereas the rabbit iliac artery is elastic and distinctly different (Bayes-Genis *et al.* 2000). Pigs develop spontaneous atherosclerosis during ageing, and the development of plaques can be induced by diet, hyperglycemia and by introducing vascular injury, most often by angioplasty. However, no consensus on the best model has been achieved, and reports of advanced plaques are limited (Artinger *et al.* 2009). Pigs have mostly been used in experimental research of cardiovascular surgery models and stenting, but also in imaging of plaques. Although the resemblance is superb, many practical and economic issues limit the use of pigs in research of atherosclerosis on a large scale.

2.2.4 Clinical models

Human atherosclerotic plaques can not be accessed without risks and, despite the progress in various imaging methods, monitoring of the progressing disease is still challenging. Although extensive histological data of human samples are available, these samples are normally taken post-mortem. Because atherosclerotic lesions can be found not only in coronary arteries, but also in large vessels such as carotid arteries, aorta, and peripheral arteries, it has been suggested that detection of vulnerable plaques in any artery could serve as an indicator of vulnerability (Dalager *et al.* 2008). Therefore, imaging studies have so far concentrated on these larger non-moving vessels, particularly carotid arteries. The carotid artery is used for monitoring the disease due to its easy accessibility via ultrasound measurements. Carotid intima-media thickness (IMT) is considered a marker of generalised atherosclerosis (Hollander *et al.* 2002). Also, it has been proposed that vulnerable plaques in the carotid artery could be used as a general marker for cardiac risk. Although it is tempting to think that the imaging of these easier targets could also be enough for the assessment of cardiac risk, the evidence is still scarce. Carotid arterectomy patients are used to test the hypotheses *in vivo* in humans, and histology samples are available.

2.3 Imaging of atherosclerosis and plaque vulnerability

Imaging is used as a clinical tool in the diagnosis and risk assessment of atherosclerosis. Traditional methods of vasculature imaging are based on detecting the narrowing of the lumen, which is not a sufficient marker of plaque vulnerability, and therefore, the use of new improved anatomic imaging and molecular imaging methods in atherosclerosis are increasingly used and further developed. These sophisticated methods are providing new information on molecular and cellular mechanisms. In the future, imaging can be used in diagnosis decision making and to guide and monitor response to therapy. In many cases, the same imaging technology and methods are applicable in experimental animals, facilitating translational research.

The structure and function of arteries can be studied with several methods. Traditional imaging is based on detection of changes in the anatomy or on physical features, such as blood flow. With molecular imaging, the function can be assessed at the cellular and molecular level, and the biological processes can be visualised and quantified. Characterisation of plaques can be performed by anatomic and molecular imaging with either invasive or non-invasive techniques. The characteristics of the techniques are summarized in Table 2. So far, none of the techniques alone has the needed requirements for molecular imaging of plaque vulnerability, but PET has the needed sensitivity for detection of micro-dose amounts of a tracer and clinical availability.

In addition, several other new invasive imaging modalities have shown progress in plaque imaging, e.g. intravascular near infrared fluorophore reflectance, optical coherence tomography, and thermography. Endothelial function can be measured non-invasively by ultrasound or tonometry, providing information on vasoreactivity, vascular compliance, and the general atherosclerotic burden (Naghavi *et al*. 2006).

2.3.1 Angiography

Coronary angiography is the standard method in the diagnosis and treatment planning for patients with acute cardiac events. In angiography, a catheter is taken to the coronary artery from the femoral or radial artery and a bolus of contrast agent is given to visualise the arteries under X-ray. Direct injection of contrast into the coronary ostia provides full visualization of the coronary tree and its narrowings, with a good spatial resolution (Brown and Zhao 2007). This technique is invasive, but during the same operation, balloon angioplasty or stenting can be performed.

2.3.2 Intravascular ultrasound

Intravascular ultrasound (IVUS) is an invasive imaging technique performed during cardiac catheterization using small, intra-coronary catheters. The strong ultrasound signal reflected from the intima and external elastic membrane allows real-time intraluminal imaging of the vessel wall and measurement of the plaque area.

Table 2: Comparison of imaging technology. Modified from Dobrucki and Sinusas 2005, Brown and Zhao 2007, Brindle 2008 and Kherlopian et al 2008.

Modality	Spatial resolution (preclinical)*	Spatial resolution (clinical)	Depth	Temporal resolution	Sensitivity (mol/L)	Molecular probe	Quantifiable	Scan time	Patient safety
Angiography	80 -200 μm	200 μm	No limit	50 ms	-	-	anatomical measurements	sec-min	invasive, inonising radiation, contrast agent risks
Ultrasound	50 μm	300–500 μm	mm-cm	20 ms	**	μg-mg	challenging	sec-min	safe, contrast agent risks
IVUS	80 -200 μm	80 -200 μm	mm-cm	20 ms	-	-	anatomical measurements	sec-min	invasive
CT	12- 50 μm	200-400 μm	No limit	83-165 ms	?	?	anatomical measurements	sec-min	ionising radiation, contrast agent risks
MRI	4-100 μm	250–500 μm	No limit	sec-min	10^{-3}-10^{-5}	μg-mg	anatomical measurements. molecular probes challenging	min-hrs	probes and contrast risks
Optical									
Bioluminescence	3–5 mm	-	1–2 mm	sec-min	10^{-15}-10^{-17}	μg-mg	no	sec-min	probes risks
Fluorescence	2–3 mm	-	<1 mm	sec-min	10^{-9}-10^{-12}	μg-mg	no	sec-min	probes risks
PET	1–2 mm	2-5 mm	No limit	10 s-min	10^{-11}-10^{-12}	ng	yes	min-hrs	ionising radiation
SPECT	0.5–1.5 mm	7-10 mm	No limit	min	10^{-10}-10^{-11}	ng	challenging	min-hrs	ionising radiation

* preclinical cameras: microPET, microSPECT, microMRI, microCT
** single microbubbles can be detected

IVUS visualises the coronary artery wall, identifies angiographically invisible plaques and classifies them as soft, fibrous, or calcified. Another advantage is the opportunity to follow biological processes "on site", e.g. the healing process of ruptured plaques has been followed with the IVUS method (Rioufol *et al*. 2004). However, IVUS can not reliably identify characteristics of the plaque that render it vulnerable. (Brown and Zhao 2007) To date, no data from large epidemiological studies assessing the predictive value of IVUS on clinical events are available, although IVUS is sometimes seen as a golden standard in plaque imaging (Brown and Zhao 2007). Nonetheless, a retrospective study did show IVUS plaque progression to be strongly correlated with risk of clinical events as predicted by clinical scoring systems (von Birgelen *et al.* 2004). Another challenge in IVUS imaging is its spatial orientation, and the inability to measure severely narrowed or occluded arteries (Duivenvoorden *et al.* 2009).

2.3.3 Ultrasound

Ultrasound images are obtained when high-frequency sound waves emitted from a transducer placed on the subject are reflected back from underlying tissue structures. Clinical ultrasound instrumentation operates at frequencies of between 7.5 and 15 MHz, with a spatial resolution of 300–500 μm. At higher frequencies (40–50 MHz) the resolution is 50–100 μm, making it suitable for relatively high-resolution imaging in small animals, although at these frequencies ultrasound penetration is limited to 5–10 mm in soft tissues (Brindle 2008). Intima-media thickness (IMT) of the carotid arteries and arterial flow can be easily measured by ultrasound and Doppler ultrasound. The IMT measurement of carotid atherosclerosis has been validated as a as a marker of risk for cardiovascular disease (Duivenvoorden *et al* 2009). The major limitation is that ultrasound provides two-dimensional pictures of the vessel wall, while atherosclerosis is a three-dimensional, irregular and eccentric disease. Furthermore, ultrasound is hampered by calcifications, which complicates measurements in subjects with more advanced atherosclerosis.

Ultrasound provides relatively low resolution anatomical data, but the relatively low cost, ease of use, sensitivity and speed of imaging make this an attractive imaging modality in the laboratory (Brindle 2008). The use of targeted microbubbles detected by a regular ultrasound device is a new prospective method. The echolucent gas-filled particles bind to their targets on the endothelium, and non-targeted particles can be used as blood-pool contrast agents (Kaufmann and Lindner 2007). However, the relatively large size of the microbubbles (1–4 μm) means that they cannot leave the intravascular space and molecular imaging is limited to this compartment.

2.3.4 Computed tomography

CT images are obtained by rotating a low-energy X-ray source and detector around the subject to acquire a series of projections. These are then used to construct a three-dimensional image. Contrast in the image arises because of differential tissue absorption of X-rays, and, although the soft tissue contrast is not optimal, contrast

agents can be used for characterisation of vasculature (Brindle 2008). Modern multidetector CT has high spatial and temporal resolution, which allows anatomical imaging of coronary arteries. It is currently able to detect, localise, and characterise some aspects of coronary plaques, such as volume, positive remodelling and calcifications (Stein *et al.* 2008). Automatic quantification of calcified areas, so-called calcium scoring, has long been suggested as a useful prognostic tool in coronary artery disease (Kaufmann *et al* 1995). Although CT has high resolution, is fast and has high throughput, the drawback is that the patient is exposed to ionising radiation.

Recently, the first attempts at using targeted contrast agents have been presented. A targeted iodinated nanoparticle contrast agent has been shown to accumulate in macrophages in the plaques and thus enable visualisation of plaques in a rabbit model (Hyafil *et al.* 2007).

2.3.5 MRI

MRI provides very high spatial and temporal resolution without ionising radiation and with high soft tissue contrast, but the sensitivity is low. MRI involves the detection of nuclear spin reorientation in an applied magnetic field. Because the interaction is so weak the technique is insensitive and imaging is usually restricted to detection of water protons to provide images of anatomy (Brindle 2008). However, there are many different mechanisms for generating contrast in the MR image. Vascular magnetic resonance imaging is a relatively new non-invasive technique in the assessment of atherosclerosis. New sequences and coils allow high resolution imaging of the walls of the aorta and, in particular, the carotid artery (Duivenvoorden *et al* 2009). In addition to imaging arterial wall dimensions, MRI also enables visualization of plaque composition. Haemorrhage, fibrous cap and lipidrich necrotic cores can readily be distinguished, providing information on plaque vulnerability (Chu *et al.* 2004).

Imaging of haemorrhagic areas or phagocytic activity is based on detection of paramagnetic iron from haem, and this could be enhanced by iron-particle contrast agents, such as small paramagnetic iron oxide (SPIO) or other formulations of iron particles. These exogenously injected iron particles are either targeted to bind specific targets, or internalised via phagocytosis (Sakalihasan and Michel 2009). The multimodality nanoparticle approach and other specific magnetic nano- or other particles have placed MRI also into the category of molecular imaging, although quantification of the signals can be demanding. Microparticles targeted for platelets and thrombosis have been shown to be feasible (von zur Muhlen *et al*. 2008). Although these probes have been used in clinical trials, the major restiriction is that due to their low sensitivity, micromolar range quantities of these agents are required (Choudhury *et al.* 2009). Therefore, there are regulatory and safety issues to be solved. However, the use of MRI in detection of vulnerable plaque morphology will be very likely in the future, especially with the development of the hybrid PET-MRI device.

2.3.6 Optical imaging

Fluorescence and bioluminescence imaging techniques are extremely sensitive and widely used in the field of cell and tissue imaging. The use of fluorescence-mediated planar and tomographic imaging of mice is increasing. In fluorescence imaging, excitation light in the visible region is used to excite fluorophores in the tissue, which emit fluorescence at longer wavelengths. Although the technique has been widely used with cultured cells it is limited *in vivo* by the depth of penetration of the excitation light. This can be increased by using light in the near-infrared (NIR) region of the spectrum (650–900 nm) when absorption by haemoglobin and water is relatively low (Brindle 2008).

Bioluminescence imaging relies on the genetic engineering of tissues to express luciferases. These are photoproteins, isolated from organisms such as the firefly, which modify their substrates and in so doing produce light, which can be detected. The advantage over fluorescence imaging is that the technique is very sensitive, as there is no background. However, like fluorescence imaging, scattering and absorption of the emitted photons limits the depth at which the luciferase label can be detected to 1–2 mm (Brindle 2008).

Although these techniques have proved useful in the laboratory, they are unlikely to translate directly into the clinical practice. The low penetrance of optical imaging restricts the use of these very sensitive methods, but with the development of catheter-mounted fibre-optic devices, intra-arterial imaging can be performed (Jaffer *et al* 2007). The limitation may be the required amount of the probe.

2.3.7 Nuclear imaging

PET and single-photon emission computed tomography (SPECT) are non-invasive methods for imaging biological and physiological processes *in vivo*. Both methods utilise radiopharmaceuticals (tracers) that are positron-emitting (in PET) or gamma-emitting (in SPECT) compounds. The radiotracers are synthesised by sophisticated, time-saving methods and with high radiopurity. The formulated tracer is injected into the patient intravenously and the distribution of the tracer is detected after a period of time or measured kinetically from the time of the injection.

The strength of nuclear imaging lies in its outstanding sensitivity even in the picomolar range, allowing very weak signals to be detected. This also means that many biological processes can be investigated without any adverse pharmacological effects from the labelled probe molecule. Another advantage is that SPECT and PET technology are already established in clinical use with commercial scanners and a range of approved and tested tracers. The most recent technical advance in nuclear imaging is the use of hybrid scanners (PET-CT or SPECT-CT) that can combine the benefits of both anatomical and molecular imaging. In fact, the anatomical localisation is mandatory for molecular imaging methods, because when the signal is specific enough, few other

landmarks are available for localisation of the detected target. Dedicated small animal PET and SPECT imaging devices that use the same technology have become available with higher spatial resolution (about 1 mm). The combination of PET and MRI is also becoming available, and will also offer further potential to plaque imaging.

SPECT

Single photon emission computed tomography (SPECT) is a tomographic imaging technique using gamma rays. It is very similar to conventional planar nuclear medicine imaging using a gamma camera. However, it is able to provide true three-dimensional information (Sakalihasan and Michel 2009). The SPECT isotopes generally have long half-lives, or the parent radionuclides from which they are made in radionuclide generators, make them more readily available, whereas the short half-lives of the PET isotopes means that their production and use often require expensive on-site cyclotron and radiochemistry facilities (Brindle 2008). SPECT has better availability with a larger number of clinical scanners, but the limited spatial resolution (7-10mm) of clinical SPECT scanners makes the method less attractive for use in plaque imaging.

PET

PET imaging utilises compounds containing radioisotopes which decay through the emission of positrons. When a positron collides with a local electron, these undergo annihilation together and produce two simultaneous high-energy 511 keV gamma rays (photons) 180 degrees apart. These gamma rays are detected by the PET scanner consisting of a ring of detectors of scintillation crystals attached to photomultiplier tubes. Coincidental events are registered and corrected for attenuation of photons, and the data are reconstructed onto tomographic images by mathematical processing. Clinical PET scanners have a spatial resolution of 2-4 mm. The ability to correct for photon attenuation and to perform kinetic modelling to quantify processes in absolute terms makes PET a leading molecular imaging technique.

The most commonly used radionucleotides are fluorine-18 (^{18}F), carbon-11 (^{11}C), nitrogen-13 (^{13}N), copper-64 (^{64}Cu) and oxygen-15 (^{15}O), which have physical half-lives ($T_{1/2}$) of 109.8 min, 20.4 min, 97 min, 12.7 h and 2.0 min, respectively. These radionucleotides are cyclotron-produced, and therefore the tracers are normally produced on-site. Generator-produced radionuclides such as gallium-68 (^{68}Ga; $T_{1/2}$ = 67.8 min) and rubidium-82 (^{82}Rb; $T_{1/2}$ = 1.25 min) are becoming available also in clinical settings. An important advantage of PET over SPECT is that positron-emitting isotopes can usually be substituted for naturally occurring atoms in the probe compound and are therefore disturb probe function to a lesser extent.

The pharmacological characters of a PET tracer need to be validated in order to calculate the distributions in the body and quantify the biological processes. These are primarily performed by *in vivo* and *ex vivo* methods using experimental animal models. The radioactivity in the tissue samples is measured using gamma counting or digital autoradiography methods, and the results can be used to estimate the feasibility of a new tracer and to calculate the effective radiation dose for the patient.

Challenges in nuclear imaging

In the case of plaque imaging, there are also certain limitations in nuclear techniques that make plaque imaging challenging. First of all, the plaques are very small targets to be detected. The modern cameras in clinical use have a spatial resolution of 4 mm, which does not allow plaque imaging without certain technical processes and good target-to-background ratio of the tracer. Correction of the partial volume effect and new reconstruction methods for resolution recovery can alleviate the problem (Soret *et al.* 2007). The animal PET cameras have the highest spatial resolution, up to 1.2 mm. However, the range of the emitted positron (the distance from the site of positron emission to the site of annihilation) can degrade the ideal resolution, and this eventually results in a small but unavoidable limit to the spatial resolution. Positron range is radionuclide-dependent, e.g. ^{18}F has lower energy than ^{11}C or ^{15}O, which results in more blurry images with ^{11}C or ^{15}O than with ^{18}F.

Another challenge for the imaging of coronary plaques is the continuous motion of the target. The temporal resolution of the scanners does not allow fast snapshot imaging of plaques, but gating techniques during image acquisition can be used to minimise the effect of cardiac motion. Electrocardiogram (ECG) gating is routinely used in cardiac studies, and techniques for respiratory gating are available for PET imaging. The motion of coronary vessels is a combination of cardiac contraction and respiratory motion, and to eliminate motion-induced image blurring, both gating techniques need to be applied simultaneously. The recent progress in dual gating has enabled the imaging of small moving objects such as coronary plaques. Dual gating can improve the signal by at least a factor of two without losing too much sensitivity (Martinez-Möller *et al.* 2007, Kokki *et al.* 2007, Alexanderson *et al.* 2008, Wykrzykowska *et al.* 2009). Whether the signal coming from a plaque is strong enough to be detected in clinical situations still needs to be confirmed. Moreover, success will also depend upon the availability of tracers with adequate target-to-background ratios (Park *et al*. 2008).

Exposure to ionising radiation is a limitation and, especially in high resolution PET-CT imaging, the doses can reach undesired levels. Therefore, the screening of healthy individuals is probably not feasible, but PET-CT imaging of selected patient populations is anticipated to guide therapy in the future.

2.4 Targets for nuclear imaging of atherosclerosis

General requirements for a tracer are affinity and specificity, a strong detectable signal with high contrast to background, and adequate physical, chemical and biological properties (Choudhury and Fisher 2009). High specificity can be obtained with antibodies or antibody fragments, but potential immunogenicity, molecular size and demanding production are limitations. Peptides and oligosaccharides are also potential high affinity ligands. Contrast can be further improved by using multiple ligands or nanoparticles with many signalling molecules, but contrast in high sensitivity nuclear imaging is mainly achieved by improving the specificity of the tracer. It is also

important to know the biokinetics of the tracer in order to quantify the target, and to make the method reproducible and predictable.

The potential targets for molecular imaging in the plaque are the cells and molecular processes involved in the process of making the plaque more vulnerable. The approach can be indirect, such as an increased metabolism of activated macrophages as a marker of active inflammatory process in the plaque, or direct, such as expression of a specific enzyme involved in the degradation of the fibrous cap. Several attempts have been made to image atherosclerosis, with the most work being done using ^{18}F-FDG (Table 3). However, imaging of a very small moving structure, in which the biological processes are partly unknown, is a great challenge, and so far no consensus or major breakthroughs have been seen.

2.4.1 Imaging of inflammation

Inflammation in the plaque is thought to be the key element creating vulnerability in plaque. Activated macrophages in the fibrous cap or shoulder regions are found as markers of vulnerable inflamed plaque. The tracers are typically targeted toward the higher metabolic activity of the macrophages, but macrophage-selective markers have also been developed.

^{18}F-FDG

The most widely used tracer for targeting the metabolic activity of inflammatory cells is 2-^{18}F-fluoro-2-deoxy-D-glucose (^{18}F-FDG). ^{18}F-FDG is a glucose analogue with a positron-emitting fluoride on the second hydroxyl position. The tracer behaves like glucose in distribution and transportation into the cells. Glucose and ^{18}F-FDG are phosphorylated in the cells by hexokinases (glucokinase in the liver), but unlike glucose, ^{18}F-FDG cannot proceed in the glycolysis pathway and remains trapped inside the cells. The uptake of ^{18}F-FDG is increased in all cells with high glucose metabolism, e.g. in cancer cells and activated leukocytes (Deichen *et al.* 2003). ^{18}F-FDG PET is a well established and widely used method in cancer detection, in the staging and assessment of response to treatment, which also makes ^{18}F-FDG the most widely used PET tracer in the world. The uptake of ^{18}F-FDG in macrophages has been demonstrated by microautoradiography (Kubota *et al.* 1994) and is thought to be increased due to the high metabolic rate and upregulated expression of the glucose transporter-1 (GLUT-1) in macrophages.

The first prospective study on imaging human carotid plaques demonstrating increased ^{18}F-FDG uptake was performed by Rudd and co-workers in 2002 (Rudd *et al.* 2002) and has been confirmed by others (Wu *et al.* 2007). Increased uptake of ^{18}F-FDG has been found in large arteries, when studying retrospectively ^{18}F-FDG scans of elderly cancer patients (Tatsumi *et al.* 2003, Paulmier *et al.* 2008). Later, correlation of ^{18}F-FDG uptake and macrophage content of the plaque has been shown in experimental animals (Zhang *et al.* 2006), in humans *in vitro* with ^{3}H-DG (Rudd *et al.* 2002),

Table 3: Recent achievements in nuclear imaging targets and tracers for atherosclerosis research.

Target	*Tracer*	*Tested in (ref)*
Inflammation		
Metabolic activity / glucose	^{18}F-FDG	Mouse (Laurberg 2007, Matter 2006) Rabbit (Zhang 2006) Human carotid plaques (Rudd 2002, Tawakol 2006, Rudd 2007) Human carotid, iliac, and femoral (Rudd 2008) Human carotid as response to treatment (Tahara 2006, Lee 2008) Human coronary (Alexanderson 2008, Wykrzykowska 2009)
Metabolic activity / choline consumption	^{18}F-FCH ^{11}C-choline	Mouse ex vivo (Matter 2006) Human (Bucerius 2008) Human (Kato 2009)
Monocyte trafficking	^{111}In-oxine	Mouse (Kircher 2008)
Monocyte chemoattractant protein-1	^{99m}Tc-MCP-1	Rabbit (Hartung 2007)
Vascular cell adhesion molecule-1	^{99m}Tc- VCAM-1 peptide, ^{18}F-4V VCAM-1 peptide	Rabbit (Broisat 2007) Mouse (Nahrendorf 2008 b)
Interleukin-2 receptor	^{99m}Tc-Interleukin-2	Human carotid plaques in response to treatment (Annovazzi 2006)
Phagocytosis by macrophages	^{64}Cu-TNP	Mouse (Nahrendorf 2008a)
Lectinlike oxidised LDLR	^{99m}Tc-LOX-1-mAb	Rabbit (Ishino 2008)
PBR receptor on macrophages	^{11}C-PK11195	Human carotid plaques (Hoppela 2007)
Enzyme targeting		
Matrix metalloproteinases	^{123}I-HO-CGS 27023A	Mouse carotid injury model (Schäfers 2004)
Matrix metalloproteinases	^{99m}Tc-RP-805	Rabbit abdominal aorta injury model (Fujimoto 2008)
Matrix metalloproteinases	^{111}In–RP782	Mouse carotid injury model (Zhang 2008)
Apoptosis		
Phosphatidylserine	^{99m}Tc-Annexin A5	Mouse (Isobe 2006) Rabbit, in response to treatment (Sarai 2007)
Caspase-3	^{18}F-Isatin	Mouse myocardial infarction (Hermann 2007)
Angiogenesis		
$\alpha_v\beta_3$ Integrin	^{99m}Tc-labelled peptide ^{18}F-galacto-RGD ^{68}Ga-DOTA-RGD	Mouse hind limb ischemia model (Hua 2005) Rat myocardial ischemia model (Higuchi 2008) Mouse (Haukkala 2009)
Thrombogenic factors		
Collagen	^{124}I-GPVI	Mouse in vivo and human in vitro samples (Schulz 2008)
Platelet aggregation	^{18}F-AppCHFppA	Rabbit (Elmaleh 2006)
Tenascin-C, Fibronectin	^{124}I-antibodies	Mouse ex vivo (von Lukowicz 2007)

and *in vivo* (Graebe *et al.* 2009). Also correlation to development of arterial thrombosis has been shown (Aziz *et al.* 2008). Reports of response to treatment have been published recently; uptake attenuation in response to statin therapy (Tahara *et al.* 2006), antioxidant therapy (Ogawa *et al.* 2006), diet intervention (in rabbits) (Worthley *et al.* 2009) and life-style change (Lee *et al.* 2008). However, some controversial findings have been reported in one study using the ApoE$^{-/-}$ mouse model of atherosclerosis with no plaque uptake (Laurberg *et al.* 2007). The predictive value of ^{18}F-FDG is under investigations. In one retrospective study of cancer patients, vascular ^{18}F-FDG was found to predict risk for future cardiovascular events, whereas calcium index related to old cardiovascular events (Paulmier *et al.* 2008). The reproducibility of carotid artery ^{18}F-FDG imaging has been also found to be good (Rudd *et al.* 2007, Rudd *et al.* 2008). These findings together demonstrate that ^{18}F-FDG PET imaging has the potential to study the plaque inflammatory process and to monitor the disease progression and response to treatment.

However, it must be noticed that the most of the studies were performed in large non-moving vessels. Imaging of coronary vessels with ^{18}F-FDG has been demonstrated (Dunphy *et al.* 2005, Alexanderson *et al.* 2008, Wykrzykowska *et al.* 2009) but histological evidence has not yet been proven. The ^{18}F-FDG imaging of coronary arteries is problematic not only because of the movement, but also due to the high uptake of the tracer into the myocardium and the dependence on metabolic condition. This can be alleviated with proper standardisation of the imaging procedure and by diet pre-treatment (Williams and Kolodny 2008).

Choline

Increased metabolic activity can also be imaged by using radiolabelled choline and choline derivatives. Choline uptake has been shown to correlate with the proliferative activity of cells (Yoshimoto *et al.* 2004), and therefore radiolabelled choline is used in the imaging of various cancers. Macrophages have also been shown to have increased ^{18}F-fluoromethylcholine (^{18}F-FCH) uptake, as shown in an experimental soft-tissue infection model (Wyss *et al.* 2004). A study by Matter *et al.,* using an ApoE$^{-/-}$ mouse model of atherosclerosis, showed marked uptake of ^{18}F-FCH in plaques with a correlation to the macrophage content (Matter *et al.* 2006). Two retrospective studies of elderly cancer patients showed uptake of ^{18}F-FCH (Bucerius *et al.* 2008) and methyl-^{11}C-choline (^{11}C-choline) (Kato *et al.* 2009) in large arteries. In both studies, the tracers were able to visualise the vessel wall in the aorta and carotid arteries, but no further analysis on the histology of the plaques, nor correlation to cardiovascular risk factors were reported. Proliferation itself may not be the reason for the increased uptake of choline in the plaques, since the overall proliferative activity has been found to be very low in human carotid plaque samples (Rekhter *et al*. 1995). The uptake is most likely based on increased choline transport in activated leukocytes.

Monocyte recruitment

The use of radiolabelled leukocytes is the golden standard in infection imaging in nuclear medicine. Autologous granulocytes are labelled irreversibly with long half-life tracer indium-111-oxine (^{111}In-oxine), injected into the patient and inflammatory loci are imaged after several hours or one day. Monocyte recruitment has been visualised also in a mouse model of atherosclerosis *in vivo* (Swirski *et al*. 2006, Kircher *et al*. 2008). Labelled monocytes were detected in the plaques of ApoE$^{-/-}$ mice up to 7 days after administration. Pre-treatment with statins markedly lowered the uptake, as shown in both *in vivo* and *ex vivo* methods, indicating that this method can be effectively used in experimental drug and treatment response settings.

The MCP-1 is a potent chemokine that stimulates monocyte migration into the intima. MCP-1 is expressed in endothelial cells and infiltrating macrophages in atherosclerotic lesions (Ylä-Herttuala *et al.* 1991). Iodine-125 (^{125}I) labelled MCP-1 has been shown to accumulate at the site of vascular injury in mice (Ohtsuki *et al.* 2001). MCP-1 is absent in healthy vessels, and its presence correlates with progression of coronary artery disease. Uptake of technetium-99m (^{99m}Tc) labelled MCP-1 has been shown to correlate with macrophage content in the rabbit atherosclerosis vascular injury model (Hartung *et al.* 2007).

The VCAM-1 is another commonly expressed pro-inflammatory moderator of monocyte recruitment. Iodine-123 (^{123}I) and 99mTc-labeled VCAM-1 specific peptides showed marked uptake in plaques in a rabbit model (Broisat *et al*. 2007). Also, a PET tracer ^{18}F-4V peptide targeting VCAM-1 (Nahrendorf *et al.* 2008b) has been introduced, but further studies are needed to demonstrate the potential for detection of vulnerable plaques.

Interleukin-2 (IL-2) is a cytokine that acts by binding to its receptor (IL2R), expressed mainly on activated T-cells and macrophages. Scintigraphy with ^{123}I- or ^{99m}Tc-labelled IL-2 has been used to image chronic inflammatory disorders and atherosclerosis. Target-to-background ratio of ^{99m}Tc-IL-2 correlated with the percentage of IL-2R-positive cells in histology, and was decreased in atorvastatin-treated patients, suggesting potential for atherosclerosis imaging (Annovazzi *et al.* 2006).

Macrophages

Activated macrophages and foam cells phagocytose oxidised LDL and other particles in the plaques. This can be utilized in imaging using labelled LDL particles or nanoparticles. ^{64}Cu-labelled nanoparticle (^{64}Cu-TNP) accumulated in the plaques of atherosclerotic mice, and the target-to-background ratio was approximately 5 in the aortic root as detected by PET (Nahrendorf *et al.* 2008a). The potential limitation of this tracer is that it also accumulated in the myocardium and the liver. Autologous radiolabelled LDL particles (^{99m}Tc-ox-LDL and ^{125}I-LDL) have been shown to accumulate in human carotid arteries *in vivo* (Virgolini *et al.* 1991, Iuliano *et al.* 2000), but slow blood clearance may limit the use of this technique. Recently, the research has been focused on epitopes and receptors for lipoproteins. LOX-1 is a cell surface

receptor for oxidised LDL, and is expressed in macrophages and endothelial cells in atherosclerotic lesions. A recent report on using ^{99m}Tc-LOX-1-mAb showed a 10-fold higher uptake in atherosclerotic than in control aorta in a rabbit model (Ishino *et al.* 2008). The tracer uptake correlated with the plaque vulnerability index, although the accumulation did not correlate with macrophage density. It is likely that since LOX-1 is expressed during the early stage of atherosclerosis, it might not be useful in distinguishing later stage plaques.

Activated macrophages express peripheral benzodiatsepine receptors (PBR). PET tracer ^{11}C-PK11195 binds to PBR and has been used in humans for assessing microglia activation in various neurogenerative disorders. N-Methyl-^{11}C-(R)-1-(2-chlorophenyl)-N-(1-methylpropyl)-3-isoquinoline carboxamide (^{11}C-PK11195) has been shown to accumulate in macrophages in an experimental lung infection model (Jones *et al.* 2002). ^{11}C-PK11195 has been suggested as a potential imaging agent for detecting inflammation associated with atherosclerosis. A pilot study showed that although the tracer binds to carotid plaques in humans, significant background binding in the nearby tissues limits the use (Hoppela *et al.* 2007).

2.4.2 Imaging of matrix degradation

Matrix metalloproteinases, especially MMP-9, have been associated with plaque progression and destabilisation of the fibrous cap, making them promising targets for detection of plaque vulnerability. Schäfers and co-workers (Schäfers *et al.* 2004) demonstrated marked uptake in injured atherosclerotic vessels using a labelled MMP inhibitor. Also, in a very recent study, the uptake of another MMP inhibitor, ^{99m}Tc-RP-805, was shown to correlate with MMP expression, and could be modulated by dietary modification and statin treatment (Fujimoto *et al.* 2008). A novel tracer, ^{111}In–RP782, has specificity for activated MMPs and also showed increased uptake in a mouse model (Zhang *et al.* 2008). In all of these studies, an injured artery model was used, raising the question of the validity of the method in human atherosclerosis. Therefore, studies in animal models with spontaneous atheromas are warranted.

2.4.3 Imaging of apoptosis

Apoptosis of macrophages and SMCs is also considered an indicator of plaque development, as well as vulnerability. The research has mainly focused on using ^{99m}Tc labelled Annexin A5 to detect phosphatidylserine on apoptotic cells. Atherosclerotic lesions in human carotid, swine, and rabbit and mouse models have been shown to take up annexin tracers and correlate to macrophage content and apoptosis (Kietselaer *et al.* 2004, Kolodgie *et al.* 2003b, Isobe *et al.* 2006). Annexin uptake has also been shown to decrease in response to treatment with caspase inhibitors in a rabbit model of atherosclerosis (Sarai *et al.* 2007) and in response to diet and statin therapy (Hartung *et al.* 2005). However, there is some debate on the specificity of the tracer. This has led to the development of other tracers targeting apoptosis. Caspase-3 activation is a downstream process and a specific marker for apoptosis. Caspase-3 binding isatins

have been developed and ^{18}F-isatin has been reported to have a high specificity in myocardial ischemia induced apoptosis (Hermann *et al.* 2008, Podichetty *et al.* 2009), but its feasibility in plaque imaging has not yet been determined.

2.4.4 Imaging of angiogenesis

Intraplaque angiogenesis results in fragile structure of the neovasculature that may lead to intraplaque haemorrhage and plaque rupture. Angiogenesis imaging has focused on the alpha-v-beta-3 ($\alpha_v\beta_3$) integrin, a transmembrane glycoprotein which mediates cell/cell and cell/ matrix interaction. Natural ligands of $\alpha_v\beta_3$ bind to this integrin via a RGD (arginine (R), glycine (G), aspartate (D)) motif. RGD-containing peptides and radiolabelled derivatives, such as ^{18}F-galacto-RGD, have been shown to target and successfully detect angiogenesis in tumour and ischemia models, and also in cancer patients (Haubner *et al.* 2005, Higuchi *et al.* 2008, Beer *et al.* 2005). $\alpha_v\beta_3$-integrin-binding tracers co-localise with macrophages in human carotid artery plaque endartrectomy samples, as shown with an optical imaging agent Cy5.5-labelled RGD (Waldeck *et al*. 2008). Recently, a MRI nanoparticle approach (Burtea *et al.* 2008) for $\alpha_v\beta_3$ integrin targeting, and a radiolabelled peptide for SPECT imaging (Hua *et al.* 2005) have been shown to detect plaques.

2.4.5 Imaging of thrombogenic factors

Exposure of extracellular matrix to vascular lumen is a prerequisite for thrombus formation and, therefore, imaging of platelets and components of ECM may have great potential for plaque imaging. Collagen-targeted ^{124}I labelled glycoprotein VI (GPVI) antibody showed increased uptake to aortic plaques in mice, and the target was also visualized in human artery samples *in vitro* (Schulz *et al.* 2008). Platelet imaging has earlier been performed with labelled platelets or platelet or fibrin-specific antibodies (Cerqueira *et al.* 1992). Recently, Elmaleh *et al* found that a competitive inhibitor of adenosine diphosphate (ADP) in platelet aggregation, the ^{18}F-labelled derivative of diadenosine oligophosphate (^{18}F-AppCHFppA), demonstrated rapid accumulation into the atherosclerotic abdominal aorta with a reasonably good target-to-background ratio. The uptake measured by PET correlated with plaque macrophage density in a rabbit model (Elmaleh *et al.* 2006). Also ^{125}I-labeled antibodies against an ECM protein tenascin-C, and fibronectin were found to accumulate in macrophage-rich sites in plaques in an experimental mouse study (von Lukowicz *et al.* 2007).

2.5 Future aspects

Molecular imaging is a key method in newly released guidelines released by The Society for Heart Attack Prevention and Eradication (SHAPE) for the assessment of risk of atherosclerotic disease. Molecular imaging of biological processes such as plaque inflammation can be expected to provide additional and probably decisive information for guiding therapy. Currently, the most widely studied tracer for plaque inflammation is ^{18}F-FDG, but although it has been proved to be feasible and

reproducible in carotid arteries (Rudd *et al.* 2007, Rudd *et al.* 2008), cardiac data are currently limited. However, these preliminary findings with the recent development in scanner and gating techniques give reason to expect that imaging inflammation in human coronary plaques may be clinically feasible in the near future.

Although the natural aim is to develop tracers for specific targets, it must be realised that it is likely that the more specific the process becomes, the weaker the detected signal will be. Thus, theoretically, tracers with multiple uptake mechanisms linked to plaque vulnerability may have an advantage. ^{18}F-FDG can be regarded as such a non-specific but practical tracer. In the light of recent findings of multiple ruptures of the plaques, imaging and prevention of thrombosis and thrombogenic factors warrant further studies. Many of the current imaging targets are such that occur during many phases of the progression of the plaque, and may therefore have potential in estimating the atherosclerotic burden, but may not be ideal in predicting future cardiac events in the short term. Therefore, response to therapy, histological evidence, or preferably both need to be shown in feasibility studies. The predictive value of a tracer is hard to determine in any model. With improving animal models, these new tracers and concepts can be studied before entering into clinical studies. Prevention trials and prospective follow-up studies in patients are needed to study the prognostic value of the method.

Imaging has high, but fairly unused potential in increasing our understanding of the progression of atherosclerosis. So far there have been a limited number of longitudinal imaging studies either in humans or experimental animals, focusing on following the atherosclerotic plaque formation and characterisation. Longitudinal studies are needed to understand the value of these imaging methods in various clinical situations. Further, it is necessary to understand better the implication of plaque characterisation in non-cardiac arteries in prediction of cardiac events. The predictive value of imaging is not only in the interest of clinicians, but it is also a priority in the pharmaceutical industry. The ongoing consortium study, the HRP Initiative BioImage study, led by academic institutions and pharmaceutical companies in US, is a good example of this importance. This large prospective, observational trial with 6800 volunteers aims to determine whether ultrasound of carotid arteries, CT, PET-CT or MRI, could be used to identify the individuals with a higher risk to develop a future heart attack or stroke. The first results of this study are expected in year 2012.

Instead of the characterisation of vulnerable plaques, perhaps it would be more beneficial to characterise the vulnerable patient since it is likely that none of the biomarkers or imaging techniques can solve this clinical problem alone. Together with possessing a vulnerable plaque, so-called vulnerable blood, characterised by high LDL cholesterol, coagulation factors and biomarkers, added to traditional risk factors would give a better probability to stage the disease and to select the subjects at intermediate to high risk of cardiovascular events (Naghavi *et al.* 2003, Naghavi *et al.* 2006) and to guide therapy.

3 OBJECTIVES OF THE STUDY

The purpose of the study was to evaluate the inflammation-targeting tracers ^{18}F-FDG, ^{11}C-PK11195, ^{18}F-galacto-RGD and ^{11}C-choline for imaging of vascular inflammation associated with atherosclerosis. Specific aims were

1. to evaluate the feasibility of the methods and the LDLR$^{-/-}$ ApoB$^{100/100}$ mouse model to be used in validation studies for atherosclerosis imaging

2. to investigate the relationship between tracer uptake and the plaque morphology, histology and immunohistology

3. to study the non-specific tracer uptake in the surrounding tissues for evaluation of feasibility of tracers in atherosclerosis imaging

4 METHODS AND EXPERIMENTAL ANIMALS

4.1 Radiotracers and metabolite analysis

4.1.1 Production of radiotracers

Radionuclides in studies I, II and IV were produced at the Accelerator Laboratory of the Åbo Akademi University, and the radiotracers were synthesised at the Radiopharmaceutical Laboratory of Turku PET Centre. In study III, ^{18}F-galacto-RDG was produced at the Laboratory of Radiochemistry, Department of Nuclear Medicine, Technical University of Munich. The molecular structures of the used positron emitting tracers are shown in Figure 2. The ^{18}F labelled tracers have $T_{1/2}$ of 110 min, and the ^{11}C labelled $T_{1/2}$ = 20 min.

^{18}F-FDG

^{18}F-FDG was synthesised according to the method described by Hamacher (Hamacher *et al.* 1986) with an automatic apparatus. The specific radioactivity at the end of synthesis was >76 MBq/nmol, and the radiochemical purity exceeded 98%.

^{18}F-fluoride

^{18}F-fluoride was produced by irradiating oxygen-18 (^{18}O) enriched water with a proton beam from the isochronous cyclotron (MGC-20) at the Turku PET Centre Accelerator Laboratory. Radiochemical and radionuclidic purity of the product exceeded 98%.

^{11}C-PK11195

The ^{11}C-PK11195 was prepared as described by Debruyne (Debryne *et al.* 2003) with slight modifications. Measurement of concentration and radiochemical purity of ^{11}C-PK11195 batches was performed by high-performance liquid chromatography (HPLC), showing purity higher than 99.5%.

^{18}F-galactol-RGD

^{18}F-galacto-(cyclo(Arg-Gly-Asp-DPhe-Val-) (^{18}F-galacto-RDG) was synthesised as described by Haubner and colleagues (2004) via nucleophilic substitution reaction of 4-nitrophenyl-2-^{18}F-fluoropropionate with cyclo(Arg-Gly-Asp-DPhe-Lys(SAA)-). The reaction product had radiochemical purity >98% and specific radioactivity of 40 MBq/nmol.

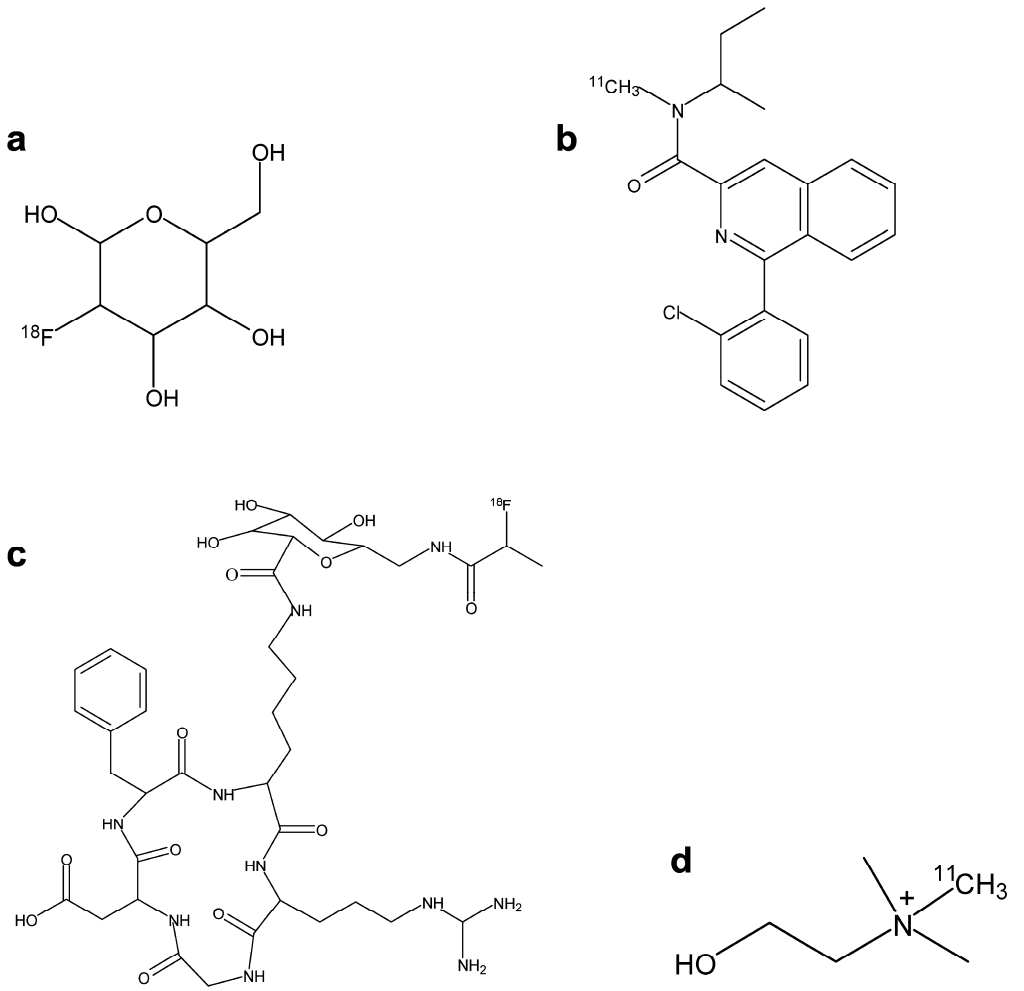

Figure 2: Molecular structure of the tracers. a: ^{18}F-FDG, b: ^{11}C-PK11195 c: ^{18}F-galacto-RGD d: ^{11}C-choline.

^{11}C-choline

^{11}C-Carbon dioxide produced by the ^{14}N(p,α)^{11}C reaction was converted to ^{11}C-methyl triflate using standard procedures (Någren and Halldin 1998). ^{11}C-Choline was produced in a reaction of ^{11}C-methyl triflate and N,N-dimethyl-2-aminoethanol using HPLC purification and analysis procedures slightly modified from a method described by Rosen *et al* (1985), with high radiochemical yield (>70%) and radiochemical purity (>99.5%). Specific radioactivity of other ^{11}C compounds in general prepared from ^{11}C-carbon dioxide and ^{11}C-methyl triflate in the Radiopharmaceutical Laboratory of the University of Turku was higher than 40 MBq/nmol, but was not specifically measured for ^{11}C-choline due to the low ultraviolet (UV) absorbance of choline.

4.1.2. Other used radiotracers

Tritium (hydrogen-3, ^{3}H) labelled PK11195 (3.145 MBq/nmol) and 2-Deoxy-D-1-^{3}H-glucose (^{3}H-DG) were kindly provided by GE Healthcare Amersham, United Kingdom. Tritium has half-life of 12.3 years and is a beta-emitter.

4.1.3. Radiometabolite analysis

Plasma radiometabolites were analysed in study IV. Blood samples (0.5-1 ml) were obtained with cardiac puncture (2 LDLR$^{-/-}$ ApoB$^{100/100}$ mice, 4 control mice) at 10 min after intravenous injection. The blood was collected into an ice-cold heparinised tube. The plasma was separated by centrifugation (2118 x g for 5 min) at +4 °C. Proteins of plasma were precipitated with acetonitrile, and supernatant, obtained after centrifugation and followed by filtration through a syringe filter (0.45 µm, Waters Corporation, USA), was analyzed by radio-HPLC.

Radiometabolite analysis was performed using an earlier described method (Roivainen *et al.* 2000). The radioactive compounds in samples were identified by comparing the retention times of authentic standards^{11}C-choline and ^{11}C-betaine. The ^{11}C-betaine was prepared *in vitro* from ^{11}C-choline by using *choline oxidase* (0.05 U/µl in ultra pure water, EC 1.1.3.17, Sigma-Aldrich).

4.2 Experimental animals

The LDLR$^{-/-}$ ApoB$^{100/100}$ mouse (strain #003000, Jackson Laboratory, Bar Harbor, ME) was used as the atherosclerotic and hypercholesterolemic animal model. These mice are deficient for both LDL receptor and ApoB48, expressing only the ApoB100 form (Veniant *et al.* 1998). The mice were kept on a Western-type diet (Teklad Adjusted Calories, consisting of 21% fat and 0.15% cholesterol without sodium cholate) for varying periods (Table 4). In studies II-IV only male mice were used, while in study I, some female mice were also used.

The LDLR$^{-/-}$ ApoB$^{100/100}$ strain is cross-bred to C57Bl background and, therefore, C57Bl mice were used as the control. C57Bl mice do not develop atherosclerosis under normal chow. The control mice were used at different ages (Table 4). The C57Bl mice used in studies I and IV had been used earlier for breeding. The C57Bl mice in studies II and III were housed only for these studies.

All mice were housed under standard conditions with lights on from 6.00 a.m. to 6.00 p.m. Food and water were provided *ad libitum*. The mice were bred in the University of Kuopio and transferred to Turku or Munich before the experiments.

Ethical considerations

The study plan was approved by the Laboratory Animal Care and Use Committee of the University of Turku, Finland (I-IV), the Laboratory Animal Care and Use Committee of the University of Kuopio, Finland (I-IV), and the regional governmental

commission of animal protection of Bavaria (Regierung von Oberbayern, München, Germany) (III).

Table 4: Animal characteristics.

Study	n males (+females)	Age (months)	Chow + Western (months) **	Weight (g)
Atherosclerotic				
I a *	7 + 4	14 ± 1	2-5+ **5-8** + 2	35 ± 8
I b *	2 + 1			
II	5	13 ± 1	10+ **3**	39 ± 8
III	12	14 ± 1	7-10+ **3-7**	40 ± 6
IV	6	17 ± 0	15 + **2**	38 ± 3
Control				
I a	9	7 ± 1	-	42 ± 4
I b	1			
II	3	9	-	28 ± 4
III	11	6 ± 2	-	30 ± 3
IV	5	13 ± 2	-	42 ± 6

* Study I a: ^{18}F-FDG Ib: ^{18}F-fluoride. **Feeding time is represented as number of months on normal chow + Western-type diet (in bold) + normal chow.

4.3 Biodistribution studies

The general study design of the biodistribution and autoradiography studies of tissue samples is presented in simplified form in Figure 3. The accumulation of intravenously (i.v.) injected tracers was measured *in vivo* (in study III) and *ex vivo* in tissue samples. There were some modifications to the protocols in each study, and the main methodological differences are presented in Table 5.

Radiotracers were injected i.v. and allowed to distribute for a specified time before the animals were sacrificed in a carbon-dioxide (CO_2) chamber or by cervical dislocation. Arterial blood was collected by cardiac puncture, tissue samples were dissected and weighed, and radioactivity was measured in a well counter (NaI(Tl) 3 × 3 inch, Bicron 3MW3/3P, Bicron, Newbury, OH, USA) or a gamma counter (1480 Wizard 3" gamma counter EG&G Wallac, Turku, Finland). All data were corrected for background radioactivity and radioactive decay and the dose remaining in the tail was also compensated for. The amount of radioactivity that had accumulated in the tissue samples or blood over the distribution period was expressed as a percentage of the injected dose per gram of tissue (%ID/g).

In the dual tracer study (III) the mice were co-injected with a short-lived PET tracer and a tritionated, long half-life, low energy tracer; the accumulation of the latter was measured from tissue sections after the primary tracer had decayed.

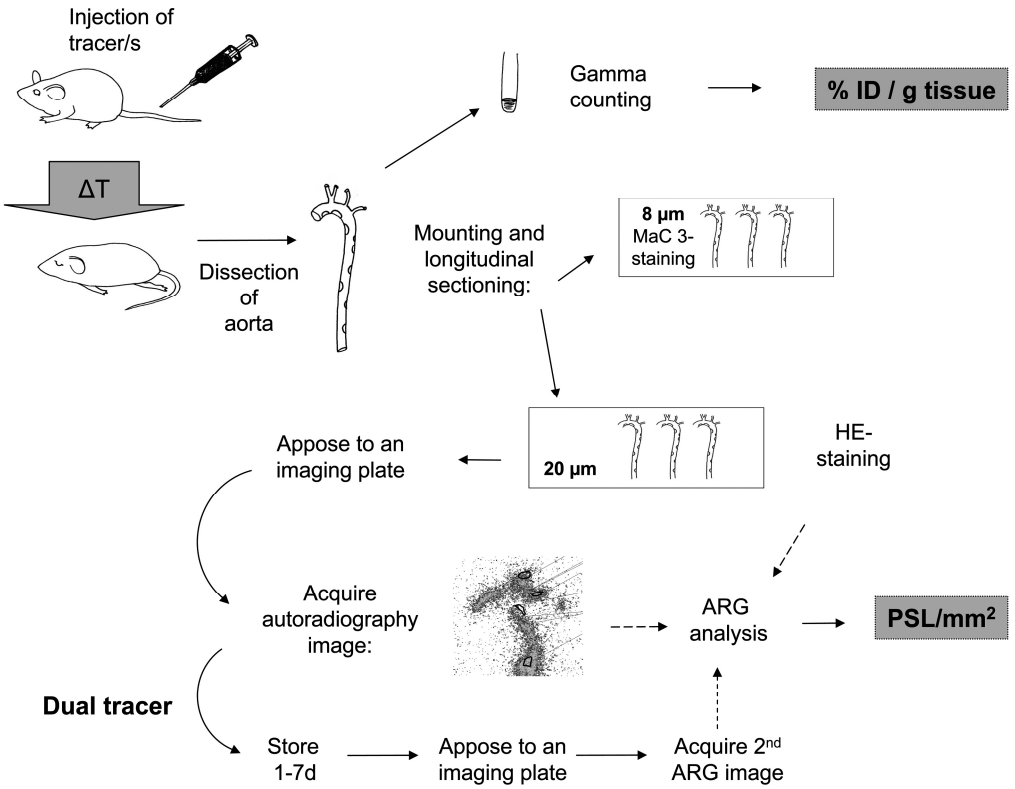

Figure 3 General study design in studies I- IV.

Table 5: Comparison of methods in studies I-IV.

Study	Tracer	Dose (MBq)	Injection	ΔT (min)	Euthanasia	Gamma-detector	IP	IP (2nd)	IP-reader
I a	^{18}F-FDG	17 ± 6				Well-counter	TR	TR	BAS5000
I b	18F	22 ± 3	awake	60	CO_2				
II	^{11}C-PK11195	23 ± 12	awake	20	CO_2	Well-counter	TR		BAS5000
III	^{18}F-galacto-RGD	28 ± 8	isoflurane anaest.	120	CO_2	Wizard	MS	TR	FLA2000
IV	^{11}C-Choline	27 ± 10	awake	10	cervical dislocation	Wizard	TR		BAS5000

IP: Imaging plate, TR: Fuji Imaging Plate BAS-TR2025, MS: Fuji Imaging Plate BAS-MS2040

4.4 Autoradiography of aortic sections

The distribution of tracers to aortic tissue was studied with digital autoradiography of $LDLR^{-/-}$ $ApoB^{100/100}$ and control mice. The aorta was dissected and blood was removed with saline rinsing. The surrounding adventitial connective tissue and fat were removed in study I, whereas in the other studies it was left attached. The aortas were frozen in mounting media (TissueTek OCT Compound, Sakura Finetek, USA) for sectioning with cryomicrotome. Sequential longitudinal 20 μm (for autoradiography) and 8 μm (for immunohistochemisty) mouse aorta sections were cut at –15°C, thaw-mounted onto microscope slides and briefly air-dried. The 20 μm sections were apposed to an imaging plate (I, II, IV: Fuji Imaging Plate BAS-TR2025, III: Fuji Imaging Plate BAS-MS2040, Fuji Photo Film Co., Ltd., Japan). After a pre-specified exposure time of at least two half-lives of the tracer, the imaging plates were scanned with the Fuji Analyser BAS-5000 (Fuji Tokyo, Japan; internal resolution of 25 μm) or in III: Fuji Analyser FLA-2000 (Fuji Tokyo, Japan; internal resolution of 50 μm). The images were analysed for count densities (photo-stimulated luminescence per unit area, PSL/mm^2) with an image analysis programme (Tina 2.1, Raytest Isotopenmessgeräte, GmbH, Straubenhardt, Germany). The background area count densities were subtracted from the image data. In study I, the results were counted as ratios against the control region (healthy wall in study I and muscle in study III). In study III, the data were also corrected for injected dose and decay. The coefficient of variation of repeated analyses was 4.5% (n=6 mice).

Regions of interest (ROIs)

After careful co-registration of autoradiography and haematoxylin-eosin (HE) stained histological images, regions of interest (ROIs) were defined according to morphology. The mean values for intensities (PSL/mm^2 values) for each ROI type were calculated.

In all studies, ROI categories included plaque and healthy vessel wall. In study I, the ROI was also drawn in the calcified area in the plaque. In studies II and IV, the plaque ROIs were defined as (1) non-inflamed plaques (mostly core areas without cell infiltration or acellular areas in the plaque), and (2) inflamed plaque (cell-rich areas in the plaques containing mostly macrophages). In studies III and IV, adventitia (including the adipose tissue surrounding the vessel) was also one of the ROI categories.

Determination of inflammation in the ROI

The uptake in the plaques was compared with the amount of inflammation in the region in studies II-IV. In study II, the ROIs were defined as non-inflamed plaque (mostly core areas without cell infiltration or acellular areas in the plaque), or inflamed plaque (cell-rich areas in the plaques containing mostly macrophages). In study III, uptake of ^{18}F-galacto-RGD was compared with plaque composition in Movat pentachrome stained sections in 34 randomly selected plaques of 8 mice (Figure 4). Proportions of connective tissue and ground substance, as well as nuclear density were determined

using automated image analysis software (Definiens Architect, Munich, Germany). Count densities were determined in the same plaques by drawing ROIs in the autoradiogram of the same or adjacent section. In study IV, randomly selected plaque ROIs (n=35) were semi-quantitatively assessed for inflammation by number of nuclei and amount of Mac-3 staining in consecutive sections. The ROIs in these plaques were divided into two categories: 1) non-inflamed was defined as having no or only occasional leukocytes in the region of interest, and 2) inflamed, having a high number of nuclei and corresponding Mac-3 positive staining in the area of the concecutive section.

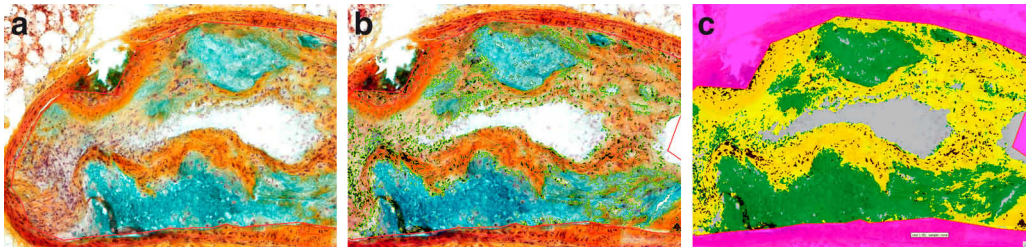

Figure 4: Movat pentachrome staining and analysis. a: Movat staining of a brachiocephalic plaque, b: definition of the analysed area (pink line), c: analysis of the plaque composition: connective tissue (yellow), ground substance (green) and nuclei (black).

Dual tracer study

The uptake of ^{18}F-galacto-RGD was compared to the uptake of ^{3}H-DG in a dual tracer approach. Six LDLR$^{-/-}$ ApoB$^{100/100}$ mice and two controls were injected with both tracers and, after autoradiography measurement of ^{18}F-radioactivity, the sections were stored for one week, exposed again for 14 days (Fuji Imaging Plate BAS-TR2025), and scanned to measure accumulated ^{3}H-radioactivity (Figure 5). The same template of ROIs was used in the ^{18}F- and 3H-autoradiographs to compare the radioactivity in exactly the same regions.

4.5 PET imaging

In study III, the biodistribution of the PET tracer was imaged *in vivo* prior to the biodistribution and autoradiography studies (Figure 5). Four LDLR$^{-/-}$ ApoB$^{100/100}$ mice and five controls were imaged with the Inveon small animal PET-CT scanner (Siemens, Knoxville, TN, USA) 75 minutes after injection of ^{18}F-galacto-RGD. PET images were acquired for 15 minutes, followed by CT angiography without moving the animal. To obtain vascular contrast, 0.2-0.3 ml of iodinated intravascular contrast agent Fenestra VC (ART, Advanced Research Technologies, Saint-Laurent, Canada) was injected. Mice were kept fully sedated with 1.5% isoflurane during injections and imaging.

PET images were reconstructed and data were normalised and corrected for randoms, dead time and decay. No corrections were made for attenuation or scatter. The PET and CT images were fused and analysed using the Inveon Research Workplace software (Siemens, Knoxville, TN, USA). Image registration was done using automatic weighted mutual information algorithm, and confirmed visually on the basis of anatomical landmarks showing physiological accumulation of the tracer, for example the kidneys, skin, liver, thymus, and bone marrow. For measurement of tracer uptake, ROIs were drawn in the bifurcation of the brachiocephalic artery and the right atrium as seen in the CT angiogram. Radioactivities in ROIs were corrected for injected radioactivity to calculate the percentage of injected dose per gram of tissue (%ID/g) by assuming that 1 ml = 1 g, and the ratio of vessel-related activity to blood pool.

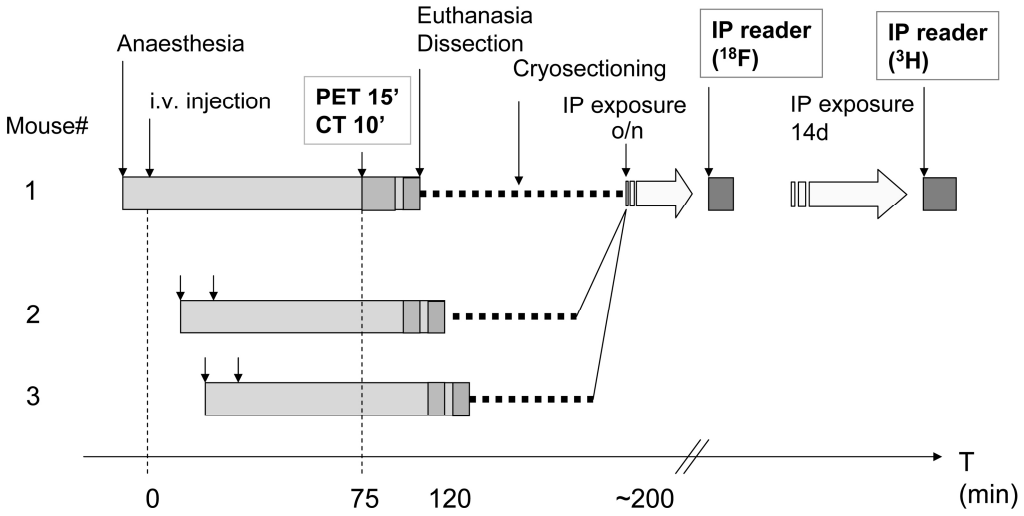

Figure 5: Study protocol in study III

4.6 *In vitro* studies

4.6.1 *In vitro* distribution of ^{18}F-FDG in human artery samples

The *in vitro* distribution of ^{18}F-FDG was studied autoradiographically using frozen sections of human arteries. Samples of heavily calcified human femoral, aortic and carotid arteries from four subjects were obtained from surgical operations and post-mortem. Artery samples were rapidly frozen in isopentane chilled with dry ice. Twenty micrometre thick cross-sections were cut at –15 °C, thaw-mounted onto microscope slides, and stored at –20 °C. The sections (n = 40) were warmed to room temperature (RT), incubated in saline for 20 min at RT and after that with 3.5 MBq of ^{18}F-FDG in 100 ml saline for 15 min at RT, washed twice for 10 s with ice-cold saline, and rinsed

in distilled water. The sections were air-dried and apposed to an imaging plate for 3 h. The imaging plates were scanned and the images were analysed for count densities as described above.

4.6.2 Specific binding

In vitro binding of ^{3}H-PK11195 in aorta sections

Twenty micrometer sections of atherosclerotic mouse aorta were prepared (study I) and stored at -20 °C. Before use the sections were warmed to room temperature (RT) and pre-incubated for 5 min at RT in 50 mM Tris-HCl buffer (pH 7.4). Immediately thereafter, the sections were incubated for 30 min at RT with 1.2 nM ^{3}H-PK11195 (3.145 MBq/nmol, Amersham, SA) in 50 mM Tris-HCl buffer. Non-specific binding was estimated in adjacent sections in the presence of 10 mM unlabelled PK11195 (ABX, Radeberg, Germany). After incubation, the slides were washed twice for 10 s with ice-cold buffer and rinsed in distilled water to remove buffer salts. The sections were air-dried and apposed to an imaging plate (Fuji Imaging Plate BAS-TR2025, Fuji Photo Film Co., Ltd., Japan) for digital autoradiography. The exposure time was seven days. The imaging plates were scanned with the Fuji Analyzer BAS-5000. The digital autoradiographic images were analyzed for count densities as described in section 4.4.

In vitro binding of ^{18}F-galacto-RGD in mouse aorta sections

In vitro binding and displacement studies were performed also for ^{18}F-galacto-RGD. 20 µm sections of atherosclerotic mouse aorta were warmed to RT, preincubated for 5 min at RT in phosphate-buffered saline (PBS), and incubated with 10 nM ^{18}F-galacto-RGD (specific radioactivity range 40-100 MBq/nmol) in PBS on a spot for 30 min at RT. Serial sections were incubated in the presence of 10 mmol of competing unlabelled cyclic RGD pentapeptide (Cilenqitide, Merck KGaA, Darmstadt, Germany). After incubation, the slides were washed twice for 5 min with PBS, rinsed in cold water, air dried, and apposed to an autoradiography imaging plate, exposured overnight and analysed as described in section 4.4.

4.6.3 Biochemical measurements

Plasma glucose level was measured in study I with an Analox GM9 glucose analyser (Analox Instruments, London, UK) using the glucose oxidase method.

4.7 Histology and immunohistochemistry

Histological features of plaques were studied in aortic tissue sections stained after autoradiography in HE or Movat pentachrome (in study III). The degree of inflammation was semi-quantitatively assessed by an experienced pathologist as the number of leukocytes in the tissue. (No leukocytes = non-inflamed aorta; occasional single leukocytes = mild inflammation; occasional leukocytes and some groups of

inflammatory cells = moderate inflammation; abundant infiltration of leukocytes = severe inflammation.)

In study II, consecutive 8 µm sections were immunostained with Mac-3 (antibody for mouse macrophages) and anti-PBR-antibody. Sections stored at -70 °C were melted, air-dried and fixed in ice-cold acetone. Endogenous peroxidase was blocked and the sections were incubated for 1 h with Mac-3 antibody. Control immunostaining was performed with IgG negative control antibody. Biotinylated secondary antibody was incubated for 30 min, followed by incubations with streptavidin-HRP and AEC + substrate chromogen according to the instructions of the manufacturer. Finally, the sections were counterstained with haematoxylin. All antibodies were from BD Pharmingen and all reagents from DakoCytomation, CA, USA.

In study III, macrophages, endothelial cells, B-cells and T-cells were detected by automated immunostaining (Ventana Medical Systems, Tucson, AZ, USA) of 8 µm serial frozen sections using the following primary antibodies: Mac-3 (BD, Heidelberg, Germany), CD31 (AbD Serotec, clone 390), CD3 (Dako, Hamburg, Germany), and B220/CD45R (clone RA3-6B2; BD Pharmingen, Heidelberg, Germany). Biotinylated goat anti-mouse (Dako) or goat anti-rabbit (Vector, Burlingame, Canada) IgG antibodies were used as secondary reagents, linked to a streptavidin-HRP-complex (Jackson Immunoresearch Laboratories, West Grove, PA, USA) and visualised with diaminbenzidin (Sigma-Aldrich, Munich, Germany). The area of Mac-3 positive staining within plaques was visually graded as small, intermediate or large.

In study IV, consecutive 8 µm sections were immunostained with Mac-3 for detection of macrophages and Ki-67 for proliferating cells. Sections stored at -70°C were melted, air-dried and fixed in phosphate-buffered formalin. After exposure to hot 10 mM citrate buffer and blocking with 3% bovine serum albumin, the sections were incubated with either Mac-3 antibody (clone M3/84, BD Pharmingen, working dilution 1:5000) or Ki-67 (clone Mib-1, Dako, Denmark; working dilution 1:2000). After peroxidase blocking, the sections were incubated (for Mac-3 staining, first by rabbit anti-rat (Dako, Denmark) polyclonal IgG antibodies) by EnVision+ System- HRP goat anti-rabbit antibody (Dako, Denmark) and visualised with diaminbenzidin (Dako, Denmark). Finally, the sections were counterstained in haematoxylin.

4.8 Statistical analyses

All results are expressed as the mean ± SD. Normality tests were performed using the Shapiro-Wilkins method. A p-value less than 0.05 was considered statistically significant.

In studies I and II, univariate correlations were calculated using the Spearman correlation method, and in study IV, the Pearson partial correlation method was used. Analysis of variance (ANOVA) was used to study the significance of differences observed in animal characteristics, and in biodistribution between atherosclerotic mice and control groups in studies I and II. In studies III and IV, Dunnett's test was used to

compare biodistribution in organs, and student's t-test for non-paired data was used when comparing the uptake between $LDLR^{-/-}ApoB^{100/100}$ and control mice.

In the autoradiography analysis, in study I, a mixed model with Tukey-Kramer corrected p-values was applied to individual mean values of ROIs. In study II, parametric ANOVA of repeated measures was used in the inter-animal comparison for the mean PSL values of radioactive uptake of the defined ROI. For intra-animal comparisons ANOVA was used. In study III and IV repeated measures ANOVA with Tukey correction was used to compare tracer uptake in the three categories of ROI's. For comparison of uptake of ^{18}F-galacto-RGD, uptake of ^{3}H-DG and histological features (study III) linear regression was calculated with a mixed model (with mouse as a random factor).

5 RESULTS

5.1 Characterisation of the animal model

All LDLR$^{-/-}$ApoB$^{100/100}$ mice had extensive atherosclerotic plaques throughout the aortic tree, especially at vascular branches. The observed plaques were heterogeneous, but predominantly of fibroatheroma type resembling type IV and V lesions (Stary *et al.* 2005). Typically, the lesions were rich in macrophage-derived foam cells, and consisted of a necrotic core, surrounded by proliferation of spindle cells (smooth muscle cells, fibroblasts) and varying amounts of ECM, including collagen and elastin. Calcifications were seen particularly in older mice. The highest prevalence of plaques and calcified plaques was observed in the arch area and the proximal part of brachiocephalic, carotid and subclavian branches. However, none of the plaques was of vulnerable type VI, characterised by surface defects with haemorrhage and thrombus formation. A few example slices of the cusp area were taken and stained with HE, showing extended plaques.

Leukocyte infiltration was observed in plaques in all atherosclerotic mice and, based on the histological and immunohistochemical analysis, the inflammation was estimated to be of moderate degree. In study III, more detailed analysis of the plaque composition was performed. Based on the results of the immunohistochemical analyses, most of the cells in the plaques, approximately 60%, were macrophages. Nuclear density was associated with macrophage number as indicated by higher density in the plaques graded as having large (n = 8) rather than small (n = 11) Mac-3 positive area (2.1 ± 1.2 vs. 1.0 ± 0.3 arbitary units (a.u.), p = 0.01). Only very few T-cells or B-cells were found. In study I, only few examples of Mac-3 staining were available, but based on the histological analysis, the inflammation was estimated to be more moderate than in the other studies.

Immunohistochemical staining with CD31 demonstrated a strong positive signal in the endothelial lining of the aorta. However, neoangiogenesis was almost absent in the plaques. Moreover, cell proliferation seemed to be very low in the plaques, since only very few occasional Ki-67 positive cells in the mouse atherosclerotic plaques were found. PBR-specific antibody stained mainly the same sites as the macrophage antibody, suggesting that macrophages are the main cell type expressing this receptor in the plaques.

5.2 Biodistribution of tracers in tissues

The uptake of ^{18}F-FDG, ^{18}F-fluoride, ^{18}F-galacto-RGD and ^{11}C-choline was significantly higher in the aorta of atherosclerotic mice than in the control mice aorta (Table 6). On the contrary, the uptake of ^{11}C-PK11195 in the whole aorta of atherosclerotic LDLR$^{-/-}$ ApoB$^{100/100}$ mice was significantly lower than in the control mice.

The uptake ^{18}F-FDG was higher in the heart of the atherosclerotic mice. The liver uptake of ^{18}F-galacto-RGD and ^{11}C-choline was higher in LDLR$^{-/-}$ApoB$^{100/100}$ mice as compared to control mice. In the other measured tissues there were no significant differences between the atherosclerotic and the control mice.

The aorta-to-plasma uptake ratio of ^{11}C-PK11195 was 22 ± 7 and the aorta-to-heart 0.6 ± 0.3 in LDLR$^{-/-}$ ApoB$^{100/100}$ mice. The ^{18}F-galacto-RGD %ID/g in the aorta was more than two-fold higher than the residual activity in the blood of the same mice ($p <$ 0.0001). For ^{11}C-choline, the aorta-to-blood and aorta-to-muscle ratios of LDLR$^{-/-}$ ApoB$^{100/100}$ mice were 5.5 ± 2.2 and 3.0 ± 0.9, respectively. ^{18}F-FDG accumulated greatly to the heart, which is probably caused by the animal feeding protocol used in this study. The availability of ^{11}C-PK11195 in the circulating blood was not found to be affected by the animal weight (p = 0.26). The biodistribution of ^{11}C-choline in the circulating blood was not found to be affected by the animal weight or strain (P = 0.08).

5.3 Biodistribution of tracers in the plaques

Autoradiography analysis was performed in the longitudinal sections of the aorta at atherosclerotic plaques and healthy vessel wall sites. The number of analysed regions was high in all studies, and the mean uptake intensities into each region were calculated for each study mouse separately. Furthermore, to avoid the confounding variability caused by the injected radioactivity dose and decay, the data were calculated as ratios (study I), dose and decay were compensated for (study III) or taken into account in statistical calculations. The observed plaque-to-wall ratios for each study are shown in Table 7.

The uptake of ^{18}F-FDG was 2.7 ± 1.1 -fold higher in the plaques compared to the healthy adjanced vessel wall (p = 0.008). In calcified plaque regions there was significantly higher uptake, 6.2 ± 3.2 (p = 0.002).

^{18}F-Fluoride showed even higher accumulation of radioactivity (17-fold, range 9-24) in non-calcified plaques and a very high (240-fold, range 188-290) accumulation in the calcified regions as compared with healthy regions. No ^{18}F-fluoride radioactivity accumulation was seen in the autoradiographs of the aorta of the control animal.

In study II, autoradiographs revealed diffuse ^{11}C-PK11195 uptake in the aorta sections, not specifically limited to the inflamed plaques. There was significantly higher accumulation of ^{11}C-radioactivity in inflamed regions compared to non-inflamed regions of the plaques (p = 0.011), but no difference was found in the accumulation in inflamed regions and the healthy vessel wall of the same animals. The uptake to cell-rich sites in plaques did not differ from the uptake to the healthy vessel wall (p = 0.1).

Average uptake of ^{18}F-galacto-RGD was significantly higher in the atherosclerotic plaques than in the adjacent, normal vessel wall or adventitia. Peak plaque-to-wall ratios in the animals varied from 1.7 to 3.0. The uptake in the aorta of controls was comparable to that in the normal vessel wall of LDLR$^{-/-}$ ApoB$^{100/100}$ mice.

Table 6: Biodistribution of tracers to aorta of atherosclerotic LDLR$^{-/-}$ ApoB$^{100/100}$ mice and in control C57Bl mice.

Study	Tracer	ΔT (min)	n (atheroscl)	n (control)	%ID/g Aorta (atherosclerotic)	%ID/g Aorta (control)	p
I a	^{18}F-FDG	60	11	9	0.41 ± 0.16	0.26 ± 0.12	0.037
I b	^{18}F-fluoride	60	3	1	3.38 ± 1.02	0.02	
II	^{11}C-PK11195	20	5	3	4.69 ± 1.29	9.00 ± 1.11	0.004
III	^{18}F-galacto-RGD	120	8	7	0.22 ± 0.04	0.15 ± 0.04	0.01
IV	^{11}C-Choline	10	6	5	4.11 ± 1.13	2.21 ± 0.65	0.0016

Table 7: Uptake of tracers (PSL/mm^2) presented as ratios.

Study	Tracer	Plaque-to-Wall (all)	Non-inflamed / *Calcified to-Wall	Inflamed-to-Wall	p**	Adventitia-to-Wall
I a	^{18}F-FDG	2.7 ± 1.1 (p = 0.008)	* 6.2 ± 3.2 (p = 0.002)	-	-	-
Ib	^{18}F-fluoride	17	* 240	-	-	-
II	^{11}C-PK11195	0.6 ± 0.2 (ns)	0.5 ± 0.1	0.8 ± 0.1	0.011	-
III a	^{18}F-galacto-RGD	1.4 ± 0.3 (p = 0.001)	correlation to nuclearity		0.01	1.0 ± 0.2 (p = 0.0004)
IIIb	^{3}H-DG	1.5 ± 0.2	-	-	-	2.1 ± 1.1
IV	^{11}C-Choline	2.3 ± 0.6 (p = 0.014)	1.41 ± 0.48	2.55 ± 0.78	<0.001	1.9 ± 0.5 (p = 0.021)

* Calcification-to-wall
** non-inflamed vs. inflamed
ND = not determined
ns = not significant

The autoradiography analysis of *ex vivo* ^{11}C-choline uptake showed significant uptake of ^{11}C-radioactivity in the plaques compared with the healthy vessel wall (plaque-to-wall ratio 2.3 ± 0.6, p = 0.014). The adjacent adventitial tissue, containing adipose tissue surrounding the vessel, also showed substantial uptake (adventitia-to-wall ratio 1.9 ± 0.5), but less than in the plaques (p = 0.02).

5.3.1 Correlation to inflammation and morphology

Histological correlates of tracer uptake were studied in serial tissue sections stained with HE, immunohistochemistry and Movat pentachrome (in study III, Figure 4). In study III, uptake of ^{18}F-galacto-RGD was associated with density of nuclei in the atherosclerotic plaques (p = 0.003). The highest uptake was seen in the lesions with the highest density of nuclei as quantified in the Movat-stained sections. Based on the results of the immunohistochemical analyses, most of the cells in the plaques, approximately 60%, were macrophages. Nuclear density was associated with macrophage number as indicated by the higher density in the plaques graded as having a large rather than a small Mac-3 positive area. In contrast to cellularity, there was no association between ^{18}F-galacto-RGD uptake and either the size of the lipid core or amount of connective tissue as seen in the analysis of the Movat –stained sections.

Nuclear density was also used as the main descriptive factor, along with the macrophage stainings of consecutive sections, in determining the non-inflamed and inflamed plaque ROIs in study II. In this study, there was a significantly higher accumulation of ^{11}C-radioactivity in inflamed regions.

In study IV, the degree of inflammation was assessed in 35 randomly selected plaque regions. The uptake was significantly higher in plaques with inflammation (n = 15), compared to non-inflamed plaques with no or only occasional nuclei (n = 20) (Figure 3). The mean plaque-to-wall ratios were 2.55 ± 0.78 vs. 1.41 ± 0.48 in inflamed and non-inflamed plaques, respectively (p < 0.001). Most of the cells in the plaques were identified as macrophages.

5.3.2 Correlation to other immunohistochemical stainings

PBR-specific antibody was found to stain mainly the same sites in the plaques as the macrophage antibody (study II), but the connection was not analysed in more detail due to the small number of samples. Immunohistochemical staining in study III with CD31 demonstrated a strong positive signal in the endothelial lining of the aorta, while neoangiogenesis was almost absent in the plaques. The CD61 antibody staining for integrin $\alpha_v\beta_3$ was not successful due to high non-specific binding. In study IV, Ki-67 staining for proliferative cells was performed. Very few occasional Ki-67 positive cells were found in the mouse atherosclerotic plaques.

5.4 Mechanism of ^{18}F-FDG binding

^{18}F-FDG was found to be bound to calcifications in *ex vivo* autoradiography of mouse aortic sections. Calcified sites are necrotic tissue, and ^{18}F-FDG is not known to bind to these sites. Possible hypotheses for the mechanisms of this observed binding were either existence of free ^{18}F-fluoride or unspecific binding of ^{18}F-FDG to inert calcifications. For the first hypothesis, uptake of ^{18}F-fluoride was tested and, for the second, *in vitro* binding studies were performed.

5.4.1 ^{18}F-Fluoride

Higher uptake of ^{18}F-fluoride was detected in the aorta of atherosclerotic mice as compared with control mouse (Table 6). Autoradiography revealed high accumulation of ^{18}F-radioactivity (17-fold, range 9-24) in non-calcified plaques and a very high (240-fold, range 188-290) accumulation in the calcified regions as compared with healthy regions. No radioactivity accumulation was seen in the aorta of the control animal (data not shown).

The data from the autoradiography analysis of ^{18}F-FDG and the above ratios were used to estimate the theoretical contribution of free fluoride originating from defluorination of ^{18}F-FDG, to the autoradiography results of ^{18}F-FDG. The amount of free ^{18}F-fluoride in the ^{18}F-FDG batch was below the detection limit of 0.3 %. It was estimated that the amount of free fluoride would have had to be more than 10-fold higher to explain the observed uptake findings in calcified and non-calcified plaques.

5.4.2 Patient samples

Analysis of *in vitro* binding of ^{18}F-FDG in calcified human artery sections revealed significant binding to the calcified regions of the artery wall. Binding to the other sites was not detected.

5.5 In vitro binding of ^{3}H-PK11195

The presence of PK11195 binding sites in the atherosclerotic plaques was verified by examining the *in vitro* competive binding of tritium-labelled PK11195 to aortic sections that had earlier been used in the *ex vivo* biodistribution study of ^{18}F-FDG (Study I, 41 sections from 5 mice). The ^{3}H-PK11195 was found to bind to the aortic sections in the sites of the plaques but also on the healthy wall (Figure 6). The specific vs. non-specific binding ratio was high (12-fold).

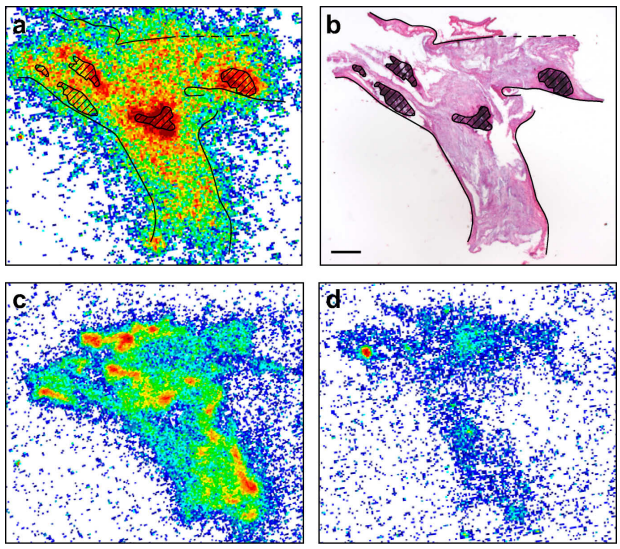

Figure 6: Comparison of ^{18}F-FDG *ex vivo* uptake and ^{11}C-PK11195 *in vitro* binding to the same mouse atherosclerotic aorta section. a: ARG image (^{18}F) and b: HE staining, with superimposed contour image of the artery and calcifications, c: ARG image (^{3}H) of the same section, *in vitro* incubation of ^{3}H-PK11195, d: ARG image (^{3}H) of consecutive section, ^{3}H-PK11195 and unlabelled PK11195. Images reprinted with permission from Springer Science+Business Media.

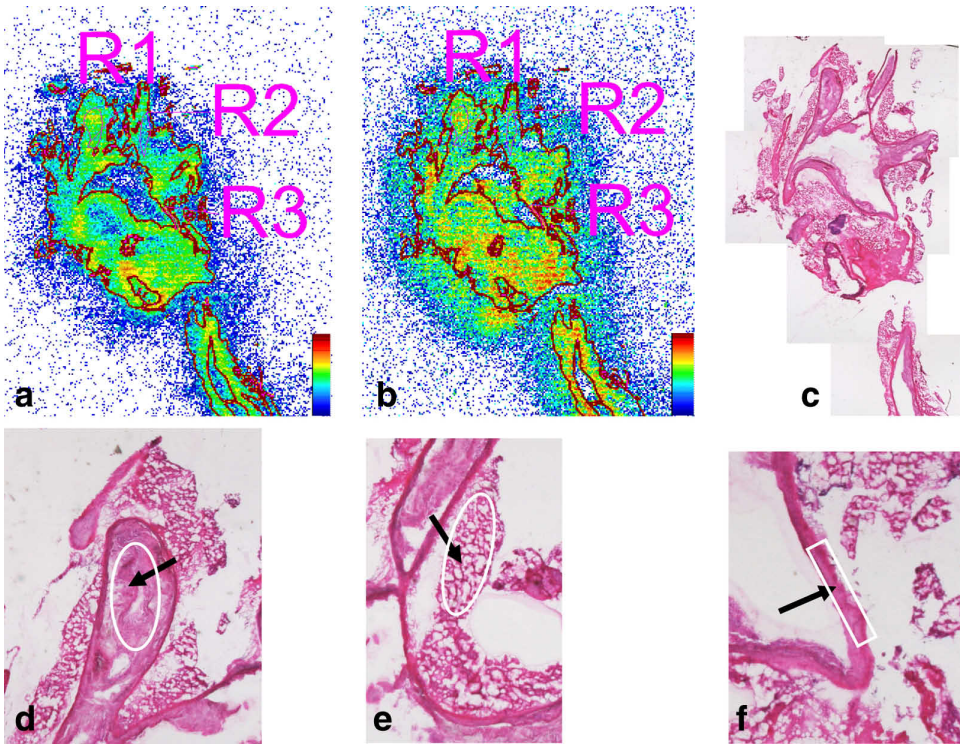

Figure 7: An example of analysis of the aortic sections. a) ^{18}F-radioactivity (^{18}F-galacto-RGD) and b) ^{3}H-radioactivity (^{3}H-DG), ARG image with contour image and ROI: R1 = plaque, R2 = adventitia, R3 = wall. c) HE-stain of the section, d) plaque, e) adventitia f) wall.

5.6 Evaluation of ^{18}F-galacto-RGD

5.6.1 Dual tracer comparison

The *in vivo* accumulation of ^{3}H- and ^{18}F-activities were measured in the same regions of interest in each aortic section. There was an association between uptakes of ^{3}H-DG and ^{18}F-galacto-RGD (Figure 7) in the atherosclerotic plaques. The highest uptakes of both tracers was found in the same plaques. When normalized to uptake in the muscle, ^{3}H- DG activity was higher than that of ^{18}F-galacto-RGD in the atherosclerotic plaques (4.0 ± 1.6 vs. 1.7 ± 0.5, p=0.02), but also in the normal vessel wall (2.7 ± 1.0 vs. 1.3 ± 0.5, p = 0.01) and adventitia (5.2 ± 2.9 vs. 1.3 ± 0.4, p =0.03). Thus, plaque-to-normal vessel wall ratios of tracers were comparable (1.5 vs. 1.4, respectively).

5.6.2 Small animal PET-CT

In vivo imaging demonstrated a focal ^{18}F-galacto-RGD signal that co-localised with calcified atherosclerotic lesions of the aortic arch as seen in the CT angiogram (Figure 8) and histology. Average ratio of ^{18}F-galacto-RGD signal in the bifurcation of the brachiocephalic artery to blood was 1.5 ± 0.2 in the LDLR$^{-/-}$ ApoB$^{100/100}$ mice and 1.1 ± 0.1 in controls (p = 0.02). The corresponding %ID/g was 0.24 ± 0.07 and 0.14 ± 0.08, respectively. Peak vessel-to-blood ratios in the hypercholesterolemic mice were 2.0 ± 0.3 and the corresponding peak %ID/g 0.32 ± 0.09.

5.6.3 *In vitro* binding of ^{18}F-galacto-RGD in mouse aorta sections

The presence of ^{18}F-galacto-RGD binding sites in the atherosclerotic plaques was verified in an *in vitro* binding and displacement study. ^{18}F-galacto-RGD was found to bind to the atherosclerotic lesions, and the binding was efficiently reduced in the presence of an unlabelled cyclic RGD peptide. The ratio of specific to non-specific binding was on average 9-fold.

5.7 Radiometabolite analysis of ^{11}C-choline

The radio-HPLC analysis of mouse plasma samples (n = 6) revealed 15 ± 7% of unchanged ^{11}C-choline at 10 min after injection. Two radiometabolites of ^{11}C-choline were observed; one of them was identified as ^{11}C-betaine and the other remained unidentified. Percentages of ^{11}C-betaine and other radiometabolite were 78 ± 7% and 9 ± 3% of total radioactivity, respectively.

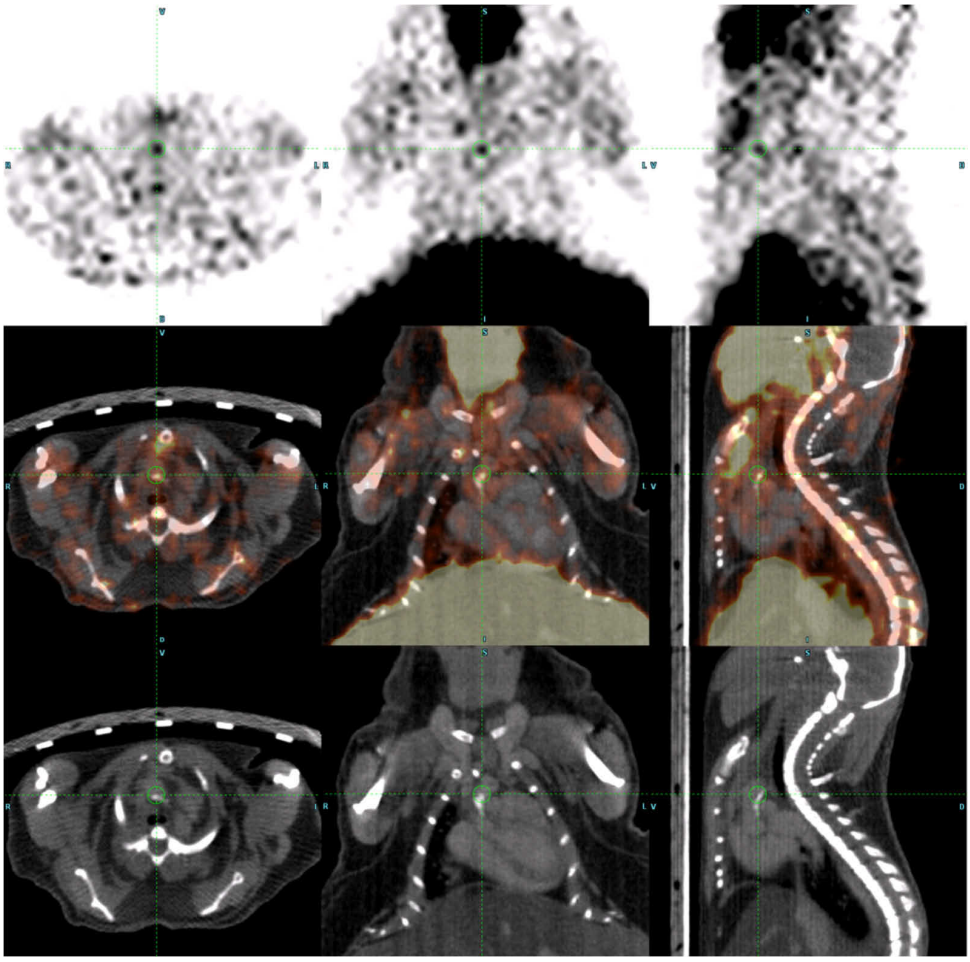

Figure 8: ^{18}F-galacto-RGD co-localises with calcified advanced plaque. a) PET image, b) co-registrated image and c) CT image

.

6 DISCUSSION

6.1 Animal model

$LDLR^{-/-}ApoB^{100/100}$ mice were chosen as the model in this study because these animals show a high prevalence of atherosclerotic plaques and increased plasma total cholesterol and triglyceride levels, as well as having the closest resemblance to human familial hypercholesterolemia (Veniant *et al.* 1998, Veniant *et al.* 2000). Most importantly, the plaque morphology resembles that of the human plaques.

In all studied $LDLR^{-/-}ApoB^{100/100}$ mice, extensive atherosclerosis was observed throughout the aorta. The plaques were mostly of fibroatheroma, or type IV according to the AHA classification (Stary *et al.* 2005), some with calcifications (type V). Despite the high age and high fat diet feeding, no plaque ruptures or thrombosis were detected. There was some animal loss during the studies, but mainly due to difficult xanthomas. The number of lost animals or the cause of death was not determined in these mice. The overall plaque burden in $LDLR^{-/-}ApoB^{100/100}$ mice has been determined before (Leppänen *et al.* 2005). At a much younger age than in the studies presented here, and after 22 weeks of diet, the aortic valve region consisted of up to 58% atherosclerotic lesions in cross-sections. The developed atherosclerotic plaques were of the fibroatheroma type and also included calcified sites in the plaques in the aortic arch region (Leppänen *et al.* 2005). The common limitation with all existing mice models of atherosclerosis is that the plaque inflammatory process is not fulminant, but rather modest, and that the plaques do not typically rupture (Jawien *et al.* 2004). The ruptures in the plaques have been claimed to be seen in the $ApoE^{-/-}$ mouse model (Jackson *et al.* 2007), but the observations are debatable (Falk *et al.* 2007).

The $LDLR^{-/-}$ $ApoB^{100/100}$ mice can be considered as a model for hypercholesterolemia. The cholesterol levels were not measured in these studies, but have been determined earlier by others. On normal chow, the cholesterol levels of adult $LDLR^{-/-}$ $ApoB^{100/100}$ mice were 230 mg/dl (5.9 mmol/l) (Veniant *et al.* 1998).

The $LDLR^{-/-}$ $ApoB^{100/100}$ mice are also considered a model for atherosclerosis, but it may be debatable whether the model represents a true atherosclerosis with vulnerable plaques, since the hard endpoints normally seen in human atherosclerosis, such as myocardial infarction, or even plaque rupture, have not been reported. The $LDLR^{-/-}$ $ApoB^{100/100}$ mice are not diabetic (Heinonen *et al.* 2007) although in study I the measured glucose levels were high. Some of the mice used in study II had been scanned with ultrasound (Saraste *et al.* 2008). The coronary arteries were processed into sections and showed substantial (30-97%) stenosis in the proximal left coronary artery, where the plaque seemed to originate from a large plaque in the ascending aorta. Half of the studied mice showed stenosis causing more than 90% of cross-sectional luminal narrowing, which is certainly consistent with severe, hemodynamically significant coronary obstruction (Tobis *et al.* 2007). These results indicate that the $LDLR^{-/-}ApoB^{100/100}$ mouse is a relevant mouse model to study marked coronary artery disease.

In control mice aortas no atherosclerosis or early signs of vascular changes were detected. The control group was chosen to be old males but, incidentally, these had a higher body mass due to a high amount of sub-peritoneal fat. This may affect the biodistribution results, if the distribution in fat tissue is substantial.

Histology and immunohistochemisty

Inflammation is considered as a key element creating vulnerability in the plaques, and therefore degree of inflammation was estimated in the studies. Assessment of inflammation in studies I, II, and IV was semi-quantitative and based on cellularity, with visually co-registering of macrophage staining in consecutive sections. In many cases the quality of the samples was not high enough to count the actual number of macrophages or other cells. Also, the accurate delineation of the plaque and vascular compartments in longitudinally cut sections is in many cases difficult. For these reasons, many traditionally used standard measures of plaque composition such as percentage of vascular area, intima-media thickness, or percentage of cell types per plaque area were not applicable. However, as was shown in study III, the cellularity count corresponded with the number of macrophages in the area, and therefore could be used as a determinant. A careful microscopic examination of the histology was always performed to rule out areas with smooth muscle cells.

Neovascularisation was not found in the mice in study III, and also the number of proliferative cells was very small. This may be due to the mouse model or the progression state of the plaques, and is further discussed in sections 6.2.3 and 6.2.4.

High fat diet feeding

The high fat diet feeding period and age of the used mice varied between the studies. At the start, limited information was available on the late progression states of atherosclerosis in these mice and, therefore, one of the aims was set to find out the best time for inducing the atherosclerosis and to study the mice. Diet withdrawal in study I resulted in less inflammation in the plaques as expected, and from thereon, the Western-type diet feeding was continued until the time of the experiments.

The mice were fed with a high fat Western-type diet containing cholesterol. This diet contains a small amount (0.15%) of cholesterol, which is enough to induce chronic systemic inflammation and atherosclerosis, independently of plasma lipid and lipoprotein levels, and to induce inflammation on the plaques of $LDLR^{-/-}$ mice (Subramanian *et al.* 2008). In our experience, prolonged high fat diet feeding induced itchy xanthomas on the skin of these animals. Switching to normal diet for a while or covering the areas with vaseline eased the problem to some extent, but still many animals had to be euthanised. Therefore, using old animals with a relatively short 2-3 month period of high fat feeding is preferable.

The animals were not fasted overnight before the experiments, but the experiments were performed mostly during the afternoon. Mice are nocturnal animals and they usually eat during the night and very seldom during the day. Nevertheless, high glucose levels in were found study I. Overnight fasting would not have been feasible,

since it would have resulted in much longer fasting than anticipated and would have compromised the animals. Fasting affects glucose metabolism and the biodistribution of some tracers (Fueger *et al.* 2006), therefore it is essential to keep the protocol fixed during the study, including the feeding pattern. Some researchers suggest a five hour fasting prior to the studies (Fueger *et al.* 2006).

6.2 Evaluation of tracers for atherosclerosis imaging

6.2.1. ^{18}F-FDG

^{18}F-FDG is a glucose analogue, which accumulates in cells in accordance with their glucose utilisation. ^{18}F-FDG PET is extensively used in imaging of cancer and inflammation. ^{18}F-FDG has been shown to detect human carotid plaques already some years ago (Rudd *et al.* 2002), and very recently also to correlate with macrophage content in the human plaque (Graebe *et al.* 2009). The correlation with inflammation had been reported earlier in experimental animal models (Tawakol *et al*. 2006, Zhang *et al.* 2006). According to these studies, inflammatory plaques seem to be characterised by increased ^{18}F-FDG uptake.

In agreement with previously published data, the results in study I show that ^{18}F-FDG accumulates in the mouse atherosclerotic aorta and atherosclerotic plaques. The findings of mouse aortic uptake of ^{18}F-FDG have been inconsistent. We found a plaque-to-wall ratio of 2.7 in *ex vivo* autoradiographs in mice. Matter and co-workers reported in the same year a similar ratio (2.6) in autoradiographs of ApoE$^{-/-}$ mouse sections (Matter *et al.* 2006). However, Laurberg and colleagues failed to show any accumulation of ^{18}F-FDG in aorta of ApoE$^{-/-}$ mice *in vivo* using a micro-PET device (Laurberg *et al.* 2007). This might be due to partial volume effects, the morphology of the plaques in this model, or the used early timepoint (Rudd *et al.* 2007b).

An unexpected finding was that significant ^{18}F-FDG uptake was detected in the calcified structures in the *ex vivo* autoradiographs of mouse atherosclerotic plaques. Two potential mechanisms for ^{18}F-FDG were tested in subsequent experiments. First, free ^{18}F-fluoride can in theory exist as an impurity in the ^{18}F-FDG batch and could cause the observed accumulation at the calcified sites. This was tested by studying a small number of mice using only ^{18}F-fluoride and, as expected, high uptake was measured in calcifications. However, from these measurements, we could calculate that the ^{18}F-FDG uptake findings cannot be explained by free ^{18}F-fluoride alone. Also the possibility that ^{18}F-FDG would be catabolised to ^{18}F is very unlikely, although the actual radioactive metabolites were not traceable in the mouse aortas owing to the small amount of radioactivity in the target tissue. Second, *in vitro* binding studies of heavily calcified human femoral arteries were performed. The results suggested a non-metabolism-dependent binding mechanism of ^{18}F-FDG, since metabolically active cells are not present in fixed post-mortem tissue sections. The most likely mechanism of ^{18}F-FDG binding to the calcified structures is entrapment of ^{18}F-FDG into the hydroxyapatite. From the current *in vitro* study it was not possible to estimate the

absolute amount of trapped ^{18}F-FDG, but the mice studies suggest that this mechanism could be significant and should also be taken into account in clinical studies.

General aspects of atherosclerosis imaging

^{18}F-FDG is now considered a promising marker for plaque vulnerability and has been used in carotid artery imaging. The ^{18}F-FDG imaging of coronary arteries is, however, problematic not only because of the movement, but also due to the high uptake of the tracer into the myocardium and the dependence on the metabolic condition. This can be alleviated with proper standardisation of the imaging procedure and diet pre-treatment (Williams *et al.* 2008).

^{18}F-Fluoride showed exceptionally high target-to-background ratios in the pilot study. ^{18}F-Fluoride imaging of plaques warrants further studies, although it is likely that it may not add to the information about calcium score measurements performed by CT.

The mice have large deposits of brown fat in the neck area. In a cold environment, brown fat utilises glucose in large amounts. Especially in mice, this affects the distribution of ^{18}F-FDG and makes the visualisation of targets around that area extremely difficult (Fueger *et al.* 2006). In addition, physical activity affects the distribution of ^{18}F-FDG (Fueger *et al.* 2006). This was not taken into account in our study (study I) or in the study by Laurberg (Laurberg *et al.* 2006); the mice were kept at room temperature. With a more optimal distribution study protocol higher target-to-background ratios could have been achieved.

6.2.2. ^{11}C-PK11195

^{11}C-PK11195 has been suggested as a potential agent for the imaging of atherosclerosis-associated inflammation. ^{11}C-PK11195 binds with high affinity to peripheral benzodiazepine receptor (PBR) found in the mitochondrial outer membrane of many peripheral cells. In the brain, only very low PBR can be found, but once activated, the glial cells express high amounts of PBR (Casellas *et al.* 2002). Therefore, ^{11}C-PK11195 is used for PET imaging of inflammation related to multiple sclerosis or other neurodegenerative diseases (Debruyne *et al.* 2003). Recent studies have suggested that ^{11}C-PK11195 accumulates in activated macrophages in the inflamed area also in the periphery, as shown in the inflamed lung in animal models and humans (Hardwick *et al*. 2005, Jones *et al.* 2002 and Jones *et al.* 2003).

The presence of PK11195 binding sites in the atherosclerotic plaque sections was investigated in study II. The binding of ^{3}H-PK11195 was found to be specific, and a patchy pattern of binding to the plaques and wall was found. The binding did not resemble the *ex vivo* ^{18}F-FDG autoradiography image, collected earlier from the same sections. Since *in vitro* binding may not correspond to *in vivo* distribution, a biodistribution study using ^{11}C-PK11195 was conducted. The uptake of ^{11}C-PK11195 was not higher in the aorta of atherosclerotic mice compared to control mice. The uptake of tracer was higher in inflamed atherosclerotic plaques than in the non-inflamed plaques, but did not exceed the uptake to other structures of the artery wall.

The antibody against PBR localised in the plaques in the same areas as the antibody against macrophages.

The lower uptake in the aorta of atherosclerotic mice compared to the aortas of the control mice may be explained by the high number and mass of core areas of the plaques observed in the aorta of atherosclerotic mice. As autoradiography analysis showed, ^{11}C-PK11195 does not accumulate in these non-inflamed sites. The atherosclerotic aortas have a higher mass due to these plaques, and therefore, the radioactivity calculated against the weight per gram of tissue is lower when accumulation in other sites is similar.

The role of PBR and the regulation of PBR expression in macrophages and other cells are poorly understood. There are controversial findings suggesting that macrophages may express PBR differently in response to their environment. A recent report by Branley and co-workers shows that although ^{3}H-PK11195 binds solely to macrophages of bronchoalveolar lavage cells in patients with interstitial lung disease (ILS), the total binding in the lung is diminished compared to that of healthy controls (Branley *et al.* 2007). They suggest that in ILS and in other inflammatory diseases like osteoarthritis (Bazzichi *et al.* 2003), the reduced expression of PBR in the macrophages may be a reflection of a pro-apoptotic and pro-inflammatory milieu.

General aspects of atherosclerosis imaging

For imaging of atherosclerotic plaques, ^{11}C-PK11195 does not seem to have an optimal target-to-background ratio, although the tracer could distinguish plaques according to activity. High uptake in the myocardium limits the use of this tracer in cardiac imaging. Although the tracer was shown to bind to carotid plaques in a pilot study conducted in humans, significant background binding, especially in the salivary glands was also seen (Hoppela *et al.* 2007). A metabolite analysis is also needed for absolute quantification, since 20 min after the injection the amount of unchanged ^{11}C-PK11195 has been shown to be 78% in human plasma (Roivainen *et al.* 2009). The short half-life of ^{11}C and the need for on-site cyclotron limit the clinical use of this tracer in atherosclerosis imaging.

6.2.3 ^{18}F-galacto-RGD

Intraplaque angiogenesis by proliferation of medial vasa vasorum has been associated with rapid plaque growth and plaque rupture (Virmani *et al.* 2005). The fragile and leaky structure of the neovasculature may lead to extravasation of red blood cells in the plaques with subsequent intraplaque haemorrhage that can predispose to plaque rupture. $\alpha_v\beta_3$ integrin is a cell surface glycoprotein receptor and it is highly expressed during angiogenesis. A peptide tracer ^{18}F-galacto-RGD binds with high affinity and selectivity to $\alpha_v\beta_3$ integrin and has been extensively validated for imaging the level of $\alpha_v\beta_3$ integrin expression in tumours (Haubner *et al.* 2001, Beer *et al.* 2005, Haubner *et al.* 2005). In atherosclerotic lesions, both macrophages and activated endothelial cells can express high levels of $\alpha_v\beta_3$ integrin (Hoshiga *et al.* 1995, Antonov *et al.* 2004).

Therefore, $\alpha_v\beta_3$ integrin expression is a potential marker of inflammation and angiogenesis in atherosclerotic lesions.

Our study provided the first evidence that ^{18}F-galacto-RGD shows specific accumulation in advanced, spontaneous atherosclerotic lesions seen in LDLR$^{-/-}$ ApoB$^{100/100}$ mice. A systematic analysis demonstrated higher ^{18}F-galacto-RGD uptake in the atherosclerotic plaques than in the normal vessel wall. In line with this, the results of the biodistribution study showed quantitatively higher uptake in the aorta of atherosclerotic than control mice. The efficient blocking of ^{18}F-galacto-RGD in *in vitro* competition studies confirmed that binding was $\alpha_v\beta_3$ integrin dependent, indicating that ^{18}F-galacto-RGD could specifically detect $\alpha_v\beta_3$ integrin expression in atherosclerotic lesions.

Previous studies have demonstrated that ^{18}F-galacto-RGD PET visualized tumours with a high level of $\alpha_v\beta_3$ integrin expression with good target-to-background ratios (Beer *et al.* 2005). More recent studies have indicated sufficient signal intensity for visualizing increased $\alpha_v\beta_3$ integrin expression in chronic skin inflammation (Pichler *et al*. 2005) and in the infarcted myocardium (Higuchi *et al.* 2008, Makowski *et al.* 2008). As expected, %ID/g of ^{18}F-galacto-RGD in the aorta was several folds lower than in $\alpha_v\beta_3$ integrin expressing tumours. However, autoradiography demonstrated that the maximal plaque-to-normal vessel wall ratios were as high as 3.0. We recently also tested ^{68}Ga-labelled RGD peptide for imaging of atherosclerosis in the same mouse model, and got equally promising results with a plaque-to-wall ratio of 1.4 (Haukkala *et al.* 2009).

In parallel with autoradiography showing the highest plaque-to-normal vessel wall ratios typically in the arch region, particularly in the bifurcation of the brachiocephalic artery, also *in vivo* imaging demonstrated ^{18}F-galacto-RGD PET signal corresponding to the advanced, calcified plaques of the aortic arch region. Calcification in advanced atherosclerotic lesions allowed localization of the vessel wall in the CT angiography. However, no uptake in the calcification itself was detected in autoradiography. Although partial volume effects related to the small size of the target are likely to influence quantitative *in vivo* analyses, our results provide evidence that visualization of $\alpha_v\beta_3$ integrin expression in atherosclerotic lesions is possible using ^{18}F-galacto-RGD PET.

Both macrophages and angiogenesis have been implicated in the progression and rupture of atherosclerotic lesions (Virmani *et al.* 2005). However, $\alpha_v\beta_3$ integrin can also be expressed by SMCs in the media of normal and diseased arteries (Hoshiga *et al.* 1995). In our study, histological analysis demonstrated that uptake of ^{18}F-galacto-RGD was associated with nuclear density in the plaques. Immunohistochemistry demonstrated that nuclear density reflected mainly the prevalence of macrophages, by far the most common cell type in the plaques. In contrast to cellularity, ^{18}F-galacto-RGD uptake did not show any association with either the amount of fibrous tissue or ground substance mainly representing the lipid core of the plaques. The results are in line with the study of Waldeck and colleagues, demonstrating that $\alpha_v\beta_3$ integrin-targeting RGD peptide labelled for optical imaging co-localised with macrophages in the vascular lesions induced by carotid artery ligation in ApoE$^{-/-}$ mice. Unlike our

tracer, this probe allowed exact co-localisation studies on the cellular level using fluorescence microscopy of tissue sections (Waldeck *et al.* 2008). The possibility for detection of $\alpha_v\beta_3$ integrin expression on macrophages of atherosclerotic lesions makes ^{18}F-galacto-RGD an attractive tracer for identification of sites of highly inflamed atherosclerotic process.

The $\alpha_v\beta_3$ integrin is perhaps best known for its essential role as a mediator of angiogenesis (Brooks *et al.* 1994). In contrast to earlier studies (Waldeck *et al.* 2008, Burtea *et al.* 2008), we found virtually no evidence of angiogenesis within the plaques, despite old age and prolonged cholesterol feeding of the animals. This is consistent with previous studies demonstrating very limited intraplaque neovascularisation in mice (Moulton *et al.* 1999, Heinonen *et al.* 2007). Therefore, it seems that neovascularisation had little influence on uptake of ^{18}F-galacto-RGD in the atherosclerotic plaques in this model. The fact that ^{18}F-galacto-RGD uptake did not differ between adventitia and the normal vessel wall in either LDLR$^{-/-}$ApoB$^{100/100}$ or control mice, also indicates that vasa vasorum expansion outside the plaques did not significantly contribute to the detected ^{18}F-galacto-RGD uptake.

We also compared ^{18}F-galacto-RGD uptake with ^{3}H-DG, a tritiated analogue of ^{18}F-FDG, by co-injection and dual tracer autoradiography. Although uptake of ^{3}H-DG appeared to be higher in the aorta, the plaque-to-wall ratio was comparable between tracers. Consistent with the results of our histological study demonstrating an association between ^{18}F-galacto-RGD uptake and macrophage density, ^{18}F-galacto-RGD and ^{3}H-DG activities were also associated in the same plaques.

General aspects of atherosclerosis imaging

^{18}F-galacto-RGD has favourable kinetic properties for imaging, such as high initial retention in the blood, rapid renal excretion and high metabolic stability (Beer *et al.* 2005, Haubner *et al.* 2004). In addition, lack of uptake of ^{18}F-galacto-RGD in the normal myocardium is an important feature when imaging the coronary arteries.

Although we found only 1.6-fold higher uptake in the plaques, on average, in the mice, considering the relatively moderate level of inflammation and the lack of neovascularisation in the plaques in our model, these results encourage the testing of ^{18}F-galacto-RGD for imaging atherosclerosis in patients. In human atherosclerotic plaques, higher degrees of inflammation and also neovascularisation are reported, which may provide a stronger signal than that seen in our study. Furthermore, tracer optimisation by multimerisation has been shown to provide increases in signal intensity from $\alpha_v\beta_3$ integrin expressing tissues (Thumshirn *et al*. 2003). Similarly to ^{18}F-FDG, ^{18}F-galacto-RGD is readily testable in humans based on the experiences from several studies involving cancer patients, thus facilitating application to clinical studies.

6.2.4 ^{11}C-Choline

Cells use choline for the synthesis of phosphatidylcholine, an essential lipid component of cell membranes, and for the synthesis of acetylcholine in the brain. All nucleated

cells have specific choline transport mechanisms, expression of which varies, being highest in the proliferative cells and cancer cells. Choline uptake can also be amplified by increased choline kinase activity. Therefore, ^{11}C-choline and the choline analogue ^{18}F-FCH have been used in PET imaging of various tumours (Hara *et al.* 1997, Hara *et al.* 1998, Tian *et al.* 2004). Radiolabelled choline is also reported to accumulate in inflamed sites in patients with rheumatoid arthritis (Roivainen *et al.* 2003), and in an experimental soft tissue infection model (Wyss *et al.* 2004). In monocyte-derived macrophages the choline transporter-like protein-1 is responsible for the transport and its expression varies in response to stimuli (Fullerton *et al.* 2006). Very recently, ^{18}F-FCH and ^{11}C-choline have been shown to visualize the vessel wall in the aorta and carotid arteries in patients (Bucerius *et al.* 2008, Kato *et al.* 2009). The radioactivity was found mainly in non-calcified vessel wall areas of elderly prostate cancer patients. Without any histological evidence, the true nature of vessel wall alterations remains unknown.

We were able to demonstrate ^{11}C-choline uptake in atherosclerotic plaques in conjunction with histomorphologic evidence. Our results revealed significantly higher uptake of tracer in inflamed mouse atherosclerotic plaques as compared with a healthy vessel wall with a plaque-to-normal wall ratio of 2.3. Importantly, the uptake in inflamed plaques was significantly higher than that to the non-inflamed plaques. Our study also showed a 1.9-fold higher uptake of ^{11}C-choline in the aortas of the atherosclerotic mice compared to the control mice. Furthermore, our findings suggest that macrophages may be responsible for the uptake of ^{11}C-choline in the plaques.

Previously, Matter and colleagues reported ^{18}F-FCH uptake in the atherosclerotic plaques of the ApoE$^{-/-}$ mouse (Matter *et al.* 2006). The autoradiography of mouse aortas showed almost five-fold higher uptake in the plaque-bearing vessel area compared to the plaque-free vessel, as well as a correlation to lipid- and macrophage stainings. In another study of experimental soft tissue infection, the target-to-background ratio of ^{18}F-FCH was 6 at its highest (Wyss *et al.* 2004). However, ^{11}C-choline and ^{18}F-FCH are two different compounds with divergent pharmacokinetic properties and, therefore, no direct comparison can be made. Moreover, it is important to notice that Matter and co-workers have used an *en face* autoradiography method, in which the thickness of analysed areas might have affected the results. Microautoradiography of the aortic sections, which is comparable to the method we have used in the present study, revealed a plaque-to-wall ratio of 3.5 with ^{18}F-FCH. Importantly, they were able to demonstrate that the level of choline kinase was similar in atherosclerotic and control aortas, suggesting that the observed difference was due to increased choline transport (Matter *et al.* 2006).

Choline uptake has been shown to correlate with the proliferative activity in the tissue (Yoshimoto *et al.* 2004). Cell proliferation has been suggested to play an important part in the progression of atherosclerotic plaques, with the main proliferative cell type in the human plaques being monocyte/macrophages, SMCs and endothelial cells (Rekhter *et al.* 1995). However, the overall proliferative activity has been found to be very low, only 0.49 % as determined by Ki-67 immunostaining in carotid plaques,

predominantly in macrophage-rich areas (Brandl *et al*. 1997). Also in the mouse atherosclerotic plaques we found only very few Ki-67 positive cells.

General aspects of atherosclerosis imaging

Due to the uptake of radiolabelled choline in several tissues, the target-to-background ratios can be expected to be moderate. In tumours the tumour-to-muscle ratios have been reported to be relatively low, e.g. 1.2–2.5 in mouse xenograft models for breast cancers (Zheng *et al.* 2004) and 1.6–3.9 in an *in vitro* study (Yoshimoto *et al.* 2004). These findings suggest that choline is not a specific marker for inflammation or for proliferation, but has, however, potential for the imaging of atherosclerosis.

Regarding the whole-body distribution of i.v. injected ^{11}C-choline in mice; our results are in accordance with previous studies (Zheng *et al.* 2002). We found that at the time point of 10 min, the target-to-background (aorta-to-blood) ratio was 5.5, indicating fast blood clearance and potential for *in vivo* PET imaging. We observed high uptake in heart and kidney, which could be problematic when imaging these targets. However, there may be differences in cardiac muscle utilization of choline between mouse and humans, since low uptake has been reported in human (Roivainen *et al.* 2009).

Intravenously administered ^{11}C-choline is catabolised rapidly in blood circulation to ^{11}C-betaine. We found that the amount of unchanged tracer was 15% in mouse plasma at 10 min after injection. Reliable radiometabolite analysis is therefore essential for quantitative PET analysis (Roivainen *et al.* 2000). There are, however, contradictory reports on the amount of betaine uptake in tissues (Yoshimoto *et al.* 2004, Brown *et al.* 2001) which can make modelling of ^{11}C-choline PET challenging.

6.3 Correlation of biodistribution to inflammation

Accumulation of tracers in the plaques was further studied according to the inflammation status. A limitation in these studies was that vulnerability of the plaques was not a predefined attribute, nor determined in other way than through assessing the inflammation. Inflammation is considered as a key event in creating vulnerability in plaques and, therefore, it is essential to know whether these tracers were able to distinguish the stable kind of plaques from inflammatory plaques. Especially for clinical application, it is more important to differentiate the inflamed sites from non-inflamed plaques, since these are pathologically very different and their vulnerability prognosis is essentially different.

For the first time, we showed that ^{11}C-PK11195, ^{18}F-galacto-RGD, and ^{11}C-choline all accumulated more in inflamed plaque when compared to non-inflamed plaque regions. The different types of plaques were not distinguished in the study of ^{18}F-FDG, but others have shown that the uptake of this tracer correlates with the number of macrophages in the plaques (Tawakol *et al.* 2005, Graebe *et al.* 2009). In our samples, it was not feasible to count the number of macrophages, and therefore, semi-quantitative methods were used. Macrophages were detected in the plaques by comparing the autoradiography sections to consecutive macrophage-stained sections

(studies II-IV). In studies II-IV, the inflammatory activity was estimated on the basis of cellularity, and the macrophages were not specifically counted in the inflamed plaque regions. However, the cellularity in the plaques was shown to correspond with the macrophage staining, as shown in study III. The plaques contained also T-cells, but in minor amounts.

6.4 Methods

When working with short half-life radioisotopes, the number of procedures must be limited and the analysis has to be carried out in a strict timeline. For these practical reasons, sectioning of the aorta was performed longitudinally as opposed to conventional cross-sectioning. This enables sectioning of the entire aorta and obtaining a large number of samples in a short time. On the other hand, we were not able to perform traditional cross-area analyses, and the immunohistology was limited to relatively thick (8 μm) cryosections consecutive to the autoradiography sections.

The measurement of radioactivity from small tissue samples or thin autoradiography sections can be problematic, if only a small proportion of the injected radioactivity is distributed to the tissue of interest. This can be compensated for by giving an animal a high dose of the radioactivity, so that some remains to be measured after the preparation time. However, then the injected radioactivity and the amount of the compound in micrograms would be much higher than in humans; this might have affected the biodistribution results, especially in the case of unspecific binding of ^{18}F-FDG (study I).

In these studies, the accumulated radioactivity was measured using different methods. The *ex vivo* measurements should be comparable with the *in vivo* measurements, and this was the case in the study III. However, the *in vitro* binding and *in vivo* biodistribution are two profoundly different things, and this should be kept in mind when interpreting the results. It must also be pointed out that the unit used in the biodistribution studies, the %ID/g tissue, does not describe the true distribution of the tracer, it merely measures the total radioactivity of the samples, including the potential radioactive metabolites. The same also applies to digital autoradiography. In addition, although the photostimulated luminescence (PSL/mm^2) has a wide dynamic range, there can be great variation in the results when detecting very low signals. Artefacts may appear in the autoradiographs at varying thicknesses of the sections, and this should be carefully examined under the microscope. Another limitation is that the digital autoradiography is also affected by the decay of radioactivity. This means that when the time for preparation of the samples varies between the animals, there are differences in the observed data. Without compensation, the results from different mice cannot be directly compared or mean values calculated. This was compensated for in such a way that the data were calculated as ratios (study I), the radioactive dose and decay were compensated for (study III), or dose and time were kept constant and the level difference was taken into account in statistical calculations.

The number of animals used in the studies was limited. However, the autoradiography analysis was performed in multiple consecutive sections covering the entire aorta and

the plaques in it. Measurements of the same plaque in consecutive sections give a better estimation of the distribution. The analysis of mouse aortic autoradiographs is challenging, causing variation in the ROI analysis, partly due to the small size of the analysed areas. This was especially seen in the healthy vessel wall, which is only a few cell layers in thickness. Interference from other nearby tissue compartments was, however, minimised by drawing ROIs for the healthy wall region farther away from the plaques. We found that the coefficient of variation of repeated analyses for this method was 4.5%.

The main results of these autoradiography studies were presented as PSL/mm^2 ratios between plaque and healthy wall. This may not be optimal in cases where the ratio was calculated from the mean values of all the measured plaque regions. In order to draw conclusions on the feasibility of the tracer for differentiating active plaques from less active ones, it would be more useful to calculate ratios separately for different types of plaques (studies II and IV), or to report maximum ratios as done in study III.

6.5 Future directions

One of the main goals of this work was to develop methods suitable for pre-clinical screening of PET imaging agents for atherosclerosis. Although good results were obtained with the current methods and the animal model used in these studies, there is still need for further optimisation, as pointed out in the previous chapter. Especially the histology and immunohistology of the mouse aortic samples are challenging and needs further improvement.

Better animal models would be useful, especially models for plaque rupture. However, surgery-induced rupture models probably have limited value in imaging studies, since the wound itself may create an artefact in the area. Pig models are interesting, since the size, anatomy and physiology are closest to humans'. Pigs also have vulnerable plaques in the coronaries (Artinger *et al.* 2009). Response to treatment and follow-up studies may well be feasible, although it must be noticed that pigs, like rabbits, are very sensitive animals; longitudinal studies can be very stressful for the animal and demanding to conduct. For both practical and economic reasons, mice are still the best option for studies needing a large number of test animals.

The tested tracers showed some favourable properties for the imaging of atherosclerosis. Further studies are either already in progress or being planned. The first study demonstrated, unexpectedly, that some fraction of ^{18}F-FDG is bound to calcifications in the plaques. However, it is possible that with a more fulminant inflammatory process, the binding to calcified regions will not prevent this tracer from being used in clinical studies. It was also later found that the animal model used in study I was not optimal, and that the Western-type diet feeding should be prolonged. Thus, this study is currently being repeated using an animal model expressing advanced inflammatory plaques. In study II, we observed a high uptake of ^{11}C-PK11195 in the surrounding tissue which may limit the clinical use of this tracer for clinical PET imaging of atherosclerosis. In study III, we found a high uptake of ^{18}F-galacto-RGD in the mouse plaques, although the level of inflammation was moderate

and there was no apparent neovascularisation in the plaques. These results encourage further testing of ^{18}F-galacto-RGD for imaging atherosclerosis in patients, since in human atherosclerotic plaques a higher degree of inflammation and also neovascularisation are reported; these may provide a stronger signal than that seen in our study. Studies of ^{18}F-galacto-RGD for the imaging of human atherosclerosis in patients are being planned at the Technical University of Munich. In study IV, we found prominent uptake of ^{11}C-choline in mouse atherosclerotic plaques; further clinical studies are needed to elucidate its value as a marker of plaque inflammation for *in vivo* imaging.

All the tested tracers are already in clinical use for other indications. Nevertheless, it was not feasible to perform testing of the tracers directly in patients. Ongoing studies in our facility have lighted some practical challenges in the imaging of human atherosclerotic plaques. Human carotid arteries are a relatively easy target for imaging, and patients can be recruited for imaging prior to endartrectomy operation, when histological samples can be obtained. However, patients with rupture-prone plaques in the carotid or coronary arteries are preferably treated urgently, leaving a very short time window for recruitment and preparations for the imaging. Technical issues in coronary artery imaging have limited the imaging of patients, but this will be probably be solved very soon. Most importantly, nuclear imaging in humans without clear indication should be limited due to their risks involved in using ionising radiation. Follow-up studies and response to treatment studies should be performed, but only with properly validated tracers and with biopsy and immunohistochemical verification. This is probably not feasible in clinical studies, at least in coronary artery disease. Moreover, when new radiotracers are introduced, careful proof-of-principle and dosimetry studies in animal models are required.

7 SUMMARY AND CONCLUSIONS

Inflammation-targeting tracers, ^{18}F-FDG, ^{11}C-PK11195, ^{18}F-galacto-RGD and ^{11}C-choline were evaluated for imaging of vascular inflammation associated with atherosclerosis in a mouse model of atherosclerosis. In summary, our results revealed:

1. Plaques in the aorta of LDLR$^{-/-}$ApoB$^{100/100}$ mice contained cell-rich, inflamed areas and acellular necrotic cores and calcifications, particularly in older mice, resembling type IV and V lesions, but not thrombosed or thrombus-prone type IV lesions even with prolonged feeding. Therefore, it is debatable whether this mouse model can be considered as a model for vulnerable plaques. However, in the evaluation of tracers for differentiation of inflammatory and non-inflammatory plaques, the LDLR$^{-/-}$ApoB$^{100/100}$ mouse model seems appropriate.
2. Quantitative autoradiography combined with carefully conducted histomorphological and immunohistochemical analysis provides essential information about the distribution of tracers at cellular level. *In vivo* imaging of atherosclerotic plaques in mice is challenging but probably feasible with a sufficient target-to-background ratio of the tracer.
3. All the tested tracers targeted inflammation in mouse atherosclerotic plaques
4. The obtained target-to-background ratios for ^{18}F-FDG, ^{18}F-galacto-RGD and ^{11}C-choline were adequate for imaging. All tracers had many desired qualities for imaging purposes, but future studies are warranted to find an optimal imaging agent for vulnerable plaque imaging.

8 ACKNOWLEDGEMENTS

This study was carried out in the Turku PET Centre, the Department of Clinical Physiology and Nuclear Medicine, University of Turku, and in Klinikum Rechts der Isar, the Technical University of Munich during the years 2004-2009. I express my sincere thanks to Professor Jaakko Hartiala, the head of the department of Clinical Physiology, Professor Juhani Knuuti, Director of the Turku PET Centre and Professor Markus Schwaiger, Head of the Department of Nuclear Medicine in TUM, for providing excellent research facilities.

I owe my deepest gratitude to my supervisors; Professor Juhani Knuuti and Adjunct Professor Anne Roivainen. Juhani, your positive and encouraging method of guidance has been very pleasant, and, I must say, I am astonished at how you are able to combine the tasks of director, scientist and clinician, and still be a great supervisor; you have always had time to share your vast knowledge and experience. Anne, you have been very kind to me right from the start and patiently shared so much time with me in discussions. I truly admire your expertise and enthusiasm. Thank you both for trusting me to make my own decisions and for giving me time to learn.

I would like to thank the members of my supervisory committee, Professor Seppo Ylä-Herttuala, and Professor Matti Poutanen, for sharing their time and visions, for being true mentors and for showing a keen interest in this project. Director Mika Scheinin and coordinator Eeva Valve are acknowledged for giving me the opportunity to work as a PhD student at the Drug Discovery Graduate School, and for their encouragement and help. I wish to express my gratitude to Professor Pirjo Nuutila, for being such an inspiring leader of the CarMet group, and also for the opportunity to broaden my academic career alongside my studies. Thank you for your guidance in scientific and other matters.

I wish to thank the official reviewers of this thesis, Professor Juha Hartikainen, and senior lecturer Lars Johansson, for their valuable and constructive criticism and comments. I thank Jacqueline Välimäki for the official language review of this thesis.

I would like to express my gratitude to my co-authors and collaborators. My sincerest thanks to Merja Haaparanta-Solin for your invaluable tutoring, especially at the beginning. Warm thanks to Päivi Marjamäki, it has been a pleasure to work with you, and I thank you for your hearty encouragement. Sincerest thanks to Antti Saraste, it has been a delight to genuinely share the many questions involved in the projects performed in Munich with you. I admire your talent, serenity and effectiveness. I thank radiochemists Kjell Någren and Nina Savisto, as well as Pauliina Luoto, for “taking the dose”, and for sharing their knowledge and time. Sincerest thanks to Johanna Silvola and Sanna Hellberg, your input has been essential, I appreciate your hard-working attitude and kindness. Anu Autio and Tiina Pöyhönen, thank you for the exciting times with the rodents and for sharing the PhD experience. From the Department of Pathology, Jukka Laine, and Sanna Soini from the Department of Pharmacy are acknowledged for their keen interest in this study. Sincere thanks to Ian Wilson and

other personnel at Turku Imanet. The personnel at the Helmholtz Zentrum Muenchen, Munich, Germany, are acknowledged for their outstanding contribution.

I have been extremely lucky to have the opportunity to work in different laboratories during this process. I wish to express my sincerest thanks to Professor Markus Schwaiger, for very fruitful collaboration and guidance, and for believing in me. The personnel in TUM are acknowledged for their excellent scientific contributions, and especially Eliane Weidl, Sybille Reder, Axel Weber and Stephan Nekolla, thank you for your hard work and kindness. From the University of Kuopio, I thank Seppo Ylä-Herttuala and Suvi Heinonen for the opportunity to visit the lab, and many thanks to Pia Leppänen, who has taken care of the mice. Also acknowledged is Professor Michael Schäfers, University of Münster, Germany, although the work itself did not end up in this thesis, for very educative laboratory visits.

I also wish to thank Irina Lisinen for her assistance with the statistical analyses, Timo Kattelus for excellent work with the pictures, Mervi Oikonen for proof-reading and discussions, Sinikka Kollanus for teaching me how to do immunohistological stainings on my samples, and Erica Nyman for doing it in the end. Many thanks to Hannele Ylipahkala for collaboration. The personnel of the Animal Centre of the University of Turku are warmly thanked for their flexible and friendly service towards me and my mice.

I want to thank the personnel at the Turku PET Centre, past and present, for a good working environment. I thank the skilled personnel of the MC-PET group, particularly Tove Grönroos, Tarja Marttila and Marko Vehmanen. Thanks to Rami Mikkola and Marko Tättäläinen for making the world of computers ever so easy, Mika Teräs and Tuula Tolvanen for their expert help with PET technology, and Mirja Jyrkinen and Sinikka Lehtola for taking care of secretarial matters. I wish to express my thanks to medical laboratory technologists Sanna Suominen and Heidi Lappalainen, Leena Tokoi, and to Henri Sipilä for help in handling the radiotracers and metabolites, and the radiographers and other personnel for their help and for lively discussions around the coffee table.

I warmly thank all my fellow researchers at the Turku PET Centre and from the ‘CarMet’ and ‘Plaque Project’ groups, especially Marco Bucci, Erika Hoppela, Gaber Komar, Riikka Lautamäki, Kari Kalliokoski and Jarna Hannukainen. In particular, I wish to thank Pauliina, Anu, Tiina, Jarkko, Tommi, Henkka and Nikke for their friendship and all the fun. It has been essential for me to have the chance to ventilate ideas with you and always find company to talk with.

I owe my deepest gratitude to my parents Raija and Markku for their unconditional love and support. My brother Petteri, Satu and Oskari, you are very precious to me. I want to thank the Kervinen family for always being there for me, and for providing a lovely, comfortable room in which to write this thesis during the past summer. Aunts Marja and Marjut, I owe my love for biology and my interest in the academic world to you. My dear godchildren Heidi, Oskari, Hilla, Pyry and Kalle; thank you for bringing joy to my life. I consider myself extremely fortunate to have so many friends in my

life; I thank you all for all the love and support. Especially Terhi, Noora, Silja, Heli, Anu, Pauliina and Lotta, who have shared the ups and downs of my life, thank you for your friendship. To my friends in Slavonic Tractor, TYYn kuoro, Petsn'boys, Littoisten Pirtapiiat and Roineen Tytöt, I say: thank you for the music, and thanks for luring me away from the office to enjoy life.

This work has been financially supported by the Finnish Cultural Foundation, the Turku University Foundation, the Ida Montin Foundation, the Aarne Koskelo Foundation, the Finnish Foundation for Cardiovascular Research, and the Instrumentarium Foundation. The work is also partly supported by EC-FP6-project DiMI (LSHBCT-2005-512146), the Finnish Centre of Excellence in Molecular Imaging in Cardiovascular and Metabolic Research, supported by the Academy of Finland, the University of Turku, Turku University Hospital and Åbo Akademi University; and Turku Centre for Disease Modelling.

Turku, November 2009

Iina Laitinen

9. REFERENCES

Agellon LB, Walsh A, Hayek T et al. Reduced high density lipoprotein cholesterol in human cholesteryl ester transfer protein transgenic mice. J Biol Chem 1991;266:10796-801.

Alexanderson E, Slomka P, Cheng V et al. Fusion of positron emission tomography and coronary computed tomographic angiography identifies fluorine 18 fluorodeoxyglucose uptake in the left main coronary artery soft plaque. J Nucl Cardiol 2008;15:841-3.

Annovazzi A, Bonanno E, Arca M, D'Alessandria C, Marcoccia A, Spagnoli LG et al. 99mTc-interleukin-2 scintigraphy for the in vivo imaging of vulnerable atherosclerotic plaques. Eur J Nucl Med Mol Imaging 2006;33:117-126.

Antonov AS, Kolodgie FD, Munn DH,.Gerrity RG. Regulation of macrophage foam cell formation by alphaVbeta3 integrin: potential role in human atherosclerosis. Am J Pathol 2004;165:247-258.

Artinger S, Deiner C, Loddenkemper C, Schwimmbeck PL, Schultheiss HP, Pels K. Complex porcine model of atherosclerosis: induction of early coronary lesions after long-term hyperlipidemia without sustained hyperglycemia. Can J Cardiol 2009;25:e109-e114.

Aziz K, Berger K, Claycombe K, Huang R, Patel R, Abela GS. Noninvasive detection and localization of vulnerable plaque and arterial thrombosis with computed tomography angiography/positron emission tomography. Circulation 2008;117:2061-70.

Badimon L, Martinez-Gonzalez J, Royo T, Lassila R, Badimon JJ. A sudden increase in plasma epinephrine levels transiently enhances platelet deposition on severely damaged arterial wall--studies in a porcine model. Thromb Haemost 1999;82:1736-42.

Bazzichi L, Betti L, Giannaccini G, Rossi A,.Lucacchini A. Peripheral-type benzodiazepine receptors in human mononuclear cells of patients affected by osteoarthritis, rheumatoid arthritis or psoriasic arthritis. Clinical Biochemistry 2003;36:57-60.

Bayes-Genis A, Kantor B, Keelan PC et al. Restenosis and Hyperplasia: Animal Models. Curr Interv Cardiol Rep 2000;2:303-8.

Beer AJ, Haubner R, Goebel M, Luderschmidt S, Spilker ME, Wester HJ et al. Biodistribution and pharmacokinetics of the alphavbeta3-selective tracer 18F-galacto-RGD in cancer patients. J Nucl Med 2005;46:1333-1341.

Bennett MR, Macdonald K, Chan SW, Boyle JJ, Weissberg PL. Cooperative interactions between RB and p53 regulate cell proliferation, cell senescence, and apoptosis in human vascular smooth muscle cells from atherosclerotic plaques. Circ Res 1998;82:704-12.

von Birgelen C, Hartmann M, Mintz GS, van Houwelingen KG, Deppermann N, Schmermund A, Böse D, Eggebrecht H, Neumann T, Gössl M, Wieneke H, Erbel R. Relationship between cardiovascular risk as predicted by established risk scores versus plaque progression as measured by serial intravascular ultrasound in left main coronary arteries. Circulation. 2004 ;110(12):1579-85.

Boyle JJ, Bowyer DE, Weissberg PL, Bennett MR. Human blood-derived macrophages induce apoptosis in human plaque-derived vascular smooth muscle cells by Fas-ligand/Fas interactions. Arterioscler Thromb Vasc Biol 2001;21:1402-7.

Brandl R, Richter T, Haug K, Wilhelm MG, Maurer PC,.Nathrath W. Topographic analysis of proliferative activity in carotid endarterectomy specimens by immunocytochemical detection of the cell cycle-related antigen Ki-67. Circulation 1997;96:3360-3368.

Branley HM, du Bois RM, Wells AU,.Jones HA. Peripheral-type benzodiazepine receptors in bronchoalveolar lavage cells of patients with interstitial lung disease. Nucl Med Biol 2007;34:553-558.

Brindle K. New approaches for imaging tumour responses to treatment. Nat Rev Cancer. 2008;8(2):94-107.

Broisat A, Riou LM, Ardisson V, Boturyn D, Dumy P, Fagret D et al. Molecular imaging of vascular cell adhesion molecule-1 expression in experimental atherosclerotic plaques with radiolabelled B2702-p. Eur J Nucl Med Mol Imaging 2007;34:830-840.

Brooks PC, Clark RA,.Cheresh DA. Requirement of vascular integrin alpha v beta 3 for angiogenesis. Science 1994;264:569-571.

Brown GD, Osman S, Wilson HK, Abogye E, Price PM, Luthra SK et al. Metabolism of [11c-Methyl]choline in tumour bearing mice and synthesis and isolation of its catabolite [11c-Methyl]betaine. J Labelled Cpd Radiopharm 2001;44:S107-S09.

Brown BG, Zhao XQ. Is intravascular ultrasound the gold standard surrogate for clinically relevant atherosclerosis progression? J Am Coll Cardiol. 2007;49(9):933-8.

Bucerius J, Schmaljohann J, Bohm I, Palmedo H, Guhlke S, Tiemann K et al. Feasibility of 18F-fluoromethylcholine PET/CT for imaging of vessel wall alterations in humans--first results. Eur J Nucl Med Mol Imaging 2008;35:815-820.

Burtea C, Laurent S, Murariu O, Rattat D, Toubeau G, Verbruggen A et al. Molecular imaging of alpha v beta3 integrin expression in atherosclerotic plaques with a mimetic of RGD peptide grafted to Gd-DTPA. Cardiovasc Res 2008;78:148-157.

Carmeliet P, Moons L, Collen D. Mouse models of angiogenesis, arterial stenosis, atherosclerosis and hemostasis. Cardiovasc Res 1998;39:8-33.

Casellas P, Galiegue S,.Basile AS. Peripheral benzodiazepine receptors and mitochondrial function. Neurochem Int 2002;40:475-486.

Cerqueira MD, Stratton JR, Vracko R, Schaible TF, Ritchie JL. Noninvasive arterial thrombus imaging with 99mTc monoclonal antifibrin antibody. Circulation 1992;85:298-304.

Cheng C, Tempel D, van Haperen R et al. Atherosclerotic lesion size and vulnerability are determined by patterns of fluid shear stress. Circulation 2006;113:2744-53.

Choudhury RP, Fisher EA. Molecular imaging in atherosclerosis, thrombosis, and vascular inflammation. Arterioscler Thromb Vasc Biol 2009;29:983-91.

Chu B, Kampschulte A, Ferguson MS et al. Hemorrhage in the atherosclerotic carotid plaque: a high-resolution MRI study. Stroke 2004;35:1079-84.

Cipollone F, Fazia M, Mezzetti A. Novel determinants of plaque instability. J Thromb Haemost 2005;3:1962-75.

Curtiss LK, Boisvert WA. Apolipoprotein E and atherosclerosis. Curr Opin Lipidol 2000;11:243-51.

Dalager S, Falk E, Kristensen IB,.Paaske WP. Plaque in superficial femoral arteries indicates generalized atherosclerosis and vulnerability to coronary death: an autopsy study. J Vasc Surg 2008;47:296-302.

Davies MJ. Anatomic features in victims of sudden coronary death. Coronary artery pathology. Circulation 1992;85:I19-I24.

Debruyne JC, Versijpt J, Van Laere KJ, De Vos F, Keppens J, Strijckmans K et al. PET visualization of microglia in multiple sclerosis patients using [11C]PK11195. Eur J Neurol 2003;10:257-264.

DeGraba TJ, Siren AL, Penix L, McCarron RM, Hargraves R, Sood S et al. Increased endothelial expression of intercellular adhesion molecule-1 in symptomatic versus asymptomatic human carotid atherosclerotic plaque. Stroke 1998;29:1405-1410.

Deichen JT, Prante O, Gack M, Schmiedehausen K, Kuwert T. Uptake of [18F]fluorodeoxyglucose in human monocyte-macrophages in vitro. Eur J Nucl Med Mol Imaging 2003;30:267-73.

Dobrucki LW, Sinusas AJ. Molecular imaging. A new approach to nuclear cardiology. Q J Nucl Med Mol Imaging. 2005;49(1):106-15.

Duivenvoorden R, de Groot E, Stroes ES, Kastelein JJ. Surrogate markers in clinical trials--challenges and opportunities. Atherosclerosis. 2009;206(1):8-16.

Dunphy MP, Freiman A, Larson SM,.Strauss HW. Association of Vascular 18F-FDG Uptake with Vascular Calcification. J Nucl Med 2005;46:1278-1284.

Elmaleh DR, Fischman AJ, Tawakol A, Zhu A, Shoup TM, Hoffmann U et al. Detection of inflamed atherosclerotic lesions with diadenosine-5',5'"-P1,P4-tetraphosphate (Ap4A) and positron-emission tomography. Proc Natl Acad Sci U S A 2006;103: 15992-15996.

Falk E, Shah PK, Fuster V. Coronary plaque disruption. Circulation 1995;92:657-71.

Falk E. Pathogenesis of atherosclerosis. J Am Coll Cardiol 2006;47:C7-12.

Falk E, Schwartz SM, Galis ZS, Rosenfeld ME. Putative murine models of plaque rupture. Arterioscler Thromb Vasc Biol 2007;27:969-72.

Farb A, Burke AP, Tang AL et al. Coronary plaque erosion without rupture into a lipid core. A frequent cause of coronary thrombosis in sudden coronary death. Circulation 1996;93:1354-63.

Farese RV, Jr., Veniant MM, Cham CM, Flynn LM, Pierotti V, Loring JF et al. Phenotypic analysis of mice expressing exclusively apolipoprotein B48 or apolipoprotein B100. Proc Natl Acad Sci U S A 1996;93:6393-6398.

Fernandez-Ortiz A, Badimon JJ, Falk E et al. Characterization of the relative thrombogenicity of atherosclerotic plaque components: implications for consequences of plaque rupture. J Am Coll Cardiol 1994;23:1562-9.

Fleiner M, Kummer M, Mirlacher M, Sauter G, Cathomas G, Krapf R et al. Arterial neovascularization and

inflammation in vulnerable patients: early and late signs of symptomatic atherosclerosis. Circulation 2004;110:2843-2850.

Fujimoto S, Hartung D, Ohshima S, Edwards DS, Zhou J, Yalamanchili P et al. Molecular imaging of matrix metalloproteinase in atherosclerotic lesions: resolution with dietary modification and statin therapy. J Am Coll Cardiol 2008;52:1847-1857.

Fullerton MD, Wagner L, Yuan Z,.Bakovic M. Impaired trafficking of choline transporter-like protein-1 at plasma membrane and inhibition of choline transport in THP-1 monocyte-derived macrophages. Am J Physiol Cell Physiol 2006;290:C1230-C1238.

Fuster V, Badimon L, Badimon JJ, Chesebro JH. The pathogenesis of coronary artery disease and the acute coronary syndromes (1). N Engl J Med 1992;326:242-50.

Galis ZS, Sukhova GK, Kranzhofer R, Clark S, Libby P. Macrophage foam cells from experimental atheroma constitutively produce matrix-degrading proteinases. Proc Natl Acad Sci U S A 1995;92:402-6.

Gimbrone MA, Jr., Nagel T, Topper JN. Biomechanical activation: an emerging paradigm in endothelial adhesion biology. J Clin Invest 1997;99:1809-13.

Glagov S, Weisenberg E, Zarins CK, Stankunavicius R, Kolettis GJ. Compensatory enlargement of human atherosclerotic coronary arteries. N Engl J Med 1987;316:1371-5.

Gough PJ, Gomez IG, Wille PT, Raines EW. Macrophage expression of active MMP-9 induces acute plaque disruption in apoE-deficient mice. J Clin Invest 2006;116:59-69.

Graebe M, Pedersen SF, Borgwardt L, Hojgaard L, Sillesen H, Kjaer A. Molecular pathology in vulnerable carotid plaques: correlation with [18]-fluorodeoxyglucose positron emission tomography (FDG-PET). Eur J Vasc Endovasc Surg 2009;37:714-21.

Goldstein JA, Demetriou D, Grines CL, Pica M, Shoukfeh M,.O'Neill WW. Multiple complex coronary plaques in patients with acute myocardial infarction. N Engl J Med 2000;343:915-922.

Hamacher K, Coenen HH,.Stocklin G. Efficient stereospecific synthesis of no-carrier-added 2-[18F]-fluoro-2-deoxy-D-glucose using aminopolyether supported nucleophilic substitution. J Nucl Med 1986;27:235-238.

Hara T, Kosaka N, Shinoura N,.Kondo T. PET imaging of brain tumor with [methyl-11C]choline. J Nucl Med 1997;38:842-847.

Hara T, Kosaka N,.Kishi H. PET imaging of prostate cancer using carbon-11-choline. J Nucl Med 1998;39:990-995.

Hardwick MJ, Chen MK, Baidoo K, Pomper MG,.Guilarte TR. In vivo imaging of peripheral benzodiazepine receptors in mouse lungs: a biomarker of inflammation. Mol Imaging 2005;4:432-438.

Hartung D, Sarai M, Petrov A, Kolodgie F, Narula N, Verjans J et al. Resolution of apoptosis in atherosclerotic plaque by dietary modification and statin therapy. J Nucl Med 2005;46:2051-2056.

Hartung D, Petrov A, Haider N, Fujimoto S, Blankenberg F, Fujimoto A et al. Radiolabeled Monocyte Chemotactic Protein 1 for the detection of inflammation in experimental atherosclerosis. J Nucl Med 2007;48:1816-1821.

Haubner R, Wester HJ, Weber WA, Mang C, Ziegler SI, Goodman SL et al. Noninvasive imaging of alpha(v)beta3 integrin expression using 18F-labeled RGD-containing glycopeptide and positron emission tomography. Cancer Res 2001;61:1781-1785.

Haubner R, Kuhnast B, Mang C, Weber WA, Kessler H, Wester HJ et al. [18F]Galacto-RGD: synthesis, radiolabeling, metabolic stability, and radiation dose estimates. Bioconjug Chem 2004;15:61-69.

Haubner R, Weber WA, Beer AJ, Vabuliene E, Reim D, Sarbia M et al. Noninvasive visualization of the activated alphavbeta3 integrin in cancer patients by positron emission tomography and [18F]Galacto-RGD. PLoS Med 2005;2:e70-

Haukkala J, Laitinen I, Luoto P et al. (68)Ga-DOTA-RGD peptide: biodistribution and binding into atherosclerotic plaques in mice. Eur J Nucl Med Mol Imaging 2009.

Heinonen SE, Leppänen P, Kholova I, Lumivuori H, Hakkinen SK, Bosch F et al. Increased atherosclerotic lesion calcification in a novel mouse model combining insulin resistance, hyperglycemia, and hypercholesterolemia.Circ Res 2007;101:1058-1067.

Hermann S, Kuhlmann M, Faust A, Kopka K,.Schafers M. Imaging of Intracellular Caspase-3 to Visualize Apoptosis [presentation 0154]. Presented at the World Molecular Imaging Congress Nice, France, September 10-13, 2008 2008;

Hermanowski-Vosatka A, Balkovec JM, Cheng K, Chen HY, Hernandez M, Koo GC, Le Grand CB et al. 11beta-HSD1 inhibition ameliorates metabolic syndrome and prevents progression of atherosclerosis in mice. J Exp Med. 2005;202(4):517-27.

Higuchi T, Bengel FM, Seidl S, Watzlowik P, Kessler H, Hegenloh R et al. Assessment of alphavbeta3 integrin expression after myocardial infarction by positron emission tomography. Cardiovasc Res 2008;78:395-403.

Hollander M, Hak AE, Koudstaal PJ, Bots ML, Grobbee DE, Hofman A et al. Comparison between measures of atherosclerosis and risk of stroke: the Rotterdam Study. Stroke 2003;34:2367-2372.

Hoppela E, Kankaanpää M, Parkkola R, Roine S, Ikonen T, Raitakari O et al. Imaging of human inflammatory plaques using [11C]-PK11195 and [18F]-FDG. J Nucl Card 2007;14: [abstract 8.15]

Hoshiga M, Alpers CE, Smith LL, Giachelli CM,.Schwartz SM. Alpha-v beta-3 integrin expression in normal and atherosclerotic artery. Circ Res 1995;77:1129-1135.

Hua J, Dobrucki LW, Sadeghi MM, Zhang J, Bourke BN, Cavaliere P et al. Noninvasive imaging of angiogenesis with a 99mTc-labeled peptide targeted at alphavbeta3 integrin after murine hindlimb ischemia. Circulation 2005;111:3255-3260.

Hyafil F, Cornily JC, Feig JE et al. Noninvasive detection of macrophages using a nanoparticulate contrast agent for computed tomography. Nat Med 2007;13:636-41.

Ishibashi S, Brown MS, Goldstein JL, Gerard RD, Hammer RE, Herz J. Hypercholesterolemia in low density lipoprotein receptor knockout mice and its reversal by adenovirus-mediated gene delivery. J Clin Invest 1993;92:883-93.

Ishino S, Mukai T, Kuge Y, Kume N, Ogawa M, Takai N et al. Targeting of lectinlike oxidized low-density lipoprotein receptor 1 (LOX-1) with 99mTc-labeled anti-LOX-1 antibody: potential agent for imaging of vulnerable plaque. J Nucl Med 2008;49:1677-1685.

Isobe S, Tsimikas S, Zhou J, Fujimoto S, Sarai M, Branks MJ et al. Noninvasive imaging of atherosclerotic lesions in apolipoprotein E-deficient and low-density-lipoprotein receptor-deficient mice with annexin A5. J Nucl Med 2006;47:1497-1505.

Iuliano L, Mauriello A, Sbarigia E, Spagnoli LG, Violi F. Radiolabeled native low-density lipoprotein injected into patients with carotid stenosis accumulates in macrophages of atherosclerotic plaque : effect of vitamin E supplementation. Circulation 2000;101:1249-54.

Jackson CL. Defining and defending murine models of plaque rupture. Arterioscler Thromb Vasc Biol 2007;27:973-7.

Jackson CL, Bennett MR, Biessen EA, Johnson JL, Krams R. Assessment of unstable atherosclerosis in mice. Arterioscler Thromb Vasc Biol 2007;27:714-20.

Jander S, Sitzer M, Schumann R, Schroeter M, Siebler M, Steinmetz H et al. Inflammation in high-grade carotid stenosis: a possible role for macrophages and T cells in plaque destabilization. Stroke 1998;29:1625-1630.

Jawien J, Nastalek P,.Korbut R. Mouse models of experimental atherosclerosis. J Physiol Pharmacol 2004;55:503-517.

Johnson J, Carson K, Williams H et al. Plaque rupture after short periods of fat feeding in the apolipoprotein E-knockout mouse: model characterization and effects of pravastatin treatment. Circulation 2005;111:1422-30.

Jones HA, Valind SO, Clark IC, Bolden GE, Krausz T, Schofield JB et al. Kinetics of lung macrophages monitored in vivo following particulate challenge in rabbits.Toxicol Appl Pharmacol 2002;183:46-54.

Jones HA, Marino PS, Shakur BH,.Morrell NW. In vivo assessment of lung inflammatory cell activity in patients with COPD and asthma.Eur Respir J 2003;21:567-573.

Kaartinen M, Penttila A, Kovanen PT. Accumulation of activated mast cells in the shoulder region of human coronary atheroma, the predilection site of atheromatous rupture. Circulation 1994;90:1669-78.

Kato K, Schober O, Ikeda M, Schafers M, Ishigaki T, Kies P et al. Evaluation and comparison of (11)C-choline uptake and calcification in aortic and common carotid arterial walls with combined PET/CT. Eur J Nucl Med Mol Imaging 2009;

Kaufmann RB, Peyser PA, Sheedy PF, Rumberger JA, Schwartz RS. Quantification of coronary artery calcium by electron beam computed tomography for determination of severity of angiographic coronary artery disease in younger patients. J Am Coll Cardiol. 1995;25(3):626-32.

Kaufmann BA, Lindner JR. Molecular imaging with targeted contrast ultrasound. Curr Opin Biotechnol 2007;18:11-6.

Khan Q, Mehta JL. Relevance of platelet-independent effects of aspirin to its salutary effect in atherosclerosis-related events. J Atheroscler Thromb 2005;12:185-90.

Kherlopian AR, Song T, Duan Q, Neimark MA, Po MJ, Gohagan JK, Laine AF. A review of imaging techniques for systems biology. BMC Syst Biol. 2008 Aug 12;2:74.

Kietselaer BL, Reutelingsperger CP, Heidendal GA et al. Noninvasive detection of plaque instability with use of radiolabeled annexin A5 in patients with carotid-artery atherosclerosis. N Engl J Med 2004;350:1472-3.

Kircher MF, Grimm J, Swirski FK, Libby P, Gerszten RE, Allport JR et al. Noninvasive in vivo imaging of monocyte trafficking to atherosclerotic lesions. Circulation 2008;117:388-395.

Kokki T, Teräs M, Sipilä HT, Noponen T,.Knuuti J. Dual Gating Method for Eliminating Motion-Related Inaccuracies in Cardiac PET [presentation M19-231]. Presented at the 2007 IEEE Medical Imaging Conference, Hawaii, USA, Oct 27-Nov 3, 2007 2007;

Kolodgie FD, Gold HK, Burke AP, Fowler DR, Kruth HS, Weber DK et al. Intraplaque hemorrhage and progression of coronary atheroma. N Engl J Med 2003 (a);349:2316-2325.

Kolodgie FD, Petrov A, Virmani R et al. Targeting of apoptotic macrophages and experimental atheroma with radiolabeled annexin V: a technique with potential for noninvasive imaging of vulnerable plaque. Circulation. 2003 (b);108:3134-9.

Kubota R, Kubota K, Yamada S, Tada M, Ido T, Tamahashi N. Microautoradiographic study for the differentiation of intratumoral macrophages, granulation tissues and cancer cells by the dynamics of fluorine-18-fluorodeoxyglucose uptake. J Nucl Med 1994;35:104-12.

Laurberg JM, Olsen AK, Hansen SB, Bottcher M, Morrison M, Ricketts SA et al. Imaging of vulnerable atherosclerotic plaques with FDG-microPET: no FDG accumulation. Atherosclerosis 2007;192:275-282.

Lee SJ, On YK, Lee EJ, Choi JY, Kim BT,.Lee KH. Reversal of vascular 18F-FDG uptake with plasma high-density lipoprotein elevation by atherogenic risk reduction. J Nucl Med 2008;49:1277-1282.

Lendon CL, Davies MJ, Born GV, Richardson PD. Atherosclerotic plaque caps are locally weakened when macrophages density is increased. Atherosclerosis 1991;87:87-90.

Leppänen P, Koota S, Kholova I, Koponen J, Fieber C, Eriksson U et al. Gene transfers of vascular endothelial growth factor-A, vascular endothelial growth factor-B, vascular endothelial growth factor-C, and vascular endothelial growth factor-D have no effects on atherosclerosis in hypercholesterolemic low-density lipoprotein-receptor/apolipoprotein B48-deficient mice. Circulation 2005;112:1347-1352.

Leskinen MJ, Kovanen PT, Lindstedt KA. Regulation of smooth muscle cell growth, function and death in vitro by activated mast cells--a potential mechanism for the weakening and rupture of atherosclerotic plaques. Biochem Pharmacol 2003;66:1493-8.

Li H, Cybulsky MI, Gimbrone MA, Jr., Libby P. An atherogenic diet rapidly induces VCAM-1, a cytokine-regulatable mononuclear leukocyte adhesion molecule, in rabbit aortic endothelium. Arterioscler Thromb 1993;13:197-204.

Libby P. Inflammation in atherosclerosis. Nature 2002;420:868-874.

Libby P, Theroux P. Pathophysiology of coronary artery disease. Circulation 2005;111:3481-3488.

Loftus IM, Naylor AR, Goodall S et al. Increased matrix metalloproteinase-9 activity in unstable carotid plaques. A potential role in acute plaque disruption. Stroke 2000;31:40-7.

von Lukowicz T, Silacci M, Wyss MT, Trachsel E, Lohmann C, Buck A et al. Human antibody against C domain of tenascin-C visualizes murine atherosclerotic plaques ex vivo. J Nucl Med 2007;48:582-587.

MacNeill BD, Jang IK, Bouma BE, Iftimia N, Takano M, Yabushita H et al. Focal and multi-focal plaque macrophage distributions in patients with acute and stable presentations of coronary artery disease. J Am Coll Cardiol 2004;44:972-979.

Mahley RW. Apolipoprotein E: cholesterol transport protein with expanding role in cell biology. Science 1988;240:622-30.

Mahmoudi M, Curzen N, Gallagher PJ. Atherogenesis: the role of inflammation and infection. Histopathology. 2007 Apr;50(5):535-46.

Makowski MR, Ebersberger U, Nekolla S,.Schwaiger M. In vivo molecular imaging of angiogenesis, targeting alphavbeta3 integrin expression, in a patient after acute myocardial infarction. Eur Heart J 2008;29:2201-

Martinez-Möller A, Zikic D, Botnar RM, Bundschuh RA, Howe W, Ziegler SI et al. Dual cardiac-respiratory gated PET: implementation and results from a feasibility study. Eur J Nucl Med Mol Imaging 2007;34:1447-1454.

Matter CM, Wyss MT, Meier P, Spath N, von Lukowicz T, Lohmann C et al. 18F-choline images murine atherosclerotic plaques ex vivo. Arterioscler Thromb Vasc Biol 2006;26:584-589.

Moreno PR, Purushothaman KR, Fuster V et al. Plaque neovascularization is increased in ruptured atherosclerotic lesions of human aorta: implications for plaque vulnerability. Circulation 2004;110:2032-8.

Moulton KS, Heller E, Konerding MA, Flynn E, Palinski W,.Folkman J. Angiogenesis inhibitors endostatin or TNP-470 reduce intimal neovascularization and plaque growth in apolipoprotein E-deficient mice. Circulation 1999;99:1726-1732.

Naghavi M, Libby P, Falk E, Casscells SW, Litovsky S, Rumberger J et al. From vulnerable plaque to vulnerable

patient: a call for new definitions and risk assessment strategies: Part I. Circulation 2003;108:1664-1672.

Naghavi M, Falk E, Hecht HS, Jamieson MJ, Kaul S, Berman D et al. From vulnerable plaque to vulnerable patient--Part III: Executive summary of the Screening for Heart Attack Prevention and Education (SHAPE) Task Force report. Am J Cardiol 2006;98:2H-15H.

Någren K, Halldin C. Methylation of amide and thiol functions with [11C]methyl trifilate, examplified by [11c]NMSP, [11c]flumazenil and [11c]methionine. Journal of Labelled Compounds and Radiopharmaceuticals 1998;41:831-841.

Nahrendorf M, Zhang H, Hembrador S, Panizzi P, Sosnovik DE, Aikawa E et al. Nanoparticle PET-CT imaging of macrophages in inflammatory atherosclerosis. Circulation 2008 (a);117:379-387.

Nahrendorf M, Keliher E, Panizzi P, Zhang H, Hembrador S, Libby P et al. Abstract 5788: VCAM-1 Targeted PET-CT Detects Inflammatory Atherosclerotic Plaques. Circulation 2008(b); 118: S_102

Narula J, Garg P, Achenbach S, Motoyama S, Virmani R,.Strauss HW. Arithmetic of vulnerable plaques for noninvasive imaging. Nat Clin Pract Cardiovasc Med 2008;5 Suppl 2:S2-10.

Nemerson Y. Tissue factor and hemostasis. Blood 1988;71:1-8.

Ogawa M, Magata Y, Kato T et al. Application of 18F-FDG PET for monitoring the therapeutic effect of antiinflammatory drugs on stabilization of vulnerable atherosclerotic plaques. J Nucl Med 2006;47:1845-50.

Ohtsuki K, Hayase M, Akashi K, Kopiwoda S,.Strauss HW. Detection of monocyte chemoattractant protein-1 receptor expression in experimental atherosclerotic lesions: an autoradiographic study. Circulation 2001;104:203-208.

Paigen B, Ishida BY, Verstuyft J, Winters RB, Albee D. Atherosclerosis susceptibility differences among progenitors of recombinant inbred strains of mice. Arteriosclerosis 1990;10:316-23.

Papalambros E, Sigala F, Georgopoulos S et al. Vascular endothelial growth factor and matrix metalloproteinase 9 expression in human carotid atherosclerotic plaques: relationship with plaque destabilization via neovascularization. Cerebrovasc Dis 2004;18:160-5.

Park SJ, Ionascu D, Killoran J, Mamede M, Gerbaudo VH, Chin L et al. Evaluation of the combined effects of target size, respiratory motion and background activity on 3D and 4D PET/CT images. Phys Med Biol 2008;53:3661-3679.

Paulmier B, Duet M, Khayat R et al. Arterial wall uptake of fluorodeoxyglucose on PET imaging in stable cancer disease patients indicates higher risk for cardiovascular events. J Nucl Cardiol 2008;15:209-17.

Pichler BJ, Kneilling M, Haubner R, Braumuller H, Schwaiger M, Rocken M et al. Imaging of delayed-type hypersensitivity reaction by PET and 18F-galacto-RGD. J Nucl Med 2005;46:184-189.

Pletcher MJ, Tice JA, Pignone M,.Browner WS. Using the coronary artery calcium score to predict coronary heart disease events: a systematic review and meta-analysis. Arch Intern Med 2004;164:1285-1292.

Podichetty AK, Wagner S, Schroer S et al. Fluorinated isatin derivatives. Part 2. New N-substituted 5-pyrrolidinylsulfonyl isatins as potential tools for molecular imaging of caspases in apoptosis. J Med Chem 2009;52:3484-95.

Pucci A, Sheiban I, Formato L et al. In vivo coronary plaque histology in patients with stable and acute coronary syndromes: relationships with hyperlipidemic status and statin treatment. Atherosclerosis 2007;194:189-95.

Rader DJ, Daugherty A. Translating molecular discoveries into new therapies for atherosclerosis. Nature 2008;451:904-13.

Rajavashisth TB, Andalibi A, Territo MC et al. Induction of endothelial cell expression of granulocyte and macrophage colony-stimulating factors by modified low-density lipoproteins. Nature 1990;344:254-7.

Ravensbergen J, Ravensbergen JW, Krijger JK, Hillen B, Hoogstraten HW. Localizing role of hemodynamics in atherosclerosis in several human vertebrobasilar junction geometries. Arterioscler Thromb Vasc Biol 1998;18:708-16.

Reddick RL, Zhang SH, Maeda N. Aortic atherosclerotic plaque injury in apolipoprotein E deficient mice. Atherosclerosis 1998;140:297-305.

Rekhter MD, Gordon D. Active proliferation of different cell types, including lymphocytes, in human atherosclerotic plaques. Am J Pathol 1995;147:668-677.

Ridker PM, Rifai N, Pfeffer MA, Sacks F, Braunwald E. Long-term effects of pravastatin on plasma concentration of C-reactive protein. The Cholesterol and Recurrent Events (CARE) Investigators. Circulation 1999;100:230-5.

Ridker PM, Brown NJ, Vaughan DE, Harrison DG,.Mehta JL. Established and emerging plasma biomarkers in the

prediction of first atherothrombotic events. Circulation 2004;109:IV6-19.

Ridker PM, Danielson E, Fonseca FA et al. Reduction in C-reactive protein and LDL cholesterol and cardiovascular event rates after initiation of rosuvastatin: a prospective study of the JUPITER trial. Lancet 2009;373:1175-82.

Rioufol G, Gilard M, Finet G, Ginon I, Boschat J, Andre-Fouet X. Evolution of spontaneous atherosclerotic plaque rupture with medical therapy: long-term follow-up with intravascular ultrasound. Circulation 2004;110:2875-80.

Rittersma SZ, van der Wal AC, Koch KT et al. Plaque instability frequently occurs days or weeks before occlusive coronary thrombosis: a pathological thrombectomy study in primary percutaneous coronary intervention. Circulation 2005;111:1160-5.

Roivainen A, Forsback S, Gronroos T, Lehikoinen P, Kahkonen M, Sutinen E et al. Blood metabolism of [methyl-11C]choline; implications for in vivo imaging with positron emission tomography. Eur J Nucl Med 2000;27:25-32.

Roivainen A, Parkkola R, Yli-Kerttula T, Lehikoinen P, Viljanen T, Mottonen T et al. Use of positron emission tomography with methyl-11C-choline and 2-18F-fluoro-2-deoxy-D-glucose in comparison with magnetic resonance imaging for the assessment of inflammatory proliferation of synovium. Arthritis Rheum 2003;48:3077-3084.

Roivainen A, Nagren K, Hirvonen J et al. Whole-body distribution and metabolism of [N-methyl-11C](R)-1-(2-chlorophenyl)-N-(1-methylpropyl)-3-isoquinolinecarb oxamide in humans; an imaging agent for in vivo assessment of peripheral benzodiazepine receptor activity with positron emission tomography. Eur J Nucl Med Mol Imaging 2009;36:671-82.

Rosen MA, Jones RM, Yano Y,.Budinger TF. Carbon-11 choline: synthesis, purification, and brain uptake inhibition by 2-dimethylaminoethanol. J Nucl Med 1985;26:1424-1428.

Rosenfeld ME, Polinsky P, Virmani R, Kauser K, Rubanyi G, Schwartz SM. Advanced atherosclerotic lesions in the innominate artery of the ApoE knockout mouse. Arterioscler Thromb Vasc Biol 2000;20:2587-92.

Ross R. Atherosclerosis--an inflammatory disease. N Engl J Med 1999;340:115-26.

Rudd JH, Warburton EA, Fryer TD, Jones HA, Clark JC, Antoun N et al. Imaging atherosclerotic plaque inflammation with [18F]-fluorodeoxyglucose positron emission tomography. Circulation 2002;105:2708-2711.

Rudd JH, Myers KS, Bansilal S, Machac J, Rafique A, Farkouh M et al. (18)Fluorodeoxyglucose positron emission tomography imaging of atherosclerotic plaque inflammation is highly reproducible: implications for atherosclerosis therapy trials. J Am Coll Cardiol 2007;50:892-896.

Rudd JH, Fayad ZA, Machac J, Weissberg PL, Davies JR, Warburton EA, Tawakol AA, Strauss HW, Fuster V. Response to 'Laurberg JM, Olsen AK, Hansen SB, et al. Imaging of vulnerable atherosclerotic plaques with FDG-microPET: no FDG accumulation'. Atherosclerosis. 2007 (b) ;192:453-4;

Rudd JH, Myers KS, Bansilal S, Machac J, Pinto CA, Tong C et al. Atherosclerosis inflammation imaging with 18F-FDG PET: carotid, iliac, and femoral uptake reproducibility, quantification methods, and recommendations. J Nucl Med 2008;49:871-878.

Sambola A, Osende J, Hathcock J et al. Role of risk factors in the modulation of tissue factor activity and blood thrombogenicity. Circulation 2003;107:973-7.

Sakalihasan N, Michel JB. Functional imaging of atherosclerosis to advance vascular biology. Eur J Vasc Endovasc Surg. 2009;37(6):728-34.

Sarai M, Hartung D, Petrov A, Zhou J, Narula N, Hofstra L et al. Broad and specific caspase inhibitor-induced acute repression of apoptosis in atherosclerotic lesions evaluated by radiolabeled annexin A5 imaging. J Am Coll Cardiol 2007;50:2305-2312.

Saraste A, Kytö V, Laitinen I, Saraste M, Leppänen P, Ylä-Herttuala S et al. Severe coronary artery stenoses and reduced coronary flow velocity reserve in atherosclerotic mouse model: Doppler echocardiography validation study. Atherosclerosis 2008;200:89-94.

Schapira K, Heeneman S, Daemen MJ. Animal models to study plaque vulnerability. Curr Pharm Des 2007;13:1013-20.

Schwartz SM, Galis ZS, Rosenfeld ME, Falk E. Plaque rupture in humans and mice. Arterioscler Thromb Vasc Biol 2007;27:705-13.

Schulz C, Penz S, Hoffmann C, Langer H, Gillitzer A, Schneider S et al. Platelet GPVI binds to collagenous structures in the core region of human atheromatous plaque and is critical for atheroprogression in vivo. Basic Res Cardiol 2008;103:356-367.

Schäfers M, Riemann B, Kopka K, Breyholz HJ, Wagner S, Schafers KP et al. Scintigraphic imaging of matrix metalloproteinase activity in the arterial wall in vivo. Circulation 2004;109:2554-2559.

Shah PK, Galis ZS. Matrix metalloproteinase hypothesis of plaque rupture: players keep piling up but questions remain. Circulation 2001;104:1878-80.

Soret M, Bacharach SL,.Buvat I. Partial-volume effect in PET tumor imaging. J Nucl Med 2007;48:932-945.

Spagnoli LG, Mauriello A, Sangiorgi G et al. Extracranial thrombotically active carotid plaque as a risk factor for ischemic stroke. JAMA 2004;292:1845-52.

Stary HC, Chandler AB, Dinsmore RE, Fuster V, Glagov S, Insull W, Jr. et al. A definition of advanced types of atherosclerotic lesions and a histological classification of atherosclerosis. A report from the Committee on Vascular Lesions of the Council on Arteriosclerosis, American Heart Association. Circulation 1995;92:1355-1374.

Stein PD, Yaekoub AY, Matta F,.Sostman HD. 64-slice CT for diagnosis of coronary artery disease: a systematic review. Am J Med 2008;121:715-725.

Stoll G, Bendszus M. Inflammation and atherosclerosis: novel insights into plaque formation and destabilization. Stroke 2006;37:1923-32.

Subramanian S, Han CY, Chiba T et al. Dietary cholesterol worsens adipose tissue macrophage accumulation and atherosclerosis in obese LDL receptor-deficient mice. Arterioscler Thromb Vasc Biol 2008;28:685-91.

Swirski FK, Pittet MJ, Kircher MF, Aikawa E, Jaffer FA, Libby P et al. Monocyte accumulation in mouse atherogenesis is progressive and proportional to extent of disease. Proc Natl Acad Sci U S A 2006;103: 10340-10345.

Tabas I. Consequences and therapeutic implications of macrophage apoptosis in atherosclerosis: the importance of lesion stage and phagocytic efficiency. Arterioscler Thromb Vasc Biol 2005;25:2255-64.

Tahara N, Kai H, Ishibashi M, Nakaura H, Kaida H, Baba K et al. Simvastatin attenuates plaque inflammation: evaluation by fluorodeoxyglucose positron emission tomography. J Am Coll Cardiol 2006;48:1825-1831.

Takaya N, Yuan C, Chu B et al. Presence of intraplaque hemorrhage stimulates progression of carotid atherosclerotic plaques: a high-resolution magnetic resonance imaging study. Circulation 2005;111:2768-75.

Tatsumi M, Cohade C, Nakamoto Y,.Wahl RL. Fluorodeoxyglucose uptake in the aortic wall at PET/CT: possible finding for active atherosclerosis. Radiology 2003;229:831-837.

Tawakol A, Migrino RQ, Hoffmann U, Abbara S, Houser S, Gewirtz H et al. Noninvasive in vivo measurement of vascular inflammation with F-18 fluorodeoxyglucose positron emission tomography. J Nucl Cardiol 2005;12:294-301.

Thumshirn G, Hersel U, Goodman SL,.Kessler H. Multimeric cyclic RGD peptides as potential tools for tumor targeting: solid-phase peptide synthesis and chemoselective oxime ligation. Chemistry 2003;9:2717-2725.

der Thusen JH, van Vlijmen BJ, Hoeben RC et al. Induction of atherosclerotic plaque rupture in apolipoprotein E-/- mice after adenovirus-mediated transfer of p53. Circulation 2002;105:2064-70.

Tian M, Zhang H, Oriuchi N, Higuchi T,.Endo K. Comparison of 11C-choline PET and FDG PET for the differential diagnosis of malignant tumors. Eur J Nucl Med Mol Imaging 2004;31:1064-1072.

Tobis J, Azarbal B, Slavin L. Assessment of intermediate severity coronary lesions in the catheterization laboratory. J Am Coll Cardiol 2007;49:839-48.

Vengrenyuk Y, Carlier S, Xanthos S et al. A hypothesis for vulnerable plaque rupture due to stress-induced debonding around cellular microcalcifications in thin fibrous caps. Proc Natl Acad Sci U S A 2006; 103:14678-83.

Veniant MM, Zlot CH, Walzem RL, Pierotti V, Driscoll R, Dichek D et al. Lipoprotein clearance mechanisms in LDL receptor-deficient "Apo-B48-only" and "Apo-B100-only" mice. J Clin Invest 1998;102:1559-1568.

Veniant MM, Sullivan MA, Kim SK, Ambroziak P, Chu A, Wilson MD et al. Defining the atherogenicity of large and small lipoproteins containing apolipoprotein B100. J Clin Invest 2000;106:1501-1510.

Virgolini I, Angelberger P, O'Grady J, Sinzinger H. Low density lipoprotein labelling characterizes experimentally induced atherosclerotic lesions in rabbits in vivo as to presence of foam cells and endothelial coverage. Eur J Nucl Med 1991;18:944-7.

Virmani R, Kolodgie FD, Burke AP, Farb A,.Schwartz SM. Lessons from sudden coronary death: a comprehensive morphological classification scheme for atherosclerotic lesions. Arterioscler Thromb Vasc Biol 2000;20:1262-1275.

Virmani R, Kolodgie FD, Burke AP, Finn AV, Gold HK, Tulenko TN et al. Atherosclerotic plaque progression and vulnerability to rupture: angiogenesis as a source of intraplaque hemorrhage. Arterioscler Thromb Vasc Biol 2005;25:2054-2061.

van der Wal AC, Becker AE, van der Loos CM, Das PK. Site of intimal rupture or erosion of thrombosed coronary atherosclerotic plaques is characterized by an inflammatory process irrespective of the dominant plaque morphology. Circulation 1994;89:36-44.

van der Wal AC, Becker AE. Atherosclerotic plaque rupture--pathologic basis of plaque stability and instability. Cardiovasc Res 1999;41:334-44.

Waldeck J, Hager F, Holtke C, Lanckohr C, von Wallbrunn A, Torsello G et al. Fluorescence Reflectance Imaging of Macrophage-Rich Atherosclerotic Plaques Using an {alpha}v{beta}3 Integrin-Targeted Fluorochrome. J Nucl Med 2008;49:1845-1851.

Whitman SC, Ravisankar P, Elam H, Daugherty A. Exogenous interferon-gamma enhances atherosclerosis in apolipoprotein E-/- mice. Am J Pathol 2000;157:1819-24.

Whitman SC, Ravisankar P, Daugherty A. Interleukin-18 enhances atherosclerosis in apolipoprotein E(-/-) mice through release of interferon-gamma. Circ Res 2002;90:E34-E38.

Williams G, Kolodny GM. Suppression of myocardial 18F-FDG uptake by preparing patients with a high-fat, low-carbohydrate diet. AJR Am J Roentgenol 2008;190:W151-W156.

Williams KJ, Tabas I. The response-to-retention hypothesis of atherogenesis reinforced. Curr Opin Lipidol 1998;9:471-4.

Winter PM, Morawski AM, Caruthers SD, Fuhrhop RW, Zhang H, Williams TA et al. Molecular imaging of angiogenesis in early-stage atherosclerosis with alpha(v)beta3-integrin-targeted nanoparticles. Circulation 2003;108:2270-2274.

Worthley SG, Zhang ZY, Machac J et al. In vivo non-invasive serial monitoring of FDG-PET progression and regression in a rabbit model of atherosclerosis. Int J Cardiovasc Imaging 2009;25:251-7.

Wu YW, Kao HL, Chen MF et al. Characterization of plaques using 18F-FDG PET/CT in patients with carotid atherosclerosis and correlation with matrix metalloproteinase-1. J Nucl Med 2007;48:227-33.

Wykrzykowska J, Lehman S, Williams G et al. Imaging of inflamed and vulnerable plaque in coronary arteries with 18F-FDG PET/CT in patients with suppression of myocardial uptake using a low-carbohydrate, high-fat preparation. J Nucl Med 2009;50:563-8.

Wyss MT, Weber B, Honer M, Spath N, Ametamey SM, Westera G et al. 18F-choline in experimental soft tissue infection assessed with autoradiography and high-resolution PET. Eur J Nucl Med Mol Imaging 2004;31:312-316.

Yanni AE. The laboratory rabbit: an animal model of atherosclerosis research. Lab Anim 2004;38:246-56.

Ylä-Herttuala S, Lipton BA, Rosenfeld ME et al. Expression of monocyte chemoattractant protein 1 in macrophage-rich areas of human and rabbit atherosclerotic lesions. Proc Natl Acad Sci U S A 1991;88:5252-6.

Yoshimoto M, Waki A, Obata A, Furukawa T, Yonekura Y,.Fujibayashi Y. Radiolabeled choline as a proliferation marker: comparison with radiolabeled acetate. Nucl Med Biol 2004;31:859-865.

Zhang J, Nie L, Razavian M, Ahmed M, Dobrucki LW, Asadi A et al. Molecular imaging of activated matrix metalloproteinases in vascular remodeling. Circulation 2008;118:1953-1960.

Zhang Z, Machac J, Helft G, Worthley SG, Tang C, Zaman AG et al. Non-invasive imaging of atherosclerotic plaque macrophage in a rabbit model with F-18 FDG PET: a histopathological correlation. BMC Nucl Med 2006;6:3

Zheng QH, Gardner TA, Raikwar S, Kao C, Stone KL, Martinez TD et al. [11C]Choline as a PET biomarker for assessment of prostate cancer tumor models. Bioorg Med Chem 2004;12:2887-2893.

von Zur MC, von Elverfeldt D, Moeller JA et al. Magnetic resonance imaging contrast agent targeted toward activated platelets allows in vivo detection of thrombosis and monitoring of thrombolysis. Circulation 2008;118:258-67.

Zureik M, Robert L, Courbon D, Touboul PJ, Bizbiz L, Ducimetiere P. Serum elastase activity, serum elastase inhibitors, and occurrence of carotid atherosclerotic plaques: the Etude sur le Vieillissement Arteriel (EVA) study. Circulation 2002;105:2638-45.

Öörni K, Kovanen PT. Lipoprotein modification by secretory phospholipase A(2) enzymes contributes to the initiation and progression of atherosclerosis. Curr Opin Lipidol 2009;20:421-7.